Interaction Notes
Note 412

BOUNDING SIGNAL LEVELS AT TERMINATIONS OF A MULTICONDUCTOR TRANSMISSION LINE BEHIND AN APERTURE

4 June 1981

W. A. Davis
M. K. Sistanizadeh

Virginia Polytechnic Institute and State University
Blacksburg VA 24061

(ABSTRACT)

This report develops a technique for bounding the maximum voltages and currents at terminations of a multiconductor transmission line (MTL) located behind an aperture-perforated conducting screen excited by an electromagnetic pulse. The electromagnetic field is coupled through a small aperture to provide the excitation of a multiconductor transmission line behind the aperture. A model is presented in terms of external and internal sources which in turn creates traveling waves on the multiconductor transmission line. The latter transfer energy to the terminations. The energy at a termination is translated to voltages and currents from which the upper bounds are determined. These upper bounds are obtained using vector norms and associated matrix norms. The formulation is presented in the frequency domain and transformed to the time domain to obtain useful upper bounds for transient analysis of multiconductor transmission line geometries with aperture excitation.

This work was sponsored by the Air Force Office of Scientific Research under Grant No. AFOSR-80-0138

TABLE OF CONTENTS

LIST OF FIGURES

LIST OF FIGURES (continued)

CHAPTER I

INTRODUCTION

In designing some systems, the designer should be able to characterize the penetration of electromagnetic pulses (EMP) or lightning signals through apertures of general shapes as well as quantify the effects of the coupled energy on transmission lines located in the vicinity of the aperture.

Apertures that are of concern to the designer are usually electromagnetically small over the spectrum of the EMP, or lightning, and their existence may be for some purpose, e.g., windows, open access holes, or they may be unintentional as in the case of cracks around doors or plates covering access ports or poor electrical seams [1]. Small in the sense of electromagnetic penetration implies that the maximum dimension of the aperture is small compared with the wavelength of the time-harmonic electromagnetic field. The analysis of the coupling (penetration) problem has been investigated by a large number of people since 1897. The first scientist to propose a solution was Lord Rayleigh [2,3], whose solution was expressed as an ascending power series of the wavenumber $k(=\frac{2\pi}{\lambda})$ where λ is the wavelength. Bethe [4] presented the results for the leading terms in the Rayleigh method by using a scalar potential function approach. Bouwkamp [5] used a set of coupled, integro-differential equations to solve the problem. Recently, some have used an integral equation approach to tackle the problem. Notable among them are Butler and Umashankar [6],[7].

The coupling of the energy from an incident electromagnetic wave to a transmission line located behind an aperture-perforated conducting screen has been investigated by many engineers and physicists in the past decade. Kajfez [8] has computed the coupled energy by the use of equivalent electric and magnetic dipole moments. He has derived the equivalent sources of a transmission line model by using both mode-matching and reciprocity techniques.

Butler and Umashankar [9] have approached the problem numerically by the method of moments, and have formulated integro-differential equations for a finite-length wire with arbitrary orientation behind an arbitrarily shaped aperture. They have also taken into consideration the scattered energy into the aperture by the wire after wire excitation. Lee and Yang [10] have solved the problem using transform techniques, and have obtained the same equivalent sources as Kajfez [8]. In addition they have determined the effects of a wire being very close to the aperture. Davis [11] has developed a model using a method spatially equivalent to Lee and Yang [10] method. He has also come up with a capacitive term in his model which is not in Lee and Yang. The importance of the capacitance occurs when the wire is close to the aperture causing a capacitive discharge of the aperture region by currents on the wire.

Davis [11] has also found a method for bounding the maximum voltage and current levels at terminations of a wire behind an aperture. In his analysis, he has approached the problem both in the frequency and time domain.

This report extends the bounding problem of a single wire to the problem of obtaining an upper bound for the computation of the voltages and currents at terminations of multiconductor transmission lines (MTL) located behind an aperture-perforated conducting screen. The computations are carried out in both frequency and time domains. There are several stages that lead to the final results.

In Chapter II, the electromagnetic field coupling through small apertures is discussed. This is then extended in Chapter III to the excitation of a MTL where a model is presented in terms of external and internal sources which in turn create traveling waves on the MTL. These waves transfer the coupled energy to the terminations. The available energy found at the terminations is translated to voltages and currents by impedance transformations. Finally, the bounds on the voltages and currents are obtained in Chapters IV and V using vector norms and associated matrix norms. The discussion is closed with the presentation of comprehensive examples which elaborate on the use of the techniques to find upperbounds on the signal levels in both the frequency and time domain.

CHAPTER II

ELECTROMAGNETIC FIELD COUPLING THROUGH SMALL APERTURE IN A CONDUCTING SCREEN

In this chapter the equivalent electric and magnetic dipoles representation of an aperture is illustrated and the basic formulas are given for this problem. The presentation is tutorial and the scope is limited to the discussion of techniques which may be encountered in application. The development follows the procedures of Butler [13].

Ideally, the problem will be discussed for a small aperture in an infinite planar screen. Of course, in practical problems, one never can encounter an infinite or totally flat screen. However, if the following conditions are satisfied, then one can replace the real world problem with an ideal one:

1. The minimum distance across the surface of the screen should be large relative to the wavelength in the medium.
2. The minimum radius of the curvature of the screen should be large compared with the wavelength
3. The point of observation should be close to the surface of the screen relative to the minimum distance across the screen.
4. The point of observation should not be close to the outer edge of the screen.
5. The edges of the aperture should not be close to the edges of the screen.

In general, the problem of concern is shown in Figure (1), where one sees an infinite conducting screen with an aperture (A) cut in it. The screen is extremely thin and separates the space into two parts, each characterized by μ (medium permeability) and ε (medium permittivity) where ε can be complex to account for a lossy medium. On each side of the screen, there are electric and magnetic sources $\bar{J}_{\pm}$ and $\bar{M}_{\pm}$ which are known impressed currents, and give rise to the excitation of the aperture.

One can show [14] that the diffracted field by a small aperture can be represented approximately by radiation from equivalent electric and magnetic dipoles. Figures (2) and (3) depict the idea of electric and magnetic dipole representation for an aperture. Note that in both cases the equivalent dipoles radiate in the presence of screen when aperture is completely closed. Also, observe that the electric dipole is in the same direction of incident electric field, whereas the magnetic dipole is in opposite direction of the incoming magnetic field.

The moments of these equivalent electric and magnetic dipoles are related to the known exciting fields by special constants called polarizabilities. (See Appendix A for details.) For the case of Figure (1), one can replace the aperture (A) by equivalent dipoles, and the moments of these dipoles can be related to the polarizabilities [11] as

$$\bar{p}_e^{\pm} = p_e^{\pm}\,\hat{z} = \pm\,\varepsilon\,\alpha_e \left[E_z^{Sc-}(\bar{r}_o) - E_z^{Sc+}(\bar{r}_o)\right]\hat{z} \qquad (1)$$

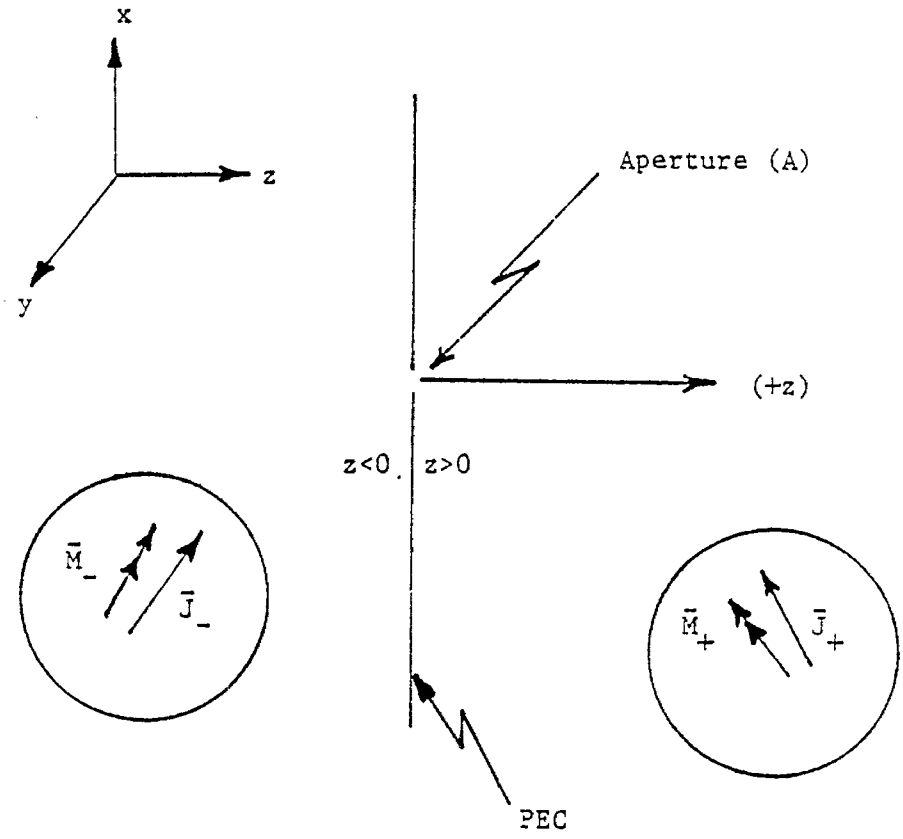

Figure (1). Location of sources with respect to the aperture and the perfect electric conductor (PEC).

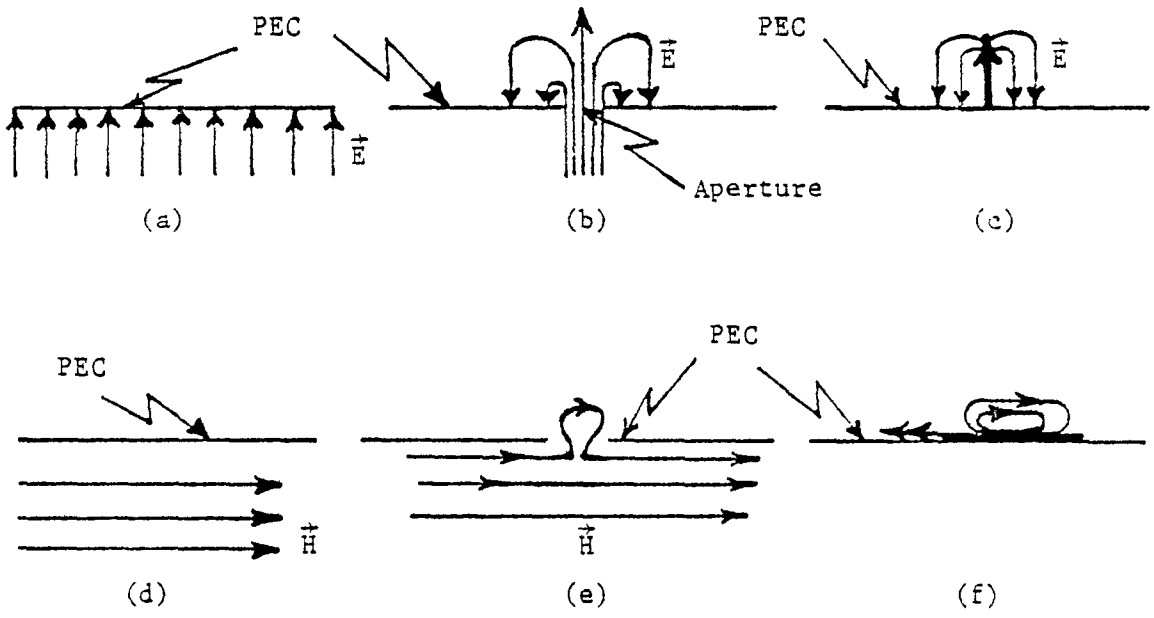

Figure (2). Equivalent electric and magnetic dipole representation of an aperture [13]: (a) electric field incident on screen without aperture, (b) electric field incident on screen with aperture, (c) equivalent electric dipole on screen with closed aperture, (d) magnetic field parallel to screen, (e) magnetic field and screen with aperture, (f) equivalent magnetic dipole on screen.

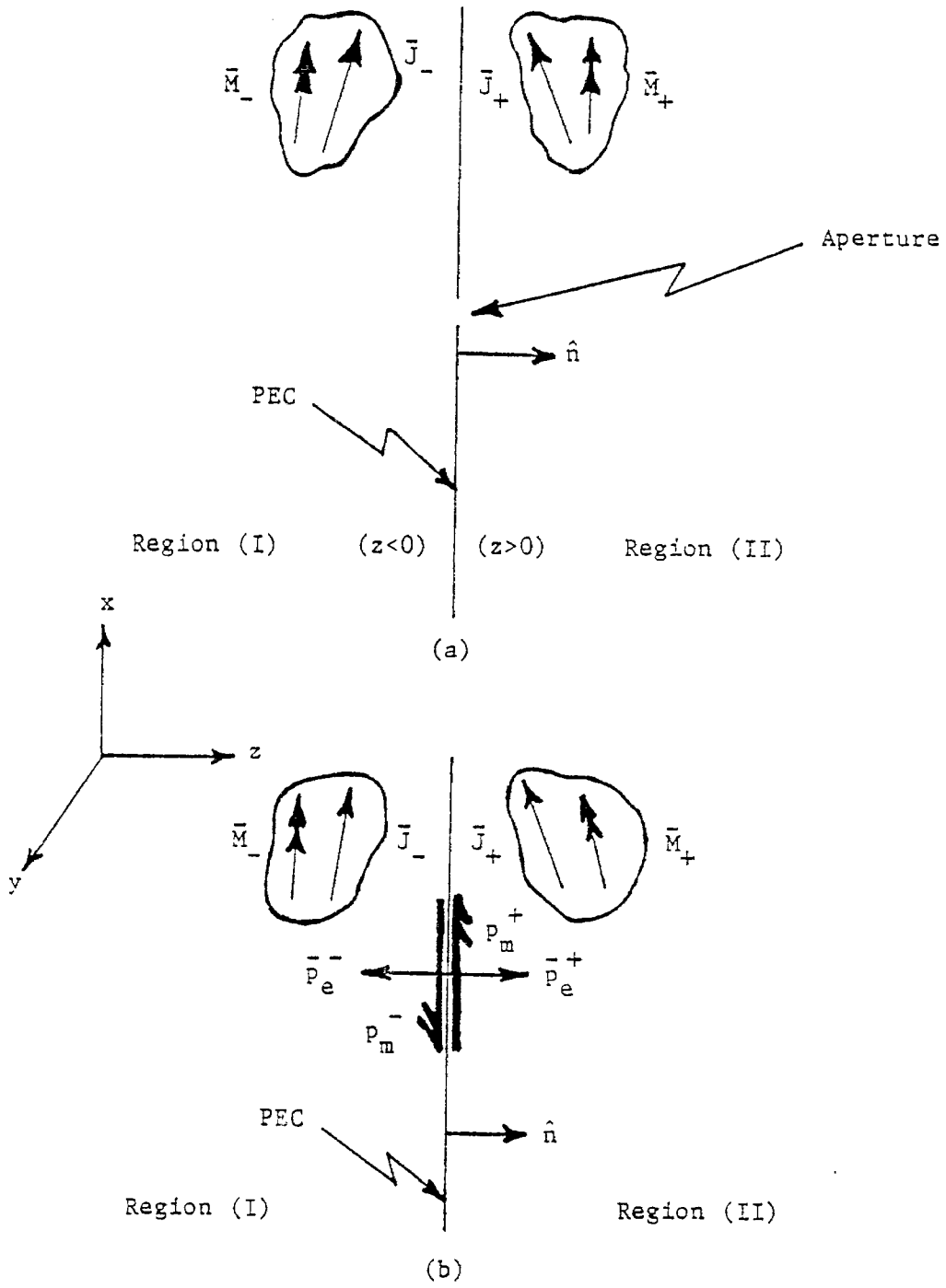

Figure (3). Equivalent problem description: (a) incident field on aperture, (b) equivalent dipole moments replacing the aperture.

$$\bar{p}_m^{\pm} = \mp \overline{\overline{\alpha}}_m \cdot \left[\bar{H}^{Sc-}(\bar{r}_o) - \bar{H}^{Sc+}(\bar{r}_o)\right] \tag{2}$$

where $\bar{p}_e^{\pm}$ is the moment of the equivalent electric dipole, $E_z^{Sc\pm}$ is called the short-circuit electric field (field which would exist if there was no aperture), $\bar{r}_o$ is the point of evaluation located in the aperture, and $\bar{H}^{Sc\pm}(\bar{r}_o)$ is the short-circuit magnetic field. The plus and minus signs represent the regions of the positive and negative z respectively.

In addition, the constants α_e and $\overline{\overline{\alpha}}_m$ are the electric and magnetic polarizabilities respectively; the latter is a dyad defined as $\overline{\overline{\alpha}}_m = (\alpha_{m,xx})\hat{x}\hat{x} + (\alpha_{m,yy})\hat{y}\hat{y}$. Thus Equation (2) can be written in component from as

$$p_{m,x}^{\pm} = \mp \alpha_{m,xx}\left[H_x^{Sc-}(\bar{r}_o) - H_x^{Sc+}(\bar{r}_o)\right] \tag{3a}$$

$$p_{m,y}^{\pm} = \mp \alpha_{m,yy}\left[H_y^{Sc-}(\bar{r}_o) - H_y^{Sc+}(\bar{r}_o)\right] \tag{3b}$$

$$\bar{p}_m^{\pm} = p_{m,x}^{\pm}\,\hat{x} + p_{m,y}^{\pm}\,\hat{y} \tag{3c}$$

The equivalent dipoles are located at $\bar{r}_o$ on the screen with the pair $\bar{p}_e^{+}$, $\bar{p}_m^{+}$ placed on the positive side of the closed surface, and $\bar{p}_e^{-}$, $\bar{p}_m^{-}$ placed on the negative side of the closed surface.

As seen from Equation (1), $\bar{p}_e^{\pm}$ is perpendicular to the screen surface while the direction of $\bar{p}_m^{\pm}$ is determined by $\bar{H}^{Sc\pm}(\bar{r}_o)$ and the shape of the aperture through $\overline{\overline{\alpha}}_m$. Now, at the present stage, one is able to calculate the field which passes through a hole in a conducting surface as well as the field which scatters back. Consider Figure (3) as depicted in the two parts. Note that the

direction of two electric dipoles are opposite to each other in two regions as are the direction of two magnetic dipoles.

Considering Figure (3b), one can write:

$$\bar{E}^{\pm}(\bar{r}) = \bar{E}^{Sc\pm}(\bar{r}) + \bar{E}^{e\pm}(\bar{r}) + \bar{E}^{m\pm}(\bar{r}) \tag{4a}$$

$$\bar{H}^{\pm}(\bar{r}) = \bar{H}^{Sc\pm}(\bar{r}) + \bar{H}^{e\pm}(\bar{r}) + \bar{H}^{m\pm}(\bar{r}) \tag{4b}$$

where $\bar{E}^{\pm}(\bar{r})$ and $\bar{H}^{\pm}(\bar{r})$ are total electric and magnetic fields present at point $(\bar{r})$ in region II or I corresponding to the (+) and (-) respectively. The (e) and (m) superscripts denote the fields of the electric and magnetic dipoles in the presence of the plane conductor, and the Sc denotes the short-circuit fields defined previously.

The electric and magnetic fields at a point $(\bar{r})$ due to electric and magnetic dipoles located at $(\bar{r}_o)$ in a homogeneous space of infinite extent are given by [13,15,16]

$$\bar{E}^{e} = -\frac{1}{\varepsilon}\nabla x(\bar{p}_e x \nabla G) \tag{5a}$$

$$\bar{H}^{e} = -j\omega\,\bar{p}_e x \nabla G \tag{5b}$$

$$\bar{E}^{m} = j\omega\,\mu\,\bar{p}_m x \nabla G \tag{5c}$$

$$\bar{H}^{m} = -\nabla x(\bar{p}_m x \nabla G) \tag{5d}$$

where G is the free space Green's Function defined as:

$$G(\bar{r},\bar{r}_o) = \frac{e^{-jk|\bar{r}-\bar{r}_o|}}{4\pi|\bar{r}-\bar{r}_o|} \tag{6}$$

Substituting Equations (5) into (4) and using image theory, one obtains:

$$\bar{E}^{\pm}(\bar{r}) = \bar{E}^{Sc\pm}(\bar{r}) - \frac{2}{\varepsilon} \nabla x[\bar{p}_e^{\pm} x \nabla G(\bar{r},\bar{r}_o)]$$

$$+ 2j\omega\mu\, \bar{p}_m^{\pm} x \nabla G(\bar{r},\bar{r}_o) \qquad (7)$$

$$\bar{H}^{\pm}(\bar{r}) = \bar{H}^{Sc\pm}(\bar{r}) - 2j\omega\bar{p}_e^{\pm} x \nabla G(\bar{r},\bar{r}_o)$$

$$- 2\nabla x[\bar{p}_m^{\pm} x \nabla G(\bar{r},\bar{r}_o)] \qquad (8)$$

If aperture reference is centered at the coordinate origin, then $\bar{r}_o$ becomes a zero vector in the above equations. The above equations are valid in the distant region of the aperture (at least one aperture dimension away).

The merit of the above approximations for computing fields depends on the electrical size of the aperture, the distance of observation point from the aperture, and the choice of the coordinate origin with respect to which the dipole moments are calculated. The details of dipole approximation are given in Appendix (B).

CHAPTER III

ELECTROMAGNETIC EXCITATION OF MULTICONDUCTOR TRANSMISSION LINES THROUGH AN APERTURE-PERFORATED CONDUCTING SCREEN

In this chapter, the electromagnetic excitation of multiconductor transmission lines (MTL) located behind an aperture-perforated conducting plane is developed using the procedures and method of Kajfez [12]. In order to do this development systematically, an aperture representation by dipoles is discussed which notationally is different from the representation introduced in chapter II. The equivalent source models are then derived using methods introduced by Kajfez [12].

Consider Figure (4) with a multiconductor transmission line parallel to the aperture on the plane. There exists an electric field in the aperture region which may be designated by $\overline{E_A}\ (z,x)$. The aperture may then be replaced with the equivalent magnetic surface current density given by

$$\vec{J}_s^{\,m}\ (x,z) = \vec{E}_A\ (x,z) \times \hat{y}$$

where $\hat{y}$ is the normal unit vector into the region of interest ($y > o$). For coupling to a MTL by a small aperture this magnetic current distribution may be replaced by the two current dipoles just above the closed aperture as shown in Figure (5). These two current dipoles have amplitudes defined by

$$\vec{c}_m = \iint \vec{J}_S^{\,m}\ (x,z)\ dxdz \qquad (9)$$

and

$$\vec{c}_e = j\omega\epsilon \iint\ (x\hat{x} + z\hat{z}) \times \vec{J}_S^{\,m}\ (x,\ z)\ dxdz. \qquad (10)$$

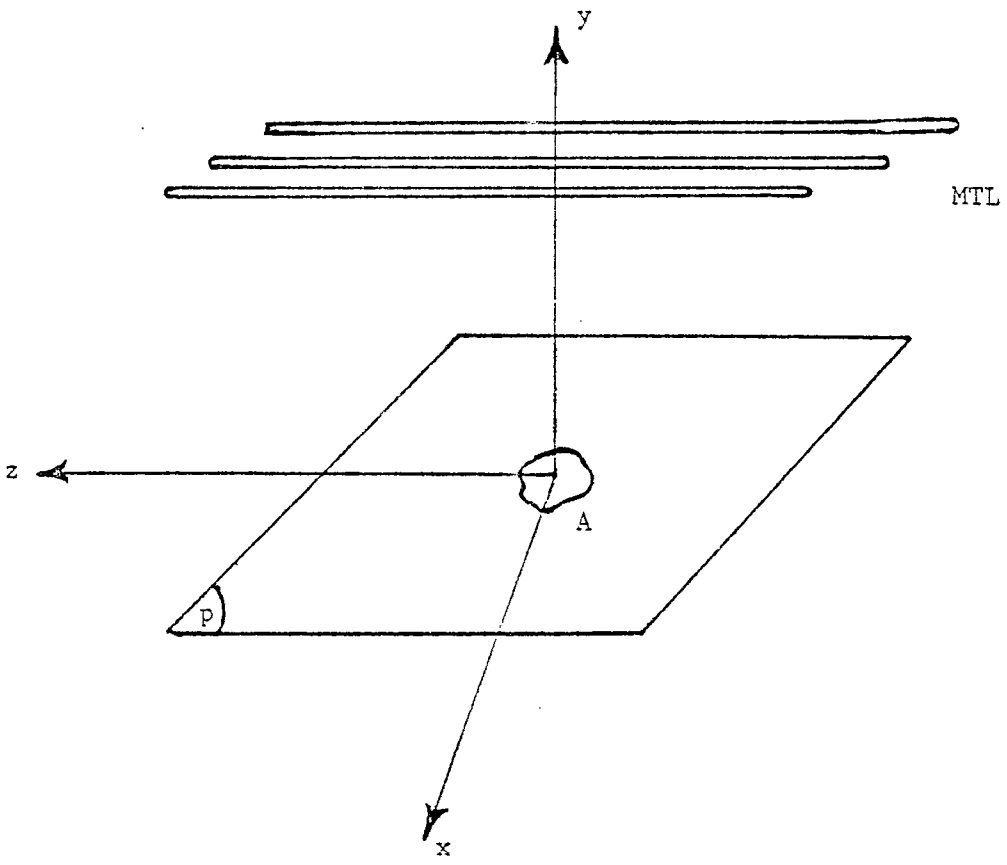

Figure (4). A MTL parallel to a plane with aperture (A).

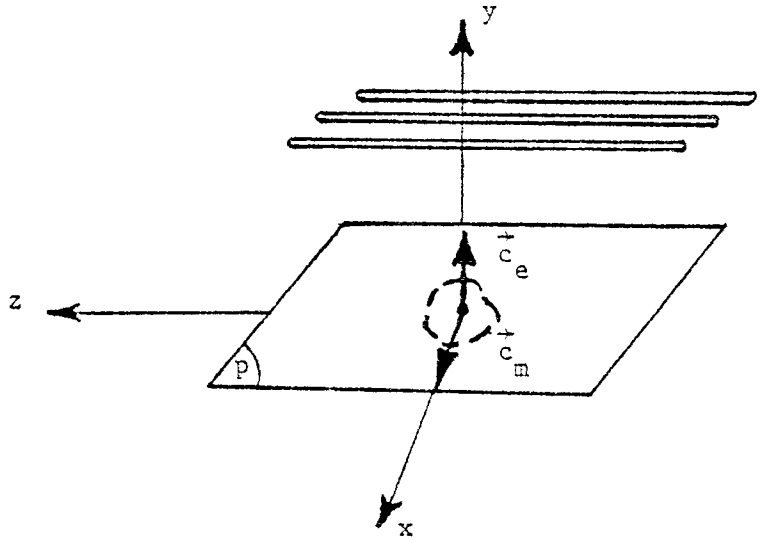

Figure (5). Aperture is replaced by equivalent current dipoles.

The derivation of Equations (9) and (10) can be found in Appendix (B).

The dipole moments $\vec{p}_e$ and $\vec{p}_m$ as introduced in Chapter II are also proportional to the above weighted integrals of the equivalent surface magnetic current [11]. From this proportionality, we may relate the current dipole amplitudes and dipole moments for $e^{j\omega t}$ by

$$\vec{c}_e = j\omega \vec{p}_e \tag{11}$$

and

$$\vec{c}_m = j\omega\mu \vec{p}_m . \tag{12}$$

The concept of polarizability (Chapter II) can be invoked here to express $\vec{c}_e$ and $\vec{c}_m$ in terms of the exterior fields. Considering Figures (6a) and 6(b), for the case of coupling to quasi-TEM (Transverse Electromagnetic) waves, only the $\hat{y}$ component of $\vec{E}$ and the $\hat{x}$ component of $\vec{H}$ are of interest. The resultant expressions are given by

$$\vec{c}_m = c_{mx}\hat{x} = -j\omega\mu\alpha_{m,xx}(H_x^{Sc-} - H_x^{Sc+})\hat{x} \tag{13}$$

$$\vec{c}_e = c_{ey}\hat{y} = j\omega\varepsilon\alpha_e(E_y^{Sc-} - E_y^{Sc+})\hat{y} . \tag{14}$$

Having introduced the preliminary notation, it is possible now to obtain equivalent sources for a MTL behind an aperture-perforated screen. Figure (5) may be redrawn for a different perspective as shown in Figure (7). Using the concept of traveling waves introduced in Appendices (D) and (E), the distribution of the electric and magnetic fields for the i^{th} mode on the MTL traveling in (+z) direction are

$$\vec{E}_i(x,y,z) = a_i\, e^{-j\beta_i z}\, \vec{e}_i(x,y) \tag{15}$$

$$\vec{H}_i(x,y,z) = a_i\, e^{-j\beta_i z}\, \vec{h}_i(x,y) . \tag{16}$$

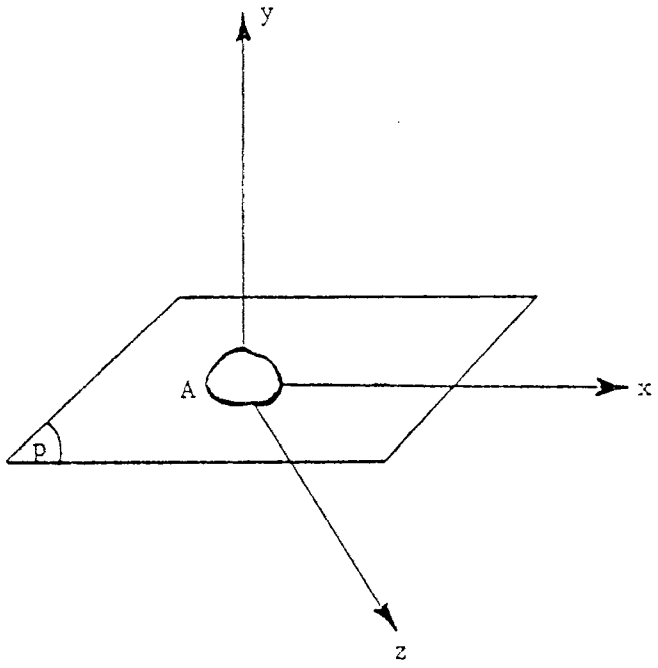

Figure (6a). Plane (p) with aperture (A).

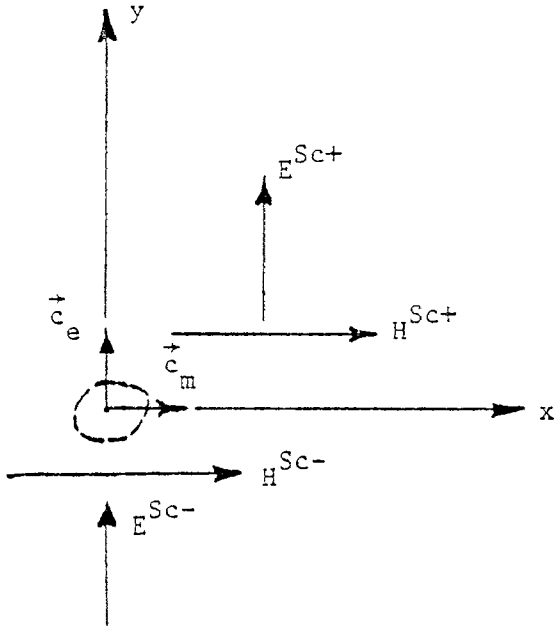

Figure (6b). Aperture replaced by a metalic lid and the associated current dipoles.

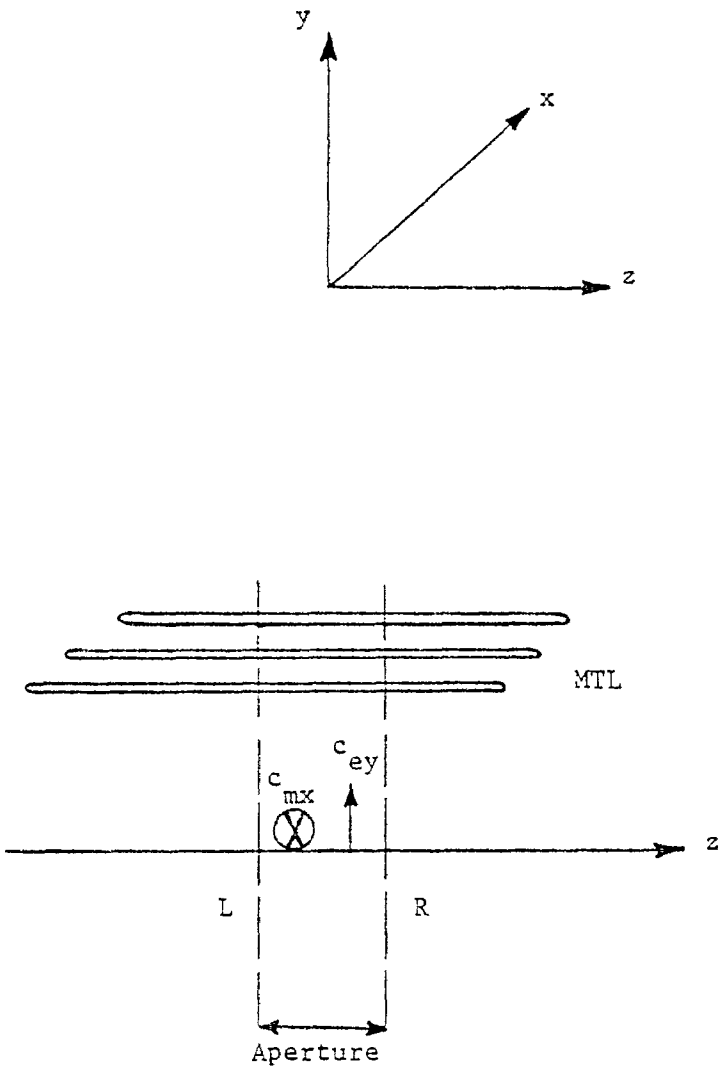

Figure (7). Aperture replaced by a metalic lid and associated current dipoles appropriately located.

where $\vec{e}_i(x,y)$ and $\vec{h}_i(x,y)$ are the power normalized modal fields over the cross section of the MTL. As depicted in Figure (7), it will be assumed that there are two infinitesimally spaced planes, denoted by (R) and (L), at each side of the aperture junction. The equivalent source model of MTL coupling will be established between these planes.

According to Appendix (F), the pair c_{mx} and c_{ey} excite the ith mode traveling in (+z) direction as

$$a_{si} = \frac{1}{2}\left[c_{mx}h_{xi}(x_0,0) - c_{ey}e_{yi}(x_0,0)\right] \tag{17}$$

where a_{si} is the source of a traveling mode in (+z) direction. The quantity $h_{xi}(x_0,0)$ is the (x) component of the ith modal magnetic-field distribution evaluated at the point ($x = x_0$) and ($y = 0$). Similarly $e_{yi}(x_0,0)$ is the y-component of the normalized electric modal field. A traveling wave source propagating in the (-z) direction, due to the pair is

$$b_{si} = -\frac{1}{2}\left[c_{mx}h_{xi}(x_0,0) + c_{ey}e_{yi}(x_0,0)\right]. \tag{18}$$

Figure (8) shows a_{si} and b_{si} sources which are convenient for analysis using scattering coefficients. Using the Dirac notation of Appendix (C), one may define the vector $|a_s\rangle$ and $|b_s\rangle$ as

$$|a_s\rangle = \begin{bmatrix} a_{s1} \\ a_{s2} \\ \cdot \\ \cdot \\ \cdot \\ a_{sN} \end{bmatrix} \quad \text{and} \quad |b_s\rangle = \begin{bmatrix} b_{s1} \\ b_{s2} \\ \cdot \\ \cdot \\ \cdot \\ b_{sN} \end{bmatrix}. \tag{19}$$

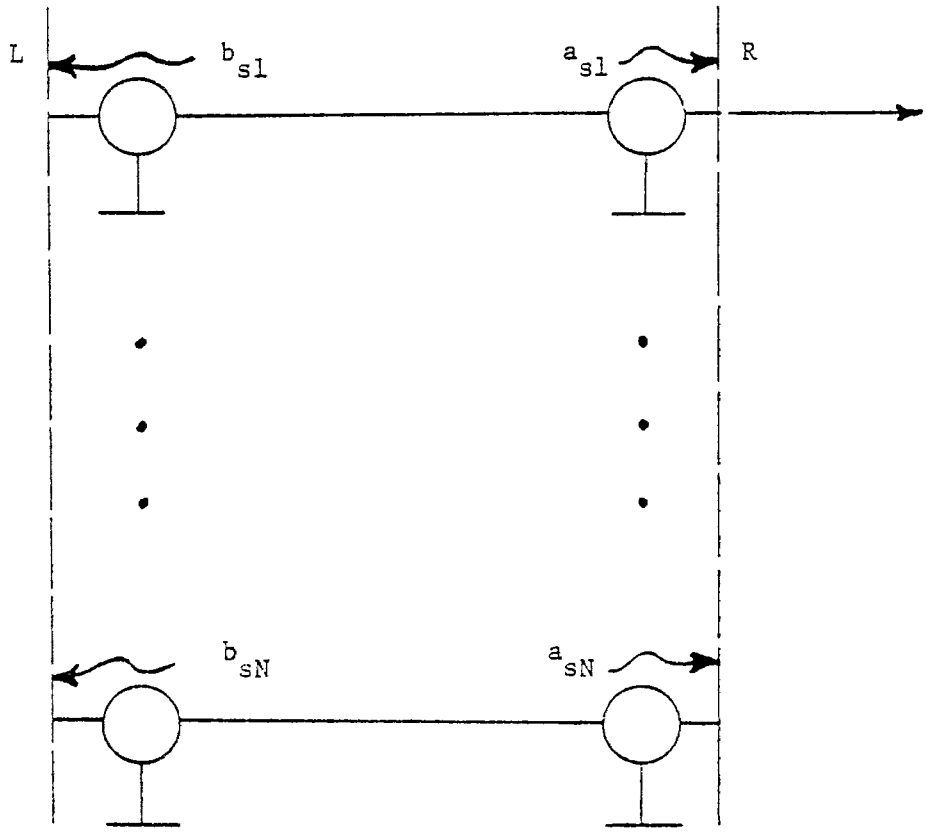

Figure (8). Traveling wave sources in (+z) and (-z) direction for each mode [12].

Define two new vectors $|a_R\rangle$ and $|b_L\rangle$ as

$$|a_R\rangle = |a_L\rangle + |a_s\rangle \tag{20a}$$

$$|b_L\rangle = |b_R\rangle + |b_s\rangle \tag{20b}$$

where $|a_R\rangle$ is the total traveling wave coming out of R (right hand reference plane) which is sum of $|a_s\rangle$ and the wave vector incoming to L (left hand reference plane). The planes R and L are shown in Figure (8). Similarly $|b_L\rangle$ is the total traveling wave coming out of L which is sum of $|b_s\rangle$ and the wave vector incoming to the R.

The equivalent circuit in terms of voltages and currents can be obtained by matrix algebra. Consider the model of voltage and current sources shown in Figure (9). The Kirchhoff laws require that

$$|V_R\rangle = |V_L\rangle + |V_s\rangle \tag{21a}$$

$$|I_R\rangle = |I_L\rangle + |I_s\rangle \tag{21b}$$

Use equation (E3) from Appendix (E) to convert the scattering representation to a voltage wave representation

$$|V_s\rangle = \underline{M}_v(|a_R\rangle - |a_L\rangle) + \underline{M}_v(|b_R\rangle - |b_L\rangle)$$

where $\underline{M}_v$ is a matrix whose columns are voltage eigenvectors. Substituting from (20a) and (20b), the above equation can be written as

$$|V_s\rangle = \underline{M}_v(|a_s\rangle - |b_s\rangle) \tag{22}$$

Invoking equations (17) and (18), one can write the components of $(|a_s\rangle - |b_s\rangle)$ as

$$(a_{si} - b_{si}) = c_{mx} h_{xi}(x_0, 0)$$

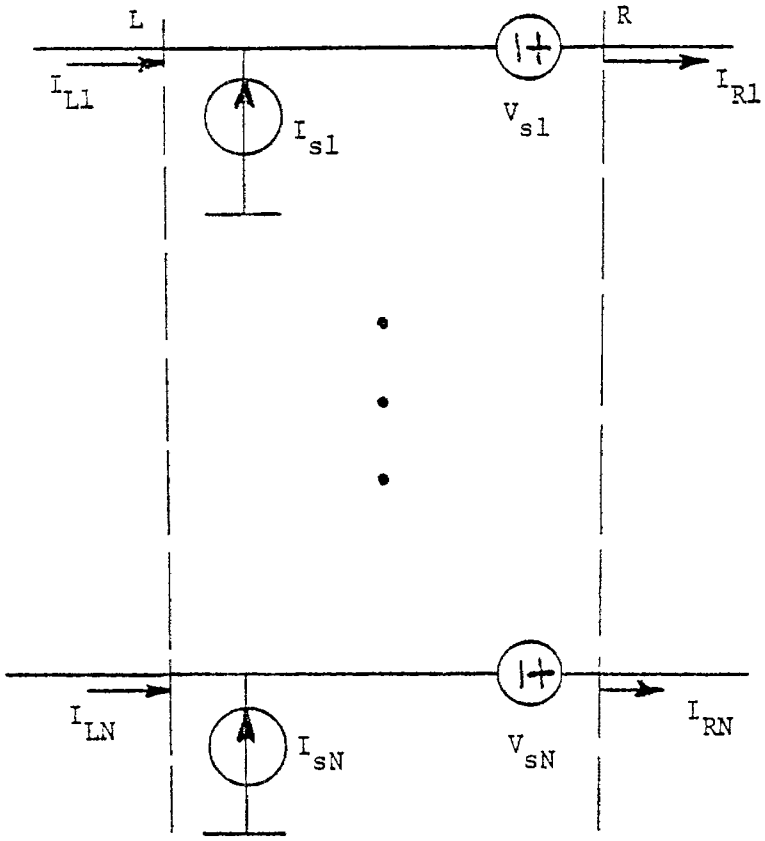

Figure (9). Voltage and current source representation for each mode [12].

This equation (22) can be written as

$$|V_s\rangle = c_{mx} \underline{M}_V \begin{bmatrix} h_{x1}(x_0,0) \\ \cdot \\ \cdot \\ \cdot \\ h_{xN}(x_0,0) \end{bmatrix}$$

Similarly using equation (E4), (17), and (18), one can write the equation for $|I_s\rangle$ as

$$|I_s\rangle = c_{ey} \underline{M}_I \begin{bmatrix} e_{y1}(x_0,0) \\ \cdot \\ \cdot \\ \cdot \\ e_{yN}(x_0,0) \end{bmatrix} \qquad (24)$$

For definitions and derivations of $\underline{M}_I$ and $\underline{M}_V$ whose columns are current and voltage eigenvectors, respectively, refer to Appendix (D). Note that in the above derivations, the energy stored in the aperture junction was neglected, therefore the Figures (8) and (9) represent the zeroth-order approximation.

The first-order equivalent circuit is now delivered for the small aperture with a MTL behind it. Consider Figure (7) again with the modification shown in Figure (10) with no incident wave coming from right. Using equation (13) and (14) and noting that the external field (or Sc^-) is zero, one can write

$$c_{mx} = +j\omega\mu \quad \alpha_{m,xx} \quad H^{sc+} \qquad (25a)$$

$$c_{ey} = -j\omega\varepsilon \quad \alpha_e \quad E_y^{sc+} \qquad (25b)$$

Decomposing electric and magnetic fields into their modal distributions, the j-th mode for each field is

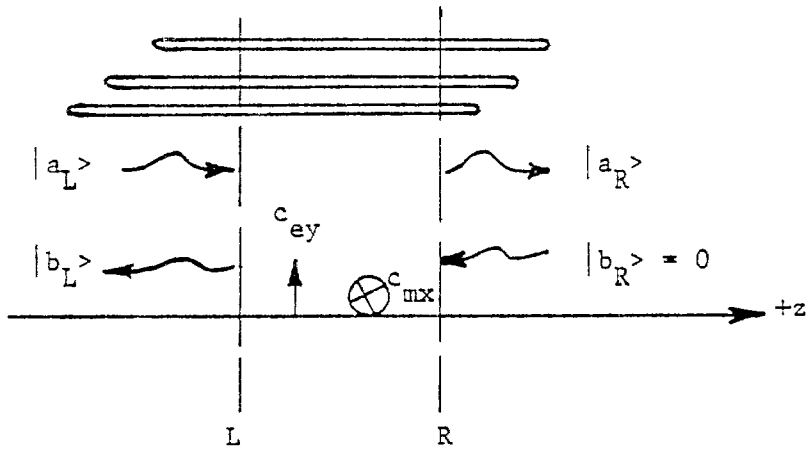

Figure (10). Incident and reflected waves on MTL with current dipoles on the closed-aperture junction [12].

$$H_{xj}^{sc+} = a_{Lj}\, h_{xj}\, (x_0,0) \tag{26a}$$

$$E_{yj}^{sc+} = a_{Lj}\, e_{yj}\, (x_0,0) \tag{26b}$$

where a_{Lj} is the amplitude of the normalized electric or magnetic field. In a similar fashion the j-th component of the amplitude of the current dipole moments are

$$c_{mxj} = j\omega\mu\,\alpha_m\, h_{xj}\, a_{Lj} \tag{27a}$$

$$c_{eyj} = -j\omega\varepsilon\,\alpha_e\, e_{yj}\, a_{Lj} \tag{27b}$$

If these moments are summed over all possible modes, then

$$c_{mx} = j\omega\mu\,\alpha_m \sum_{j=1}^{N} h_{xj}\, a_{Lj} \tag{28a}$$

$$c_{ey} = -j\omega\varepsilon\,\alpha_e \sum_{j=1}^{N} e_{yj}\, a_{Lj} \tag{28b}$$

According to equations (17) and (18), the following can be written for the ith mode of the wave in (+z) direction

$$a_{Ri} = \frac{1}{2}[c_{mx}\, h_{xi} - c_{ey}\, e_{yi}] + (a_{Li}) \tag{29a}$$

$$b_{Li} = -\frac{1}{2}[c_{mx}\, h_{xi} + c_{ey}\, e_{yi}] \tag{29b}$$

Now substituting (28a) and (28b) in the above equations one obtains:

$$a_{Ri} = \frac{1}{2}[j\omega\mu\,\alpha_m\, h_{xi} \sum_{j=1}^{N} h_{xj}\, a_{Lj} + j\omega\varepsilon\,\alpha_e\, e_{yi} \sum_{j=1}^{N} e_{yj}\, a_{Lj}] + a_{Li} \tag{30a}$$

$$b_{Li} = -\frac{1}{2}[j\omega\mu\,\alpha_m\, h_{xi} \sum_{j=1}^{N} h_{xj}\, a_{Lj} - j\omega\varepsilon\,\alpha_e\, e_{yi} \sum_{j=1}^{N} e_{yj}\, a_{Lj}] \tag{30b}$$

Define two real, symmetric matrices $\underline{H}$ and $\underline{E}$ as

$$[H]_{ij} = \frac{1}{2}\,\omega\mu\,\alpha_m\, h_{xi}\, h_{xj} \tag{31a}$$

$$[E]_{ij} = \frac{1}{2} \omega \varepsilon \alpha_e \, e_{yi} \, e_{yj} \tag{31b}$$

Equations (30a) and (30b) can then be written in terms of $\underline{E}$ and $\underline{H}$ as

$$|a_R\rangle = (\underline{I} + j\,\underline{H} + j\,\underline{E})\,|a_L\rangle \tag{32a}$$

$$|b_L\rangle = (-j\,\underline{H} + j\,\underline{E})\,|a_L\rangle \tag{32b}$$

where $\underline{I}$ is an identity matrix.

The signal flow graph of equations (32a) and (32b) is shown in Figure (11) where $|a_s\rangle$ and $|b_s\rangle$ represent the zeroth-order equivalent source models. One may define the transmission matrix $\underline{T}$ as

$$\underline{T} = \underline{I} + j\,\underline{H} + j\,\underline{E} \tag{32c}$$

and the reflection matrix $\underline{R}$ as

$$\underline{R} = -j\,\underline{H} + j\,\underline{E} \tag{32d}$$

Then equations (32a) and (32b) can be written as:

$$\begin{bmatrix} |b_L\rangle \\ |a_R\rangle \end{bmatrix} = \begin{bmatrix} \underline{R} & \underline{T} \\ \underline{T} & \underline{R} \end{bmatrix} \begin{bmatrix} |a_L\rangle \\ |0\rangle \end{bmatrix} \tag{32c}$$

Incorporating the same analysis for $|b_R\rangle$, one obtains the complete source free signal flow expressions as

$$\begin{bmatrix} |b_L\rangle \\ |a_R\rangle \end{bmatrix} = \begin{bmatrix} \underline{R} & \underline{T} \\ \underline{T} & \underline{R} \end{bmatrix} \begin{bmatrix} |a_L\rangle \\ |b_R\rangle \end{bmatrix} \tag{32d}$$

In the next chapter, this signal flow representation and the aperture signal flow sources are combined as the basic model of aperture coupling to a multiconductor transmission lines.

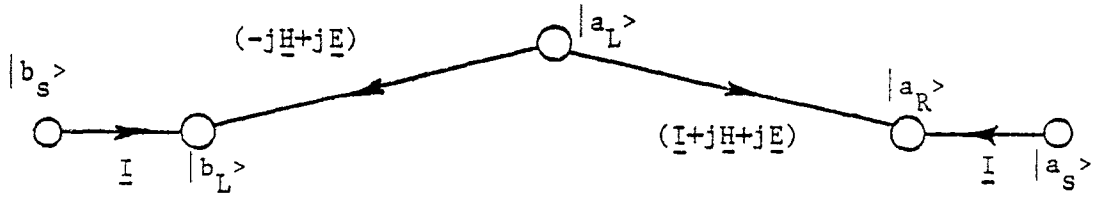

Figure (11). Signal flow graph of equations (32a) and (32b).

CHAPTER IV

BOUNDING VOLTAGE AND CURRENT AT A TERMINATION OF THE MULTICONDUCTOR TRANSMISSION LINES

In this chapter, the procedures for calculation of maximum voltage and current at a termination of MTL over a small aperture excited by an external electromagnetic pulse is formulated. Consider the aperture representation to be as shown in Figure (12).

Figure (12) can be represented by the corresponding signal flow graph in Figure (13). In Figure (13) $\underline{T}$ and $\underline{R}$ represent the transmission and reflection matrices as derived in equations (32c) and (32d). The quantities $|a_s\rangle$ and $|b_s\rangle$ are the source representations as obtained in equations (17) and (18). The quantities $\underline{\Gamma}_4$ and $\underline{\Gamma}_3$ are termination reflection matrices as computed in equations (E15) and (E17). Finally, $\underline{\Phi}_R$ and $\underline{\Phi}_L$ are the propagation matrices whose elements are exponential functions of (z) representing the phase or time delays as

$$\begin{Bmatrix} \underline{\Phi}_R \\ \underline{\Phi}_L \end{Bmatrix} = \begin{Bmatrix} \text{Diag } [e^{-j\beta_1 \ell_4}, \ldots, e^{-j\beta_N \ell_4}] \\ \text{Diag } [e^{-j\beta_1 \ell_3}, \ldots, e^{-j\beta_N \ell_3}] \end{Bmatrix} \tag{33}$$

where β_i is the phase constant for each mode. As shown in Figure (12) the origin is taken to be the region of the aperture for computation purposes. Thus, $|a_R(0)\rangle$ and $|b_R(0)\rangle$ represent the traveling waves immediately to the right of the aperture and $|a_L(0)\rangle$ and $|b_L(0)\rangle$ denote the traveling waves immediately to the left of the aperture.

One can deduce the following equations by method of signal flow theory:

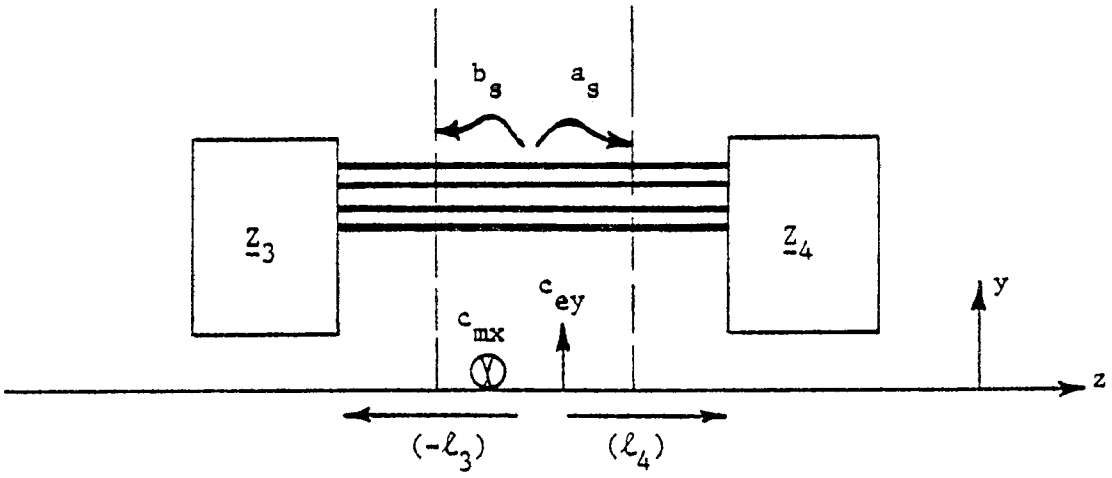

Figure (12). Terminated MTL over an aperture.

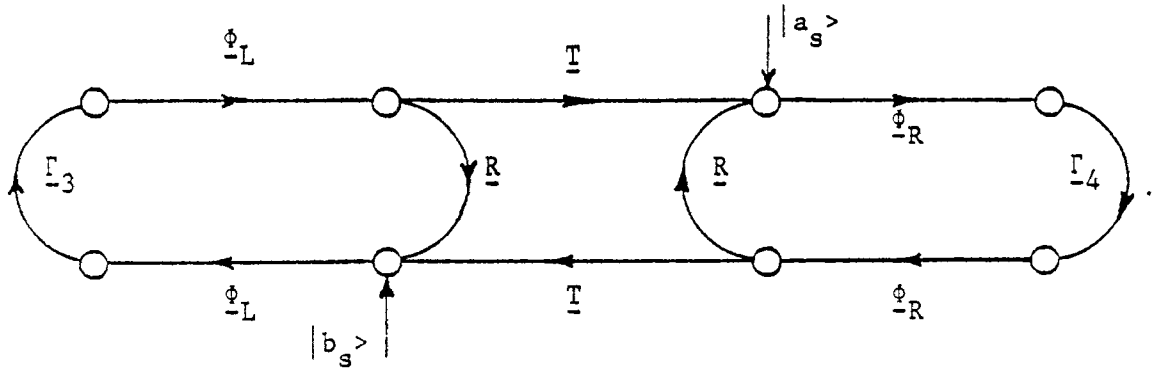

Figure (13). Signal flow graph of Figure (12).

$$|a_R(0)> = \underline{T}\,|a_L(0)> + \underline{R}\,|b_R(0)> + |a_s> \tag{34a}$$

$$|b_L(0)> = \underline{T}\,|b_R(0)> + \underline{R}\,|a_L(0)> + |b_s> \tag{34b}$$

Also at terminations $\underline{\Gamma}_4$ and $\underline{\Gamma}_3$ one can write

$$|a_R(\ell_4)> = \underline{\Phi}_R\,|a_R(0)> \tag{35a}$$

$$|b_R(\ell_4)> = \underline{\Phi}_R^{-1}\,|b_R(0)>, \tag{35b}$$

$$|b_L(-\ell_3)> = \underline{\Phi}_L\,|b_L(0)> \tag{36a}$$

$$|a_L(-\ell_3)> = \underline{\Phi}_L^{-1}|a_L(0)>, \tag{36b}$$

and

$$|b_R(\ell_4)> = \underline{\Gamma}_4\,|a_R(\ell_4)> \tag{37a}$$

$$|a_L(-\ell_3)> = \underline{\Gamma}_3\,|b_4(-\ell_3)> \; . \tag{37b}$$

Substituting equations (35) and (36) in (37), one can conclude that

$$|b_R(0)> = \underline{\Phi}_R\,\underline{\Gamma}_4\,\underline{\Phi}_R\,|a_R(0)> \tag{38a}$$

$$|a_L(0)> = \underline{\Phi}_L\,\underline{\Gamma}_3\,\underline{\Phi}_L\,|b_L(0)> \tag{38b}$$

Having introduced equations (34) and (38), one can solve for $|a_R(0)>$, $|b_R(0)>$, $|a_L(0)>$, and $|b_L(0)>$. For this first-order formulation, $|b_L(0)>$ can be shown to be

$$|b_L(0)> = [(\underline{I} - \underline{R}\,\underline{\Phi}_L\,\underline{\Gamma}_3\,\underline{\Phi}_L) - \underline{T}(\underline{\Phi}_R^{-1}\,\underline{\Gamma}_4^{-1}\,\underline{\Phi}_R^{-1} - \underline{R})^{-1}(\underline{T}\,\underline{\Phi}_L\,\underline{\Gamma}_3\,\underline{\Phi}_L)] \times$$
$$[|b_s> + \underline{T}(\underline{\Phi}_R^{-1}\,\underline{\Gamma}_4^{-1}\,\underline{\Phi}_R^{-1} - \underline{R})^{-1}\,|a_s>] \tag{39a}$$

Similarly $|a_R(0)>$ can be obtained as

$$|a_R(0)\rangle = [(\underline{I} - \underline{R}\,\underline{\Phi}_R\,\underline{\Gamma}_4\,\underline{\Phi}_R) - \underline{T}(\underline{\Phi}_L^{-1}\,\underline{\Gamma}_3^{-1}\,\underline{\Phi}_L^{-1} - R)^{-1}\,(\underline{T}\,\underline{\Phi}_R\,\underline{\Gamma}_4\,\underline{\Phi}_R)]$$

$$\times\,[|a_s\rangle + \underline{T}(\underline{\Phi}_L^{-1}\,\underline{\Gamma}_3^{-1}\,\underline{\Phi}_L^{-1} - \underline{R})^{-1}\,|b_s\rangle]. \qquad (39b)$$

For almost all practical problems of interest, one can neglect $\underline{R}$ and assume $\underline{T}$ to be unity, meaning that there are negligible reflections on the MTL due to the aperture. In fact, Kajfez [12] has shown that the reflected amplitudes are approximately one percent (or less) of the amplitudes of the incident modes. Therefore substituting $\underline{R} = \underline{0}$ and $\underline{T} = \underline{I}$ into equations (39a) and (39b), one obtains the following equations:

$$|b_L(0)\rangle = [\underline{I} - \underline{\Phi}_R\,\underline{\Gamma}_4\,\underline{\Phi}_R\,\underline{\Phi}_L\,\underline{\Gamma}_3\,\underline{\Phi}_L]^{-1}[|b_s\rangle + \underline{\Phi}_R\,\underline{\Gamma}_4\,\underline{\Phi}_R\,|a_s\rangle] \qquad (40a)$$

$$|a_R(0)\rangle = [\underline{I} - \underline{\Phi}_L\,\underline{\Gamma}_3\,\underline{\Phi}_L\,\underline{\Phi}_R\,\underline{\Gamma}_4\,\underline{\Phi}_R]^{-1}[|a_s\rangle + \underline{\Phi}_L\,\underline{\Gamma}_3\,\underline{\Phi}_L\,|b_s\rangle] \qquad (40b)$$

The above two equations are the zeroth-order formulation.

Having derived $|b_L(0)\rangle$ and $|a_R(0)\rangle$, one can use equations (36a) and (36b) to solve for $|b_R(0)\rangle$ and $|a_L(0)\rangle$ as

$$|b_R(0)\rangle = [\underline{\Phi}_R^{-1}\,\underline{\Gamma}_4^{-1}\,\underline{\Phi}_R^{-1} - \underline{\Phi}_L\,\underline{\Gamma}_3\,\underline{\Phi}_L]^{-1}[|a_s\rangle + \underline{\Phi}_L\,\underline{\Gamma}_3\,\underline{\Phi}_L\,|b_s\rangle] \qquad (41a)$$

$$|a_L(0)\rangle = [\underline{\Phi}_L^{-1}\,\underline{\Gamma}_3^{-1}\,\underline{\Phi}_L^{-1} - \underline{\Phi}_R\,\underline{\Gamma}_4\,\underline{\Phi}_R]^{-1}[|b_s\rangle + \underline{\Phi}_R\,\underline{\Gamma}_4\,\underline{\Phi}_R\,|a_s\rangle \qquad (41b)$$

Figure (14) represents the zeroth-order signal flow graph for the terminated MTL over an aperture.

Having formulated simple expressions for $|a_R(0)\rangle$ and $|b_L(0)\rangle$, one can calculate $|a(z)\rangle$ and $|b(z)\rangle$ at any point on the line. Specifically for voltage at (ℓ_4) termination, one obtains the following:

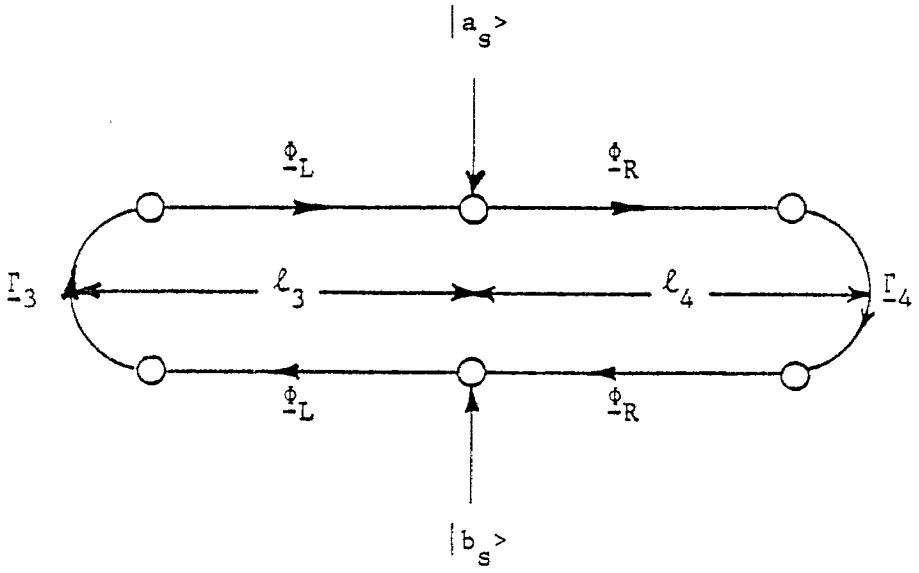

Figure (14). The zeroth-order signal flow graph.

$$|V(z)> = \underline{M}_V[|a(z)> + |b(z)>]$$

$$|V(\ell_4)> = \underline{M}_V[|a(\ell_4)> + |b(\ell_4)>]$$

However, $|a(\ell_4)>$ and $|b(\ell_4)>$ can be represented as follows from Figure (14):

$$|a(\ell_4)> = \underline{\Phi}_R \; |a_R(0)> \tag{42a}$$

$$|b(\ell_4)> = \underline{\Gamma}_4 \;\; \underline{\Phi}_R \;\; |a_R(0)> \; . \tag{42b}$$

Therefore,

$$|V_4> = |V(\ell_4)> = \underline{M}_V[\underline{I} + \underline{\Gamma}_4] \; \underline{\Phi}_R \; |a_R(0)> \tag{43a}$$

Substituting (40b) into (43a), one obtains

$$|V_4> = \underline{M}_V[\underline{I} + \underline{\Gamma}_4](\underline{\Phi}_R)[\underline{I} - \underline{\Phi}_L \; \Gamma_3 \; \underline{\Phi}_L \; \underline{\Phi}_R \; \underline{\Gamma}_4 \; \underline{\Phi}_R]^{-1} \; x$$

$$[|a_s> + \underline{\Phi}_L \; \underline{\Gamma}_3 \; \underline{\Phi}_L \; |b_s>] \tag{43b}$$

Using equation (E4) and substituting from (43a) one can also obtain any expression for $|I_4>$ as

$$|I_4> = |I(\ell_4)> = \underline{M}_I[\underline{I} - \underline{\Gamma}_4][\underline{I} + \underline{\Gamma}_4]^{-1} \; \underline{M}_V^{-1} \; |V_4> \tag{44}$$

In order to find an upper bound for the voltage or current at a termination, $|V>$ and $|I>$ should be maximized in some mathematical sense. The best mathematical procedure for bounding vectors or matrices is the calculation of their norms. The norm of a vector or a matrix is a single number which gives both a conceptual and mathematican evaluation of the size of the vector (or matrix) in the same sense that the modulus does for a complex number. The norm of a vector $|a>$ is denoted by $\| \; |a> \|$ and satisfies the following relations [17]:

$$\| |a> \| > 0 \quad \text{unless } |a> = \underline{0}$$

$$\| \beta|a> \| = |\beta| \, \| |a> \| \text{ for } \beta = \text{complex scalar}$$

$$\| |a> + |b> \| \leq \| |a> \| + \| |b> \|$$

$$\| |a> - |b> \| \geq \| |a> \| - \| |b> \|$$

The p-norm of a vector is defined as

$$\| |a> \|_p = (|a_1|^p + |a_2|^p + \ldots + |a_n|^p)^{\frac{1}{p}}, \; p = 1,2,\ldots,\infty \; . \tag{45}$$

For the case of $p = \infty$, this norm becomes

$$\| |a> \|_\infty = \max_i |a_i| \tag{46}$$

Similarly, the associated norm of a matrix $\underline{A}$ is denoted by $\| \underline{A} \|$ and satisfies the following relations:

$$\| \underline{A} \| > 0 \quad \text{unless } \underline{A} = 0$$

$$\| \beta \underline{A} \| = |\beta| \, \| \underline{A} \| \text{ for } \beta = \text{complex scalar}$$

$$\| \underline{A} + \underline{B} \| \leq \| \underline{A} \| + \| \underline{B} \| \quad \text{(triangle inequality)}$$

$$\| \underline{A} \, \underline{B} \| \leq \| A \| \, \| B \|$$

The norm of a matrix for special values of (p) is defined as

$$\| \underline{A} \|_1 = \max_j \sum_i |a_{ij}| \tag{47a}$$

$$\| \underline{A} \|_2 = \sqrt{\max(\text{eigenvalue } \underline{A}^\dagger \underline{A})} \tag{47b}$$

$$\| \underline{A} \|_\infty = \max_i \sum_j |a_{ij}| \tag{47c}$$

where (†) denotes complex conjugate transpose. Before going further, there is another identity which will be used, not proved in this discussion, and is given by

$$\| (\underline{I} - \underline{A})^{-1} \|_p = \| \underline{I} + \underline{A} + \underline{A}^2 + \ldots + \underline{A}^N + \ldots \|_p = \frac{1}{1 - \| \underline{A} \|_p} \quad (48)$$

where $\| \underline{A} \| < 1$.

Also, as noted from equations (45) and (46), the two-norm of a vector is greater or equal to its corresponding infinity-norm since

$$\sqrt{|x_1|^2 + |x_2|^2 + \ldots + |x_n|^2} \geq \sqrt{|x_{i_{max}}|^2}$$

Thus, the two norms satisfy the inequality

$$\| |x> \|_2 \geq \| |x> \|_\infty \ . \quad (49)$$

For passive terminations, which are the cases of interest, the two-norm of the termination reflection matrix $\underline{\Gamma}$ satisfies

$$\| \underline{\Gamma} \|_2 \leq 1. \quad (50)$$

This is due to the fact that reflected power from a termination is always less than or equal to incident power for physically realizable systems.

The following mathematical derivation illustrates the proof for existence of equation (50). If $|a>$ is defined as a power wave vector incident on a passive termination with reflection matrix $\underline{\Gamma}$, then the power of the reflected waves $|b>$ cannot be greater than the incident

power:

$$< b|b > \leq < a|a > \qquad \text{for physically realizable systems}$$

or

$$< b|b > = < a|\underline{\Gamma}^{\dagger}\underline{\Gamma}|a > \leq < a|a > \tag{51}$$

Similarly, for any eigenvector $|u_i>$ of matrix $\underline{\Gamma}^{\dagger}\underline{\Gamma}$ with eigenvalue λ_i one obtains

$$< u_i|\Gamma^{\dagger}\Gamma|u_i > = \lambda_i < u_i|u_i >$$

But according to equation (51)

$$< u_i|\Gamma^{\dagger}\Gamma|u_i > \leq < u_i|u_i > .$$

Therefore

$$(\lambda_i) < u_i|u_i > \leq < u_i|u_i >$$

or

$$(\lambda_i \leq 1)$$

Particularly

$$\lambda_{max} \leq 1$$

or

$$\sqrt{\lambda_{max}} \leq 1 \tag{52}$$

The above equation is the definition of the two-norm of matrix $\underline{\Gamma}$, and thus

$$\| \underline{\Gamma} \|_2 \leq 1 \tag{53}$$

At this stage, one can start analyzing equation (43b) by taking the infinity-norm of $|V_4>$ as

$$\| |V_4> \|_\infty = \|\underline{M}_V \ (\underline{I}+\underline{\Gamma}_4)\underline{\Phi}_R[\underline{I} - \underline{\Phi}_L\underline{\Gamma}_3\underline{\Phi}_L\underline{\Phi}_R\underline{\Gamma}_4\underline{\Phi}_R]^{-1} [|a_s> + \underline{\Phi}_L\underline{\Gamma}_3\underline{\Phi}_L|b_s>] \|_\infty$$

Using the triangle inequality for norms and other relations as introduced previously, the above equation is easily shown to be

$$\| |V_4> \|_\infty \leq \|\underline{M}_V\|_\infty [\| \underline{I} \|_\infty + \|\underline{\Gamma}_4\|_\infty] \| \underline{\Phi}_R\|_\infty \| [\underline{I} - \underline{\Phi}_L\underline{\Gamma}_3\underline{\Phi}_L\underline{\Phi}_R\underline{\Gamma}_4\underline{\Phi}_R]^{-1} \|_\infty$$

$$[\| |a_s> \|_\infty + \| \underline{\Phi}_L\|_\infty \|\Gamma_3\|_\infty \ \|\underline{\Phi}_L\|_\infty \| |b_s>\|_\infty]$$

Invoking equations (48) and (43b), the above inequality can be expressed as

$$\| |V_4> \|_\infty \leq \|\underline{M}_V\|_\infty [\| \underline{I} \|_2 + \|\underline{\Gamma}_4 \|_2] \| \underline{\Phi}_R\|_2 \ \frac{1}{1 - \|\underline{\Phi}_L\underline{\Gamma}_3\underline{\Phi}_L\underline{\Phi}_R\underline{\Gamma}_4\underline{\Phi}_R\|_2}$$

$$[\| |a_s> \|_2 + \|\underline{\Phi}_L \|_2 \|\underline{\Gamma}_3 \|_2 \|\underline{\Phi}_L\|_2 \| |b_s>\|_2] \quad (54)$$

Using equation (33), one obtains

$$\| \underline{\Phi}_L \|_2 = \| \underline{\Phi}_R \|_2 = 1 \quad (55)$$

Substituting equations (55) and (53) into equation (54), one has ($\| \underline{I}\|_2 = 1$)

$$\| |V_4\|_\infty \leq \|\underline{M}_V\|_\infty \ \frac{2}{1 - \| \underline{\Phi}_L\underline{\Gamma}_3\underline{\Phi}_L\underline{\Phi}_R\underline{\Gamma}_4\underline{\Phi}_R \|_2} [\| |a_s> \|_2 + \| |b_s> \|_2] \quad (56)$$

The norm in the denominator may be expanded as

$$\| \underline{\Phi}_L\underline{\Gamma}_3\underline{\Phi}_L\underline{\Phi}_R\underline{\Gamma}_4\underline{\Phi}_R \|_2 \leq \|\underline{\Phi}_L\|_2 \| \underline{\Gamma}_3\|_2 \| \underline{\Phi}_L\|_2 \| \underline{\Phi}_L\|_2 \| \underline{\Gamma}_4\|_2 \| \underline{\Phi}_R\|_2$$

or by substitution

$$\| \underline{\Phi}_L \underline{\Gamma}_3 \underline{\Phi}_4 \underline{\Phi}_R \underline{\Gamma}_L \underline{\Phi}_R \|_2 \leq 1 \ .$$

But in order to make the righthand side of equation (56) a finite quantity, one has to mathematically introduce the practical losses associated with each mode travelling on the MTL as

$$\begin{Bmatrix} \underline{\Phi}_R \\ \underline{\Phi}_L \end{Bmatrix} = \begin{Bmatrix} \text{Diag}\left[e^{-\gamma 1 z}, \ldots, e^{-\gamma N z}\right] \\ \text{Diag}\left[e^{+\gamma 1 z}, \ldots, d^{+\gamma N z}\right] \end{Bmatrix} \tag{57}$$

where

$$\gamma_i = \alpha_i + j\ \beta_i \tag{58}$$

α_i is a decay constant for each mode.

Therefore by (47b)

$$\begin{aligned} \| \underline{\Phi}_R \|_2 &= \max_i \left(e^{-\alpha_i \ell_4}\right) \\ \| \underline{\Phi}_L \|_2 &= \max_i \left(e^{-\alpha_i \ell_3}\right) \end{aligned} \tag{59}$$

where (ℓ_4) and (ℓ_3) are right and left termination distances from the aperture as depicted in Figure (12). The above equation can also be written as

$$\begin{aligned} \| \underline{\Phi}_R \|_2 &= e^{-(\alpha_{i_{min}})\ell_4} \\ \| \underline{\Phi}_L \|_2 &= e^{-(\alpha_{i_{min}})\ell_3} \end{aligned} \tag{60a}$$

Equation (56) may now be expressed as

$$\| |V_4> \|_\infty \leq \| \underline{M}_V \|_\infty \frac{2}{1 - e^{-(\sigma_R + \sigma_L)}} [\| |a_s> \|_2 + \| |b_s> \|_2]$$

where

$$\sigma_R = +2\alpha_{i_{min}} \ell_4$$

$$\sigma_L = +2\alpha_{i_{min}} \ell_3$$

If σ_T is defined as the sum $(\sigma_R + \sigma_L)$, then

$$\sigma_T = 2\alpha_{i_{min}} (\ell_4 + \ell_3) = 2\alpha_{i_{min}} \ell_T \tag{60b}$$

thus

$$\| |V_4> \|_\infty \leq \| \underline{M}_V \|_\infty \frac{2}{(1 - e^{-\sigma_T})} [\| |a_s> \|_2 + \| |b_s> \|_2] \tag{61}$$

The quantity σ_T may also be interpreted to include losses in the termination corresponding to non-unity bounds on the $|\underline{\Gamma}_i>$ and to include radiation loss both back through the aperture and in coupling to higher order modes.

It is computationally advantageous to replace $\| \underline{M}_V \|_\infty$ with the two-norm which is consistent with

$$\| |V_4> \|_\infty \leq \| |V_4> \|_2 . \tag{62}$$

This may be seen by determining the two-norm which by equation (D27) and (D31) is

$$\| \underline{M}_V \|_2 = \sqrt{\max_i \left(\frac{v_i}{\lambda_i} \right)} \tag{63}$$

where the λ_i's are the eigenvalues of the MTL matrix L^{-1} which is the

inverse of induction matrix of the MTL. Also using the triangle inequality, one obtains

$$\| |a_s\rangle \|_2 \leq [\tfrac{1}{2} \| c_{mx}|h_x\rangle \|_2 + \tfrac{1}{2} \| -c_{ey}|e_y\rangle \|_2]$$

and

$$\| |b_s\rangle \|_2 \leq [\tfrac{1}{2} \| -c_{mx}|h_x\rangle \|_2 + \tfrac{1}{2} \| -c_{ey}|e_y\rangle \|_2] .$$

Since

$$\| c_{mx}|h_x\rangle \|_2 = \| -c_{mx}|h_x\rangle \|_2$$

$$\| -c_{ey}|e_y\rangle \|_2 = \| c_{ey}|e_y\rangle \|_2$$

equation (61) may be written as

$$\| |V_4\rangle \|_\infty \leq \frac{2}{(1-e^{-\sigma T})} \sqrt{\max_i \left(\frac{v_i}{\lambda_i}\right)} \left[\| c_{mx}|h_x\rangle \|_2 + \| c_{ey}|e_y\rangle \|_2\right] \tag{64}$$

Finally, since the vector $|V\rangle$ defines the voltage on a MTL with respect to ground, the maximum voltage of interest, in other words the voltage between any two lines, is bound by

$$|\Delta V|_{max} \leq 2 \| |V_4\rangle \|_\infty$$

Using the above inequality, equation (64) may be written as

$$|\Delta V|_{max} \leq \frac{4}{(1-e^{-\sigma T})} \sqrt{\max_i \left(\frac{v_i}{\lambda_i}\right)} \left[\| c_{mx}|h_x\rangle \|_2 + \| c_{ey}|e_y\rangle \|_2\right] \tag{65}$$

which is the desired upperbound.

Substituting for c_{mx} and c_{ey} from equations (13) and (14), equation

(65) can be expressed as:

$$|\Delta V|_{max} \leq \frac{4\omega}{1 - e^{-\sigma T}} \sqrt{\max(\frac{\nu_i}{\lambda_i})} \left[\mu |\alpha_m|_{bound} |H_x^{sc}| \; \| \; |h_x> \|_2 \right.$$

$$\left. + \varepsilon \; |\alpha_e|_{bound} |E_y^{sc}| \; \| \; |e_y> \|_2 \right] \tag{66}$$

Having determined a maximum bound on the termination voltage, one can calculate a maximum bound on the termination current using equation (43a) and (43b) to simply obtain

$$\| \; |I_4> \|_\infty \leq \frac{\| \underline{M}_I \|_2}{\| \underline{M}_V \|} \| \; |V_4> \|_2 \tag{67}$$

or

$$|I_{max}| = \frac{|\Delta V|_{max}}{2} \frac{\| \underline{M}_I \|_2}{\| \underline{M}_V \|_2} \tag{68}$$

Invoking equations (D28) and (D32), one can calculate $\| \underline{M}_I \|_2$ in the same way as $\| \underline{M}_V \|_2$ to obtain

$$\| \underline{M}_I \|_2 = \sqrt{\max(\text{eigenvalue of } \underline{M}_I^\dagger \underline{M}_I)} = \sqrt{\max(\frac{\lambda_i}{\nu_i})} \tag{69}$$

Therefore equation (68) can be written as:

$$|I|_{max} = \frac{|\Delta V|_{max}}{2} \sqrt{\frac{\max(\lambda_i/\nu_i)}{\max(\nu_i/\lambda_i)}} \tag{70}$$

or

$$|I|_{max} = \frac{|\Delta V|_{max}}{2} \sqrt{\frac{1}{\max\left(\frac{v_i}{\lambda i}\right)\min\left(\frac{v_i}{\lambda_i}\right)}} \qquad (71)$$

Therefore by equations (66) and (71) one has a bound on both voltage and current at a passive termination located at some distance from the aperture. Although the above formulations all have been based on the fact that the termination is to the right of the aperture at a distant (ℓ_4), equations (66) and (71) provide a general frequency domain upper bound at any point on the MTL. It should be noted that the losses due to the aperture or termination can be taken into account by modifying σ_T as previously suggested.

The next chapter transforms these results to transient domain, and includes the important multiple reflection phenomenon.

CHAPTER V

TRANSIENT ANALYSIS

The previous discussions were based entirely on the frequency domain analysis where each mode was treated as steady state sinusoidal function of time. In this section the transient (time-domain) analysis is considered together with the multiple reflection phenomenon.
A quasi-TEM analysis of the MTL is discussed in Appendix (E). It is assumed that this quasi-TEM waveform is non-dispersive, in other words an arbitrary waveform is transmitted by each mode without distortion, and the waveform at the distance (ℓ_4) is a replica of the transmitted waveform delayed in time by ($\frac{\ell_4}{v_i}$) where v_i is the velocity of the mode. Mathematically, this is expressed as

$$a_i(\ell_4,t) = a_i(o,t-\frac{\ell_4}{v_i}) \tag{72}$$

The signal flow graph for the time domain is given in Figure (15) where terminations are located at distances (ℓ_4) and (ℓ_3) to the right and left of the aperture. If the $\underline{\Phi}_R$ matrix of the previous chapter is given by

$$\underline{\Phi}_R = e^{-j\beta\ell_4}\,\underline{I} \tag{73}$$

then

$$|a_R(\ell_4,t)> = |a_R(o,t-\tau_4)> \tag{74}$$

where

$$\tau_4 = \frac{\ell_4}{v} \tag{75}$$

The above formulation implies that all the modes have the same velocity

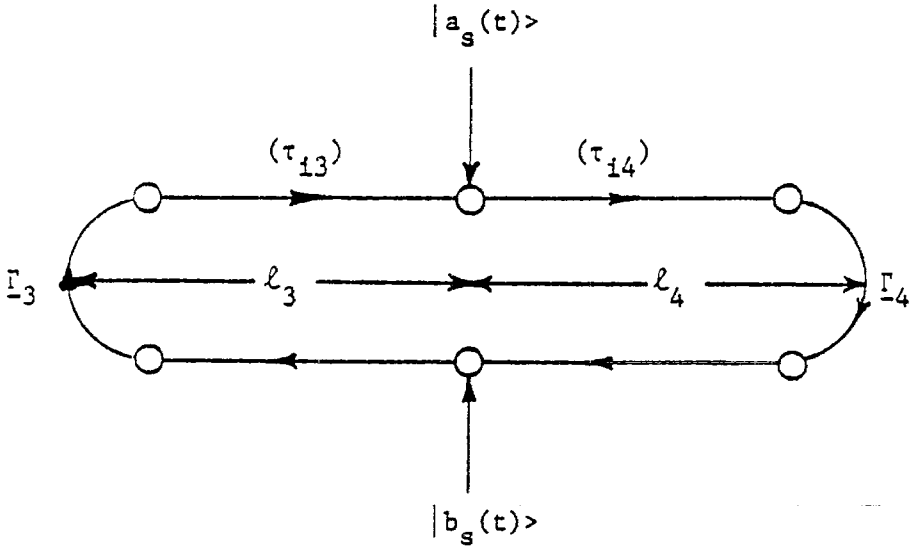

Figure (15). Time domain analysis of aperture excitation.

and consequently the same phase constant. Therefore it takes τ_4 units of time for all modes to impinge on the termination. On the other hand if the $\underline{\Phi}_R$ matrix is

$$\underline{\Phi}_R = [\delta_{ij}\ e^{-j\beta_i \ell_4}] \tag{76}$$

then

$$|a_R(\ell_4,t)> = |[a_{R_i}(o,t-\tau_i)]> \tag{77}$$

where

$$\tau_i = \frac{\ell_4}{v_i} \tag{78}$$

In this case, each mode has its own characteristic time constant (τ_i), and the formulation is much more complicated. In the following analysis, there are three major assumptions that should be kept in mind: 1) The propagation matrices $\underline{\Phi}_R$ and $\underline{\Phi}_L$ are taken to be constant. Mathematically, it is written as

$$\begin{Bmatrix} \underline{\Phi}_R \\ \underline{\Phi}_L \end{Bmatrix} = \begin{Bmatrix} e^{-j\beta\ell_4} \\ e^{+j\beta\ell_3} \end{Bmatrix} \underline{I} \tag{79}$$

where β is defined as

$$\beta = \frac{\omega}{v}$$

Also the variable (τ) corresponding to the transit time from ($-\ell_3$) to ($+\ell_4$) is defined as

$$\tau = \left(\frac{\ell_3 + \ell_4}{v}\right) ;$$

2) Terminations are assumed to be passive and resistive which implies that the elements of termination matrices $\underline{\Gamma}_4$ and $\underline{\Gamma}_3$ are real and constant; 3) The medium permittivity (ε) is taken to be that of free space (ε_o) so that all the modes travel with speed of light ($v = c$). The above three assumptions imply the worst case conditions for the whole system in terms of the voltage built up at terminations as a consequence of having the highest possible speed for each mode traveling on the MTL. This directly relates to minimal mode attenuation between successive multiple reflections. Also as implied in Figure (15), the aperture transmission and reflection matrices are assumed to be unity and zero as given by

$$\begin{aligned} \underline{\Gamma} &= \underline{I} \\ \underline{R} &= \underline{0} \end{aligned} \tag{80}$$

This assumption simplifies the formulation and calculation of the problem and due to the very small effect of $\underline{\Gamma}$ and $\underline{R}$ for problems of interest [12], it is a good approximation to the exact solution.

In Chapter IV, the termination voltage was calculated as

$$|V_4> = \underline{M}_V[\underline{I} + \underline{\Gamma}_4]\ \underline{\Phi}_R\ |a_R(0)> \ .$$

In the time domain, $\underline{\Phi}_R|a_R(0)>$ is replaced by a series of incident and reflected waves constituting the multiple reflection phenomenon as

$$|V_4(t)> = \underline{M}_V[\underline{I}+\underline{\Gamma}_4]\Big\{|a_s(t-\tau_4)> + \underline{\Gamma}_3\underline{\Gamma}_4|a_s(t-\tau_4-2\tau)>$$

$$+ \ldots + (\underline{\Gamma}_3\underline{\Gamma}_4)^n\, a_s(t-\tau_4-n(2\tau))> + \ldots +$$

$$\underline{\Gamma}_3|b_s(t+\tau_4-2\tau)> + \underline{\Gamma}_3\underline{\Gamma}_4\underline{\Gamma}_3|b_s(t+\tau_4-2(2\tau))>$$

$$+ \ldots + (\underline{\Gamma}_3\underline{\Gamma}_4)^n\underline{\Gamma}_3|b_s(t+\tau_4-n(2\tau))> + \ldots \Big\} \qquad (81)$$

The above equation can be best understood by observing Figure (16). At time (t), $|a_s(t)>$ travels (Γ_4) units of time to reach the right termination. After being reflected by $\underline{\Gamma}_4$, the wave travels (τ) units of time to reach the left termination, and again is reflected by $\underline{\Gamma}_3$. Finally, it travels (τ) units of time to impinge on the right termination. This process continues indefinitely as

$$(\underline{\Gamma}_3\underline{\Gamma}_4)^n \,|\, a_s(t-\tau_4-n(2\tau))> .$$

Similarly, one can deduce that the process for $|b_s(t)>$ takes the form

$$(\underline{\Gamma}_3\underline{\Gamma}_4)^n\underline{\Gamma}_3 \,|\, b_s(t+\tau_4-n(2\tau))> .$$

Equation (81) can now be simplified to

$$|V_4> = \underline{M}_V[\underline{I}+\underline{\Gamma}_4][\sum_{n=0}^{\infty}(\underline{\Gamma}_3\underline{\Gamma}_4)^n|a_s(t-\tau_4-n(2\tau))> +$$

$$\sum_{n=0}^{\infty}(\underline{\Gamma}_3\underline{\Gamma}_4)^n\underline{\Gamma}_3|b_s(t+\tau_4-2(n+1)\tau)>] \qquad (82)$$

Due to the losses of the aperture, the terminations, and the MTL, the above equation may be modified to include such losses as

$$|V_4> = \underline{M}_V[\underline{I}+\underline{\Gamma}_4][\sum_{n=0}^{\infty}e^{-\rho n}(\underline{\Gamma}_3\underline{\Gamma}_4)^n|a_s(t-\tau_4-n(2\tau))> +$$

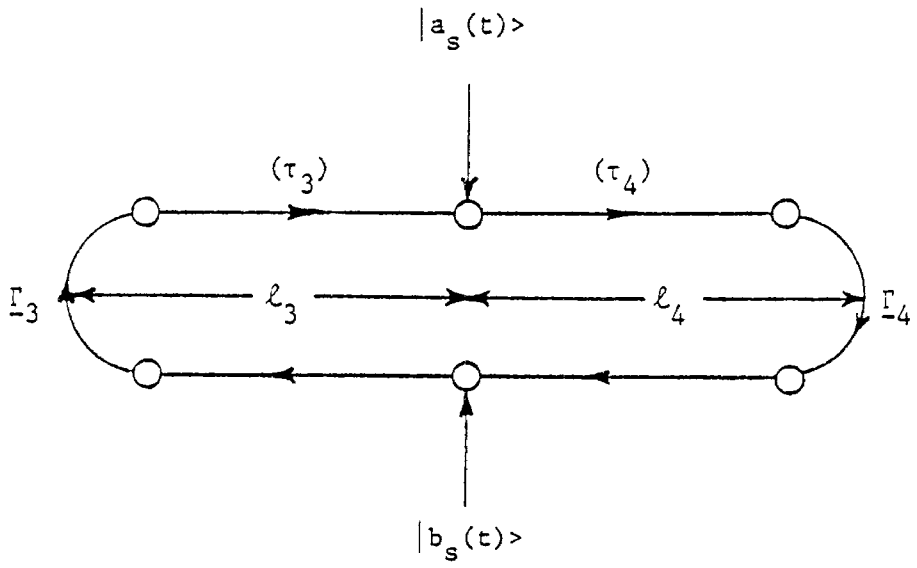

Figure (16). Multiple reflection phenomenon.

$$\sum_{n=0}^{\infty} e^{-\rho n}(\underline{\Gamma}_3\underline{\Gamma}_4)^n\underline{\Gamma}_3|b_s(t+\tau_4-2(n+1)\tau)>] \qquad (83)$$

where $(e^{-\rho n})$ takes into account the system loss for each time that a wave travels twice the length of the MTL and passes over the aperture. In order to simplify the computation of equation (83), one can use a pole expansion method of the Singularity Expansion Method (SEM) [18]. This expansion may be written for simple poles of a general function F(t) as

$$F(t) = \sum_{j=1}^{m} f_j\, e^{s_j t}\, u(t) \qquad (84)$$

where the s_j's are simple poles of the transform of F(t), and f_j's are residues due to each pole. Using the format of equation (84) in equation (83), one can write

$$|a_s(t-\tau_4-n(2\tau))> = \sum_{j=1}^{m}|a_{s_j}(0)>e^{s_j(t-\tau_4-n(2\tau))}u(t-\tau_4-n(2\tau)) \qquad (85)$$

$$|b_s(t+\tau_4-2(n+1)\tau)> = \sum_{j=1}^{m}|b_{s_j}(0)>e^{s_j(t+\tau_4-2(n+1)\tau)} u(t+\tau_4-2(n+1)\tau) \qquad (86)$$

where (s_j) is the propagation constant for each external made in the function expansion. If equations (85) and (86) are substituted in equation (83), one obtains

$$|V_4> = M_V[\underline{I}+\underline{\Gamma}_4][\sum_{j=1}^{m}|a_{s_j}(0)>\sum_{n=0}^{N} e^{s_j(t-\tau_4-n(2\tau))}e^{-on}+$$

$$\sum_{j=1}^{m} |b_{s_j}(0)\rangle \sum_{n=0}^{M} e^{s_j(t+\tau_4-2(n+1)\tau)} e^{-\rho n}] \qquad (87)$$

where, due to the unit step functions,

$$N = \text{Integer}\left[\frac{t-\tau_4}{2\tau}\right] \qquad (88a)$$

$$M = \text{Integer}\left[\frac{t+\tau_4-2\tau}{2\tau}\right] \qquad (88b)$$

for N and M non-negative. If N or M is negative, the corresponding series is deleted.

In order to obtain an upper bound on the voltage at the termination, one should take the two-norm of equation (87). Using the matrix and vector norm properties introduced previously along with the triangle inequality, one obtains

$$\| |V_4\rangle \|_2 \leq \| \underline{M}_V \|_2 \left[1 + \| \underline{\Gamma}_4 \|_2\right] \left\{ \sum_{j=1}^{m} \left[\| |a_{s_j}(0)\rangle \|_2 \left(\left| \sum_{n=0}^{N} e^{s_j(t-\tau_4-n(2\tau))} e^{-\rho n} \right| \right) + \| |b_{s_j}(0)\rangle \|_2 \left(\left| \sum_{n=0}^{M} e^{s_j(t+\tau_4-2(n+1)\tau)} e^{-\rho n} \right| \right) \right] \right\} \qquad (89)$$

If s_j, the propagation constant, is decomposed into its real and imaginary part as

$$s_{(j)} = -\eta_{(j)} + j\,\xi_{(j)}$$

then

$$\left| \sum_{n=0}^{N} e^{s_j(t - \tau_4 - n(2\tau))} e^{-\rho n} \right| \leq \sum_{n=0}^{N} e^{-\eta_j(t - \tau_4 - n(2\tau))} e^{-\rho n}$$

and

$$\left| \sum_{n=0}^{M} e^{s_j(t + \tau_4 - 2(n+1)\tau)} e^{-\rho n} \right| \leq \sum_{n=0}^{M} e^{-\eta_j(t + \tau_4 - 2(n+1)\tau)} e^{-\rho n}$$

The quantities $(-\eta_j)$ and (ξ_j) represent the decay and phase constants respectively for each mode.

One can use the finite geometrical series to simplify the above expressions as

$$\sum_{n=0}^{N} e^{-\eta_j(t - \tau_4 - n(2\tau))} e^{-\rho n} = e^{-\eta_j(t - \tau_4 - 2N\tau)} e^{-\rho N} \left[\frac{1 - e^{-(N+1)(2\eta_j\tau - \rho)}}{1 - e^{-(2\eta_j\tau - \rho)}} \right] \tag{90}$$

and

$$\sum_{n=0}^{M} e^{-\eta_j(t + \tau_4 - 2(n+1)\tau)} e^{-\rho n} = e^{-\eta_j(t + \tau_4 - 2\tau - 2M\tau)} e^{-\rho M} \left[\frac{1 - e^{-(M+1)(2\eta_j\tau - \rho)}}{1 - e^{-(2\eta_j\tau - \rho)}} \right] \tag{91}$$

Equations (90) and (91) hold only when

$$2\eta_j\tau > \rho$$

or

$$2\eta_j\tau < \rho$$

For the case when $(2\eta_j\tau = \rho)$, one may obtain

$$\sum_{n=0}^{N} e^{-\eta_j(t-\tau_4-n(2\tau))}e^{-\rho n} = (N+1)\ e^{-\eta_j(t-\tau_4)} \tag{92}$$

and

$$\sum_{n=0}^{M} e^{-\eta_j(t+\tau_4-2(n+1)\tau)}e^{-\rho n} = (M+1)\ e^{-\eta_j(t+\tau_4-2\tau)} \tag{93}$$

At this stage, one can start computing a numerical upper bound on the voltage at the termination.

The maximum value for both $e^{-\eta_j(t-\tau_4-2N\tau)}$ and $e^{-\eta_j(t+\tau_4-2\tau-2M\tau)}$ is unity which occur approximately when (N) and (M) are replaced by their respective values given in equations (88).

In order to find an upper bound for the remaining terms in equations (90) and (91), one can set M equal to N and compute the values of N for which the remaining terms are maximum. That is

$$\frac{\partial}{\partial N}\left[e^{-\rho N}\left\{\frac{1-e^{-(N+1)(2\eta_j\tau-\rho)}}{1-e^{-(2\eta_j\tau-\rho)}}\right\}\right] = 0 \tag{94}$$

After taking the derivative and solving for N denoted by N', one obtains

$$N' = \frac{\ln(2\eta_j\tau/\rho)}{(2\eta_j\tau-\rho)} - 1 \tag{95}$$

The above value for N' maximizes the equation which can be verified by showing that the second derivative is negative. Since N' must be greater than or equal to zero for the correct solution, one must compute (95) and replace N' with

$$N_{max} = \max [0, N'] \tag{96}$$

Substituting N_{max} in equations (90) and (91), one obtains

$$\sum_{n=0}^{N} e^{-\eta_j (t - \tau_4 - n(2\tau))} e^{-\rho n} \leq \left\{ \exp \left[\rho + \frac{\ln\left(\frac{2\eta_j \tau}{\rho}\right)}{1 - \frac{2\eta_j \tau}{\rho}} \right] \right\} \left\{ \frac{\left(1 - \frac{\rho}{2\eta_j \tau}\right)}{1 - e^{-(2\eta_j \tau - \rho)}} \right\} \tag{97a}$$

and

$$\sum_{n=0}^{M} e^{-\eta_j (t + \tau_4 - 2(n+1)\tau)} e^{-\rho n} \leq \left\{ \exp \left[\rho + \frac{\ln\left(\frac{2\eta_j \tau}{\rho}\right)}{1 - \frac{2\eta_j \tau}{\rho}} \right] \right\} \left\{ \frac{\left(1 - \frac{\rho}{2\eta_j \tau}\right)}{1 - e^{-(2\eta_j \tau - \rho)}} \right\} \tag{97b}$$

for N' greater than zero and unity otherwise. For the case when $(2\eta_j \tau = \rho)$, equations (92) and (93) are used and the results can be shown to be

$$\sum_{n=0}^{N} e^{-\eta_j (t - \tau_4 - n(2\tau))} e^{-\rho n} \leq \begin{cases} \left(\frac{1}{\rho}\right) e^{(\rho - 1)}, & \rho \leq 1 \\ 1, & \rho > 1 \end{cases} \tag{98}$$

The above results also hold for the summation over M.

Equations (97a) and (97b) may be simplified notationally by defining a new variable γ as

$$\gamma = 2\eta_j \tau \ .$$

Hence, the above-mentioned equations can be written as

$$\sum_{n=0}^{N} e^{-\eta_j (t - \tau_4 - n(2\tau))} e^{-\rho n} \leq \left\{ \exp\left[\rho + \frac{\rho \ln(\rho/\gamma)}{\gamma - \rho} \right] \right\} \left[\frac{1 - (\rho/\gamma)}{1 - e^{(\rho - \gamma)}} \right] \tag{99}$$

and similar simplified result holds for summation over M. If (ρ) is zero, the system has ideally no internal loss and the upper bound of the voltage at the termination will be maximum. Thus the worst case condition suggests no loss. Substituting zero for (ρ) in equation (99), one obtains

$$\left\{ \begin{array}{l} \sum_{n=0}^{N} e^{-\eta_j (t - \tau_4 - n(2\tau))} e^{-\rho n} \\ \sum_{n=0}^{M} e^{-\eta_j (t + \tau_4 - 2(n+1)\tau)} e^{-\rho n} \end{array} \right\} \leq \frac{1}{(1 - e^{-\gamma})} \tag{100}$$

Finally, substituting equation (100) in equation (89), one obtains the voltage upper bound as

$$\left\| |V_4\rangle \right\|_2 \leq \left\| \underline{M}_V \right\|_2 \left[1 + \left\| \underline{\Gamma}_4 \right\|_2 \right] \left\{ \sum_{j=1}^{m} \frac{\left[\left\| |a_{s_j}(0)\rangle \right\|_2 + \left\| |b_{s_j}(0)\rangle \right\|_2 \right]}{(1 - e^{-2\eta_j \tau})} \right\} \tag{101}$$

With the simplifications of equations (53) and (63), equation (101) becomes

$$\left\| |V_4\rangle \right\|_2 \leq 2\sqrt{\max_i (\frac{v}{\lambda_i})} \left\{ \sum_{j=1}^{m} \frac{\left[\left\| |a_{s_j}(0)\rangle \right\|_2 + \left\| |b_{s_j}(0)\rangle \right\|_2 \right]}{(1 - e^{-2\eta_j \tau})} \right\} \qquad (102)$$

As discussed in chapter IV , the maximum voltage between any two lines is

$$\left| \Delta V \right|_{max} \leq 2 \left\| |V_4\rangle \right\|_2$$

Therefore

$$\left| \Delta V \right|_{max} \leq 4\sqrt{\max_i (\frac{v}{\lambda_i})} \left\{ \sum_{j=1}^{m} \frac{\left[\left\| |a_{s_j}(0)\rangle \right\|_2 + \left\| |b_{s_j}(0)\rangle \right\|_2 \right]}{(1 - e^{-2\eta_j \tau})} \right\} \qquad (103)$$

One can use equation (70) to obtain an upper bound on the current as

$$\left| I \right|_{max} = \frac{|\Delta V|_{max}}{2} \sqrt{\frac{1}{\max_i (\frac{v}{\lambda_i}) \min_i (\frac{v}{\lambda_i})}} \qquad (104)$$

If $|a_{s_j}(0)\rangle$ and $|b_{s_j}(0)\rangle$ are replaced by their equivalent expressions in $|h_x\rangle$ and $|e_y\rangle$, then equation (103) becomes

$$\left| \Delta V \right|_{max} \leq 4\sqrt{\max_i (\frac{v}{\lambda_i})} \left\{ \sum_{j=1}^{m} \frac{\left[\left\| c_{mx}(0) |h_x\rangle \right\|_2 + \left\| c_{ey}(0) |ey\rangle \right\|_2 \right]}{(1 - e^{-2\eta_j \tau})} \right\} \qquad (105)$$

In time domain, c_{mx} and c_{ey} can be expressed as

$$c_{mx} = -\mu \alpha_{m,xx} \frac{\partial}{\partial t} [H_x^{sc-}(t)] \tag{106a}$$

and

$$c_{ey} = \varepsilon \alpha_e \frac{\partial}{\partial t} [E_y^{sc-}(t)] \tag{106b}$$

where

$$H_x^{sc-}(t) = (H_x^{sc-}) \sum_{j=1}^{m} f_j e^{s_j t} \tag{107a}$$

$$E_y^{sc-}(t) = (E_y^{sc-}) \sum_{j=1}^{m} f_j e^{s_j (t)} \tag{107b}$$

Taking derivatives from equations (107a) and (107b), and substituting in equations (106a) and (106b) respectively, equation (105) can be written as

$$\left| \Delta V \right|_{max} \leq 4 \sqrt{\max_i (\frac{v}{\lambda_i})} \left\{ \sum_{j=1}^{m} \frac{|s_j||f_j|}{(1-e^{-2\eta_j \tau})} \left[\mu \left| \alpha_{m,xx} \right|_{bound} \left| H_x^{sc-} \right| \right\| |h_x> \|_2 + \varepsilon \left| \alpha_e \right|_{bound} \left| E_y^{sc-} \right| \| |ey> \|_2 \right] \right\} \tag{108}$$

for a lossless MTL.

Equations (108) and (104) suggest a computational method for upper bound signal levels in time domain at a termination of MTL behind an aperture-perforated conducting screen.

In the next chapter, the resultant equations will be used to compute an upper bound signal level for a specific problem both in frequency and time domains.

CHAPTER VI

COMPUTATIONS OF SIGNALS UPPER BOUNDS FOR A PARALLEL-PLATE TWO-CONDUCTOR TRANSMISSION LINE

In this chapter, the results of previous discussions along with Appendices are used to compute an upper bound for the voltage and the current at a termination of a parallel-plate two-conductor transmission line located behind a circular aperture. Hopefully, this example will help the reader understand fully the concepts and the procedures used in previous discussions in computations of upper bounds.

The four basic equations which fully describe upper bounds on the voltage and the current in both time and frequency domains, as derived in chapters IV and V, are

$$\left|\Delta V\right|_{max} \leq \frac{4\omega}{1-e^{-\sigma_T}} \sqrt{\max_i \left(\frac{v_i}{\lambda_i}\right)} \left[\mu \left|\alpha_m\right|_{bound} \left|H_x^{sc-}\right| \left\| |hx\rangle \right\|_2 + \varepsilon \left|\alpha_e\right|_{bound} \left|E_y^{sc-}\right| \left\| |ey\rangle \right\|_2\right] \tag{66}$$

$$\left|I\right|_{max} = \frac{\left|\Delta V\right|_{max}}{2} \sqrt{\frac{1}{\max\left(\frac{v_i}{\lambda_i}\right) \min\left(\frac{v_i}{\lambda_i}\right)}} \tag{71}$$

$$\left|\Delta V\right|_{max} \leq 4 \sqrt{\max_i \left(\frac{v}{\lambda_i}\right)} \left[\mu \left|\alpha_m\right|_{bound} \left|H_x^{sc-}\right| \left\| |hx\rangle \right\|_2 + \varepsilon \left|\alpha_e\right|_{bound} \left|E_y^{sc-}\right| \left\| |ey\rangle \right\|_2\right] \left[\sum_{j=1}^{m} \frac{|s_j||f_j|}{1-e^{-2n_j\tau}}\right] \tag{108}$$

$$|I|_{max} = \frac{|\Delta V|_{max}}{2} \sqrt{\frac{1}{\max_i (\frac{v}{\lambda_i}) \min_i (\frac{v}{\lambda_i})}} \qquad (104)$$

The parameters used in this particular problem are the same as the ones introduced in an example by Kajfez [12] which facilitate comparison of results.

There are a few concepts that should be mentioned before proceeding to actual computations. By transmission line theory, the induction matrix $\underline{L}$ is related to the induction coefficient matrix $\underline{K}'$ as

$$\underline{L}^{-1} = c^2 \underline{K}'$$

where c is the speed of light in vacuum. The matrix $\underline{K}'$ describes the capacitance relationships of the homogeneous MTL and is evaluated for the system filled with a vacuum. This matrix depends only on the geometry of the system. The quantities λ_i's appearing in all the above-mentioned formulas are the eigenvalues of the L^{-1} matrix, and the v_i's are the corresponding modal velocities related to the eigenvalues $(-\beta_i^2)$ of the matrix $(-\omega^2 \underline{L}\,\underline{K})$ as

$$v_i = \frac{\omega}{\beta_i}$$

where $\underline{K}$ is the same matrix as $\underline{K}'$ except that it is evaluated with the true values of permittivity of the medium contained in the system.

The parallel-plate two-conductor transmission line is located behind a circular aperture of diameter d = 2 cm which is positioned at

$z = 0$ as shown in Figure (17). The transmission line is terminated by matrices $\underline{Z}_4$ and $\underline{Z}_3$ representing passive terminations located distances of 5m and 7m from the aperture respectively. The cross section of the transmission line is shown in Figure (18). There are three layers of dielectrics separating two strip conductors of width W. The thickness of dielectrics are denoted by h_1, h_2, h_3, and are assumed to be much smaller than the width W.

The computations of both the sources and the induction matrix require knowledge of the quasi-static modes on the MTL. In order to obtain the electrostatic field, a unity potential is applied to conductor a, while conductor b and the shield are held at zero potential. Then, the normalized fields in three regions are

$$\vec{E}_{1A} = \frac{1}{h_1}\,\vec{a}_y,\quad E_{2A} = 0,\quad \vec{E}_{3A} = \frac{-1}{h_3}\,\vec{a}_y \tag{109}$$

Similarly, a unity potential may be applied to conductor b while conductor a and the shield are held at zero potential. Then, the normalized fields in three regions are

$$\vec{E}_{1B} = 0,\quad \vec{E}_{2B} = \frac{-1}{h_2}\,\vec{a}_y,\quad \vec{E}_{3B} = \frac{1}{h_3}\,\vec{a}_y \tag{110}$$

Computation of the elements of the induction coefficient matrix $\underline{K}$ is accomplished by integrating the electric flux through the closed surface S_a around the conductor a as

$$Q_a = \int_{S_a} \varepsilon \vec{E} \cdot \vec{ds} \tag{111a}$$

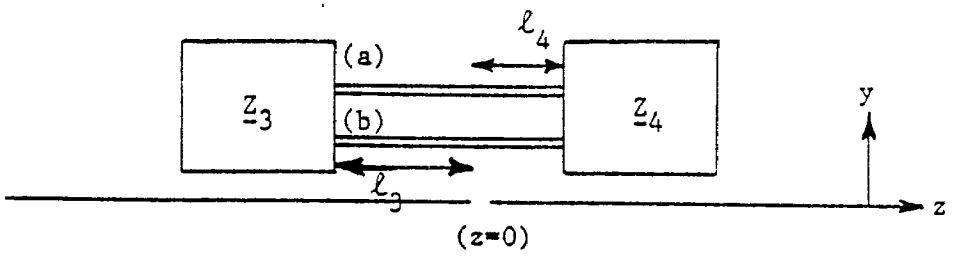

Figure (17). Two-conductor transmission line behind an aperture.

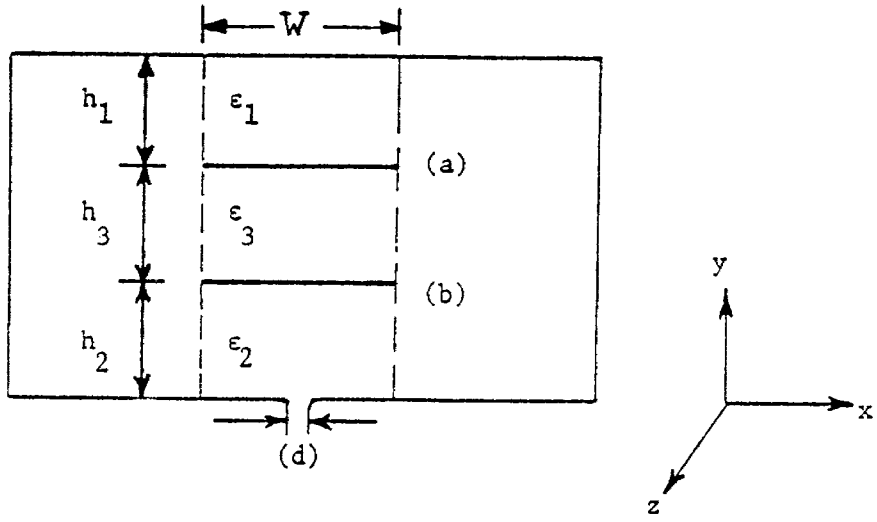

Figure (18). Cross section of two-conductor transmission line [12].

or

$$Q_a = \int_{S_a} \varepsilon \vec{E_A} \cdot \vec{ds} + \int_{S_a} \varepsilon \vec{E_B} \cdot \vec{ds} \tag{111b}$$

Equation (111b) can be written as

$$Q_a = K_{aa} + K_{ab} \tag{111c}$$

where K_{aa} and K_{ab} are the elements of $\underline{K}$ and depend only on the geometry of the system. By equations (111c), (111b), and (109), the coefficient K_{aa} is

$$K_{aa} = \varepsilon_1 \int_{x=-\frac{w}{2}}^{x=\frac{w}{2}} \vec{E_{1A}} \cdot \vec{a_y} \, dx - \varepsilon_3 \int_{x=-\frac{w}{2}}^{\frac{w}{2}} \vec{E_{3A}} \cdot \vec{a_y} \, dx$$

$$= W \left[\frac{\varepsilon_1}{h_1} + \frac{\varepsilon_3}{h_3} \right] \tag{112}$$

Similarly, the other induction coefficients are found as

$$K_{ab} = K_{ba} = - W \frac{\varepsilon_3}{h_3} \tag{113}$$

$$K_{bb} = W \left[\frac{\varepsilon_3}{h_3} + \frac{\varepsilon_2}{h_2} \right] \tag{114}$$

For this particular example, the following parameters are used to enable comparison to the transient results of Kajfez [12]:

$$h_1 = 2\text{cm}$$

$$h_2 = 2\text{cm}$$

$$h_3 = 1\text{cm}$$

$$W = 10cm$$

$$\varepsilon_{1r} = 1.0$$

$$\varepsilon_{2r} = 1.0$$

$$\varepsilon_{3r} = 2.0$$

Substituting these parameters in equations (112), (113), and (114), one obtains

$$\underline{K} = \begin{bmatrix} K_{aa} & K_{ab} \\ K_{ba} & K_{bb} \end{bmatrix} = \varepsilon_0 \begin{bmatrix} 25 & -20 \\ -20 & 25 \end{bmatrix}$$

where (ε_0) is the permittivity of vacuum. If all three dielectrics are assumed to be air ($\varepsilon_1 = \varepsilon_2 = \varepsilon_3 = \varepsilon_0$), then the induction coefficient matrix, denoted by $\underline{K}'$, becomes

$$\underline{K}' = \varepsilon_0 \begin{bmatrix} 15 & -10 \\ -10 & 15 \end{bmatrix}$$

Thus $\underline{L}^{-1}$ can be obtained as

$$\underline{L}^{-1} = c^2 \underline{K}' = \frac{1}{\mu_0} \begin{bmatrix} 15 & -10 \\ -10 & 15 \end{bmatrix}$$

where μ_0 is the permeability of vacuum. The corresponding eigenvalues of $\underline{L}^{-1}$ can be computed as

$$\lambda_1 = \frac{5}{\mu_0}$$

$$\lambda_2 = \frac{25}{\mu_0}$$

The eigenvalues $(-\beta_i^2)$ of the matrix $\underline{B} = (-\omega^2 \underline{L}\,\underline{K})$ and the corresponding eigenvectors can be obtained as

$$\beta_1^2 = \left(\frac{\omega}{c}\right)^2 , \quad |\zeta_1\rangle = \frac{1}{\sqrt{2}} \begin{bmatrix} 1 \\ 1 \end{bmatrix}$$

$$\beta_2^2 = \frac{9}{5}\left(\frac{\omega}{c}\right)^2 , \quad |\zeta_2\rangle = \frac{1}{\sqrt{2}} \begin{bmatrix} 1 \\ -1 \end{bmatrix}$$

and the corresponding modal velocities are computed using the relation $v_i = \frac{\omega}{\beta_i}$ as

$$v_1 = c$$

$$v_2 = \frac{\sqrt{5}}{3} c$$

where c is the speed of light in vacuum.

To determine the sources, the previous results must be extended to compute the aperture modal function $|e_y\rangle$ and $|h_x\rangle$.
By equation (D31), the matrix $\underline{M}_V$ which transforms a power wave to its corresponding voltage value is obtained by computing the voltage eigenvectors $|\phi_i\rangle$ given by equation (D27). Substituting the particular values of λ_i, v_i, and $|\zeta_i\rangle$ in equations (D27) and (D31) one obtains

$$\underline{M}_V = \begin{bmatrix} \phi_{a1} & \phi_{a2} \\ \phi_{b1} & \phi_{b2} \end{bmatrix} = \begin{bmatrix} 6.14 & 2.37 \\ 6.14 & -2.37 \end{bmatrix}$$

Similarly, by equations (D29) and (D32), one can compute the matrix $\underline{M}_I$ which transforms a power wave to its corresponding current value as

$$\underline{M}_I = \begin{bmatrix} \psi_{a1} & \psi_{a2} \\ \psi_{b1} & \psi_{b2} \end{bmatrix} = \begin{bmatrix} 0.0814 & 0.2108 \\ 0.0814 & -0.2108 \end{bmatrix}$$

By definition, the electric field of the nth mode traveling in positive (z) direction is

$$\vec{E}_n(x,y,z) = a_n \vec{e}_n e^{-j\beta_n z} \tag{115}$$

where $\vec{e}_n$ is normalized for unit power.

By selecting $a_n = 1$, one has

$$\vec{E}_n(x,y,0) = \vec{e}_n(x,y)$$

The corresponding voltage vector for ($a_n = 1$) and ($b_n = 0$) is obtained from equation (E3) as

$$|V_n\rangle = |\phi_n\rangle = \begin{bmatrix} \phi_{an} \\ \phi_{bn} \end{bmatrix}$$

If the potentials on the two conductors are selected equal to ϕ_{an} and ϕ_{bn} as shown in Figure (19), then the modal function $\vec{e}_n$ of the nth mode can be obtained as

$$e_{yn} = \phi_{an} (E_{2A})_y + \phi_{bn} (E_{2B})_y = \frac{-\phi_{bn}}{h_2} \tag{116}$$

Extending this result to both modes ($n = 1,2$), one obtains

$$|e_y\rangle = \frac{-1}{h_2} \begin{bmatrix} \phi_{b1} \\ \phi_{b2} \end{bmatrix}$$

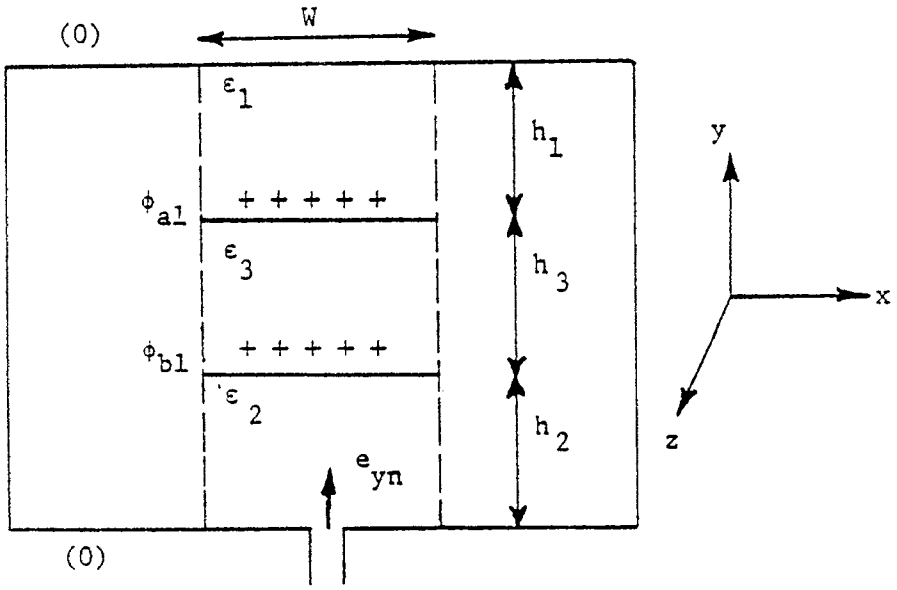

Figure (19). Computation of the modal electric field e_{yn} [12].

which gives

$$|e_y\rangle = \begin{bmatrix} -307.0 \\ +118.5 \end{bmatrix}$$

for the problem of interest.

The modal function $\overrightarrow{h_n}(x,y)$ is equal to the magnetic field $\overrightarrow{H_n}(x,y,0)$ inside the transmission line when the current on conductor (a) and (b) are respectively selected to be ψ_{an} and ψ_{bn} as shown in Figure (20). The currents are assumed to be uniformly distributed over the conductor surfaces. An elementary computation using Ampere's law and magnetic flux conservation gives the following:

$$h_{xn} = \frac{\psi_{an}\, h_1 + \psi_{bn}(h_1 + h_3)}{W(h_1 + h_2 + h_3)} \tag{117}$$

where ψ_{an} and ψ_{bn} are obtained from the matrix $\underline{M}_I$ which transforms a power wave to its corresponding current value. The vector $|h_x\rangle$ for the problem of interest becomes

$$|h_x\rangle = \begin{bmatrix} 0.814 \\ -0.421 \end{bmatrix}$$

The external short circuit fields are needed to complete the bounding process. For an incident wave with transverse magnetic (TM) polarization as shown in Figure (21), one has

$$E_y^{sc-} = 2E_0 \sin\theta, \quad H_x^{sc-} = \frac{-2E_0}{\eta_0} \sin\alpha \tag{118}$$

The incident parameters chosen by Kajfez [12] are

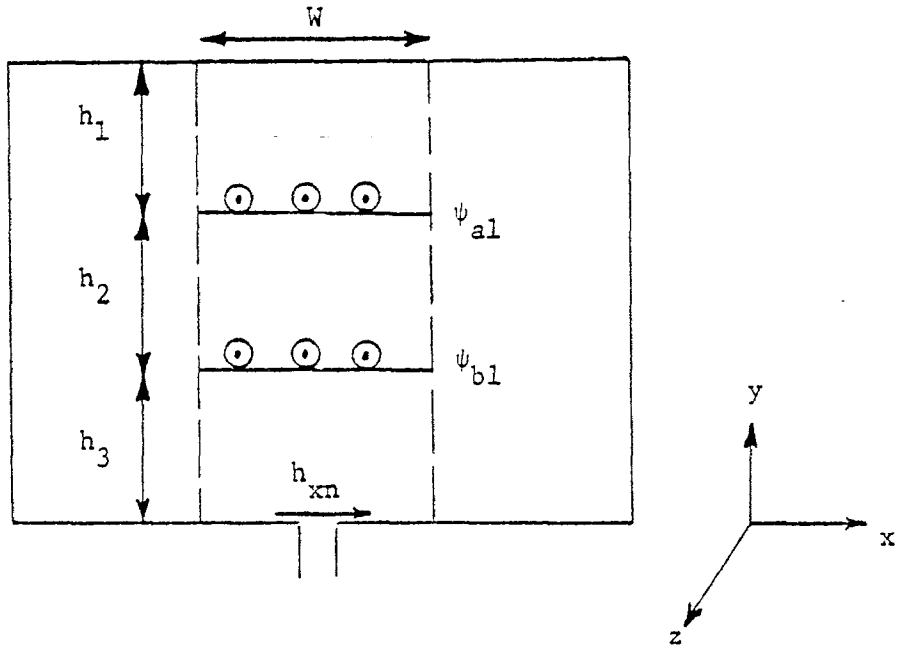

Figure (20). Computation of the modal magnetic field h_{xn} [12].

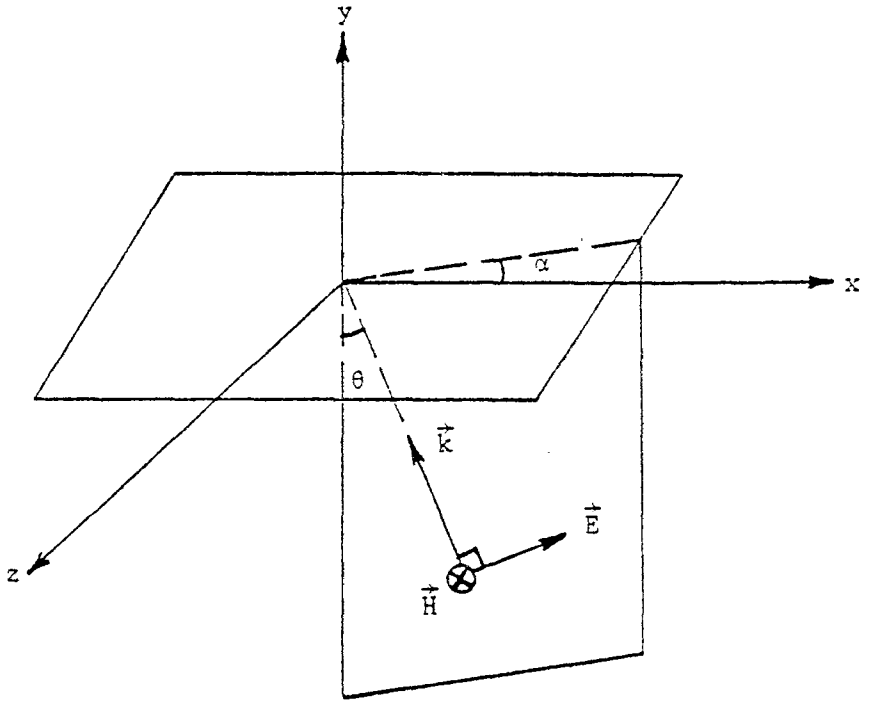

Figure (21). Transverse Magnetic (TM) polarization incident on the aperture [12].

$$\theta = 45^\circ \ , \quad \alpha = 30^\circ \ , \quad E_0 = 100 \text{ KV/m}, \quad \eta_0 = \sqrt{\frac{u}{\varepsilon}}$$

In order to obtain a numerical value for equation (66) one must compute the norms and absolute values for the following quantities:

$$\left\| |h_x> \right\|_2 = \sqrt{(0.814)^2 + (0.421)^2} = 0.9164 \text{ A/m}$$

$$\left\| |e_y> \right\|_2 = \sqrt{(307)^2 + (118.5)^2} = 329.1 \text{ V/m}$$

$$\left| H_x^{sc-} \right| = \left| \frac{-E_0}{\eta_0} \sin\alpha \right| = 132.6 \text{ A/m}$$

$$\left| E_y^{sc-} \right| = \left| 2E_0 \sin\theta \right| = 141.4 \text{ KV/m}$$

$$\alpha_m = \left(\frac{d^3}{6} \right) = 1.333 \times 10^{-5}$$

$$\alpha_e = \left(\frac{d^3}{12} \right) = 6.666 \times 10^{-7}$$

Assuming $(\alpha_i)_{min} = {}^{1dB}/_{100ft}$, one obtains

$$20 \log_{10} \left[e^{-(\alpha_i)_{min}(100ft)} \right] = -1$$

or

$$(\alpha_i)_{min} = 3.777 \times 10^{-3}$$

and by equation (60b), σ_T becomes

$$\sigma_T = 90.652 \times 10^{-3}$$

Now, one can substitute all the available data into equations (66) and (71) to obtain

$$|\Delta V|_{max} \leq (\omega) \quad (191.4 \times 10^{-9}) \text{ V}$$

$$|I|_{max} \leq (\omega) \quad (3.287 \times 10^{-9}) \text{ A}$$

If the dielectric is replaced by a vacuum and the incident angle is set ($\theta = 90^{\circ}$, $\alpha = 90^{\circ}$) for maximum short circuit fields, the upper bounds are

$$|\Delta V|_{max} \leq (\omega)(4.76 \times 10^{-7}) \text{ V}$$

and

$$|I|_{max} \leq (\omega)(7.06 \times 10^{-9}) \text{ A}$$

This forms a useful frequency-domain bound for the problem presented with a voltage less than 10 Volts for frequencies below 3.3 MHz.

For comparison, this problem has been solved exactly for open-circuit terminations on the MTL. For such a case

$$\underline{\Gamma}_3 = \underline{\Gamma}_4 = \underline{I}.$$

Determining the $|a_s\rangle$ and $|b_s\rangle$ of equations (43b) from (13), (14), (17) and (18), the results were computed and are plotted in Fig. 22 along with the bound. A modified bound is also plotted which represents the actual bound of the particular problem. The difference in bounds is 4.1 which seems slightly unreasonable until the bounding approach is examined. A factor of two arises in the bound to account for a differential mode which does not occur in the case considered. The triangle inequality used in the bound of $|a_s\rangle$ and $|b_s\rangle$ contributes another 1.5. The product of the 2-norms of $\underline{M}_V$ and $|e_y\rangle$ versus the ∞-norm of $(\underline{M}_V|e_y\rangle)$ contributes a 1.29 factor. A small contribution also occurs due to some of the neglected loss terms. In light of these observations, the resultant bound is very reasonable.

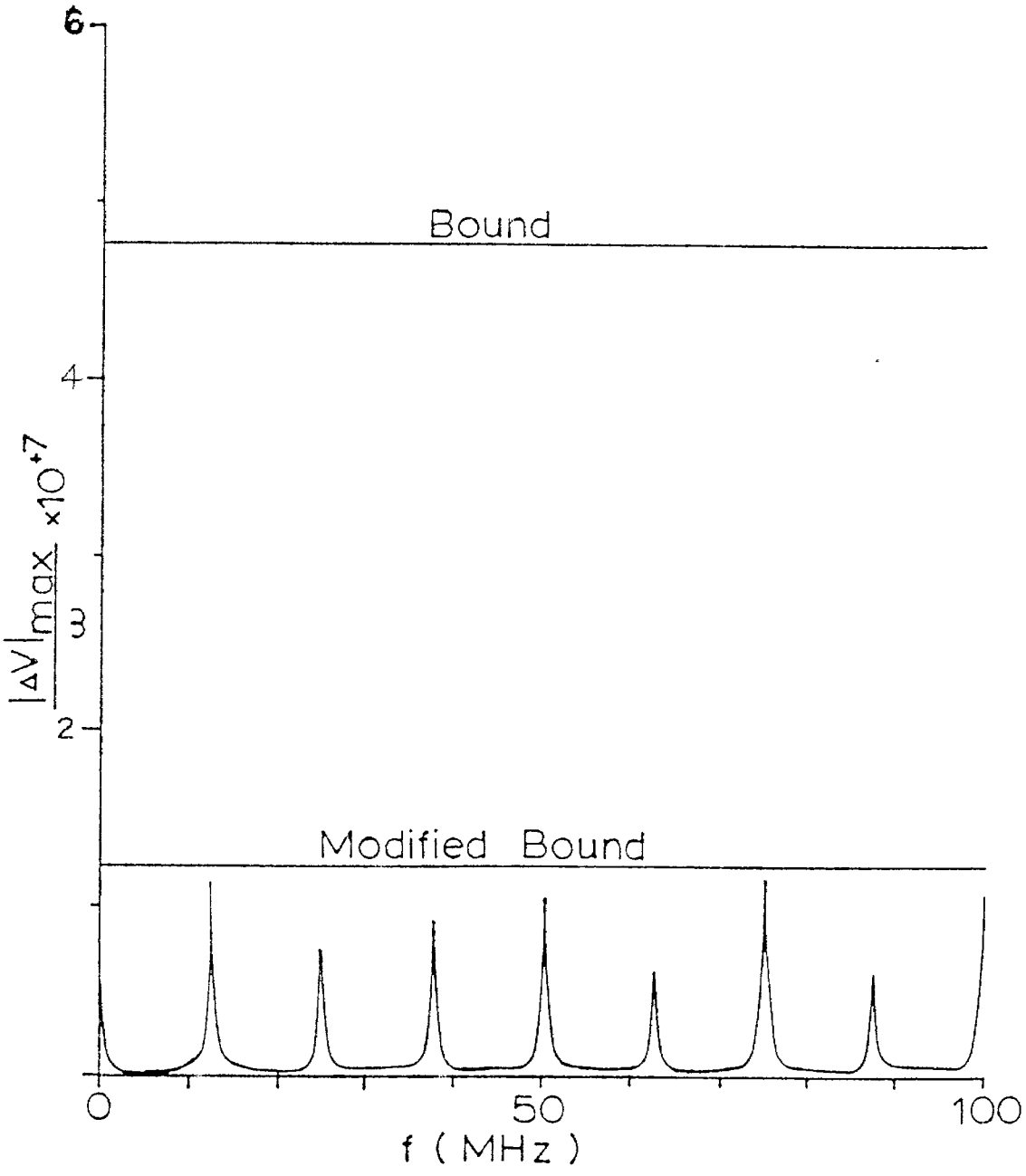

Figure 22. Open-circuit example.

For the Transient Analysis, the external incident fields given by equation (118) should be modified in order to take into account the time variations as

$$E_y^{sc-}(t) = 2E_0F(t)\sin\theta, \quad H_x^{sc-}(t) = \frac{-2E_0}{\eta_0}F(t)\sin\alpha \tag{119}$$

where for EMP a suitable function is

$$F(t) = e^{-\alpha t} - e^{-\beta t}. \tag{120}$$

Kajfez's date [12] are

$$\alpha = 3 \times 10^6 \text{ sec}^{-1}$$

$$\beta = 10^8 \text{ sec}^{-1}$$

Equation (120) is in the format of equation (84) with $|f_j| = 1(j=1,2)$, $\eta_1 = \alpha$, and $\eta_2 = \beta$. Using equations (108) and (104) for the vacuum filled lines with Kaifez's data, one obtains

$$|\Delta V|_{max} \leq (1.8959)\ V$$

$$|I|_{max} \leq (0.0281)\ A$$

where $|H_x^{sc-}|$ and $|E_y^{sc-}|$ in equation (108) correspond to the expressions of equation (119) without the F(t).

Kajfez [12] has obtained a result for this problem with moderately mismatched terminations. He has obtained a maximum voltage peak of about (0.27) volts for conductor (a) and (0.25) volts for conductor (b). Although at first glance, it may appear that the result obtained in this discussion (1.9 volts) is not reasonable at almost ten times that of Kajfez, it should be noted that for upperbound computations it is in reasonable agreement. The reason being that Kajfez has not computed worst case conditions and thus in solving the problem he has not deviated from the actual parameters regarding the termination. With his moderate mismatch, multiple reflection phenomenon have not affected the bound due to the loss. Also, in computation of various variables, he has used the true permittivity of the system. In this discussion, the use of multiple reflection phenomenon has had a negligible effect on the bound. At several stages of computation, other matrix norm inequalities such as

$$\| \underline{AB} \| \leq \| \underline{A} \| \quad \| \underline{B} \|$$

and

$$\| \underline{A} + \underline{B} \| \leq \| \underline{A} \| + \| \underline{B} \|$$

have been used extensively. These inequalities have contributed twice or more to the exact values, and therefore $|\Delta V|_{max}$ may be reasonably as small as

$$|\Delta V|_{max} \lesssim 0.95 \text{ volts}$$

In the transient analysis, the velocity of all the modes have been assumed to be the velocity of light in a vacuum which is actually larger than the true velocities of the modes in their respective media. In addition, the upperbound has had a factor of two to account for the

possible potential difference between wires and not just to ground. Taking all these factors into account, one can readily observe that the (1.9) volts for a bound on the voltage is indeed in reasonable agreement with Kajfez's calculations.

CHAPTER VII

UPPER SIGNAL BOUNDS FOR ADDITIONAL CANONICAL PROBLEMS

A more complete understanding of the bounding procedures will be presented in this chapter in connection with the upper bounds of three additional canonical problems. These problems are two parallel thin wires behind an aperture, parallel thin and thick wires behind an aperture, and a wire between an aperture-perforated parallel-plate transmission line. The latter two represent a wire at the surface of a cable bundle and a wire between bulkheads respectively.

As in the previous chapter, we use the bounds of equations (66), (71), (108), or (104) as appropriate. Let us first concentrate on the voltage represented by equation (66) below:

$$|\Delta V|_{max} \leq \frac{4\omega}{1 - e^{-\sigma T}} \sqrt{\max\left(\frac{v_i}{\lambda_i}\right)} \left[\mu |\alpha_m|_{bound} \left\| H_x^{sc-} \right\| \left\| h_x \right\|_2 + \varepsilon |\alpha_e|_{bound} \left\| E_y^{sc-} \right\| \left\| e_y \right\|_2 \right] \qquad (66)$$

Equation (66) was actually obtained from an upper bound on the power along the transmission line. The square root is the upper bound on the transformation from power waves to voltage waves. The factor of four accounts for the wire to wire voltage rather than just the wire to ground voltage in addition to the total termination voltage, which can not exceed twice the incident voltage wave. The quantity $(1 - e^{-\sigma T})$ accounts for the total multiple reflections with σ_T representing the loss per round-trip transit. The remaining terms represent the traveling wave sources due to the aperture. The ω results from a time-

derivative in the aperture current dipole moment representation, with α_m and α_e the required components of the dyadic aperture polarizabilities. The $|h_x\rangle$ and $|e_y\rangle$ vectors are associated with the multiconductor transmission line (MTL) fields at the aperture as required for the source determination using the reciprocity theorem.

For a particular problem as shown in Figure 12 of Chapter IV the radian frequency ω is assumed known and the loss σ_T must be estimated. This loss is due to power absorbed in the terminations, or line, and radiated in other neglected modes or back through the aperture. For simplicity, we shall set σ_T equal to only the line loss which will be estimated at 1dB/100ft., typical of standard transmission lines in the high frequency (HF) range.

In order to facilitate the field calculations associated with the sources, the medium is assumed to be homogeneous. In general, we shall use the parameters of a vacuum, μ_o and ε_o, which provide a maximum value of v_i to be 3×10^8 m/s. The bounds on the polarizabilities are obtained from the geometry of the aperture. In general, these bounds may be determined from the polarizabilities of an ellipse which circumscribes the aperture. The H_x^{sc-} and E_y^{sc-} are obtained from the exterior problem which is assumed to have been solved.

The remaining quantities λ_i, $|h_x\rangle$, and $|e_y\rangle$ are determined from the geometry of the MTL. The equations defining the MTL are given in Appendix D as

$$\frac{d}{dz}|V\rangle = -j\omega\underline{L}|I\rangle \tag{D1}$$

and

$$\frac{d}{dz} | I > = -j\omega \underline{K} | V > \tag{D2}$$

The parameters λ_i are the eigenvalues of $\underline{L}^{-1}$. If the medium is a vacuum as assumed, these are simply the eigenvalues of $c^2\underline{K}$ where c is the speed of light 3×10^8 m/s. The induction coefficient matrix $\underline{K}$ may be determined by either solving n boundary value problems using Laplace's equation for the n wires or determining the potentials due to charge distributions on the wires. The latter has been used where a line charge Q_i has been assumed and the associated potentials been determined. These results are used to determine the matrix $\underline{K}$ from the vector equation

$$| V > = \underline{P} | Q > \tag{12}$$

with the elements of $| V >$ and $| Q >$ associated with the corresponding wires. The matrix $\underline{K}$ is the inverse of $\underline{P}$ from which the λ_i may be found.

In determining $\underline{P}$, the electric field in the medium is required which is also used to explicitly determine E_y at the aperture for each Q_i. The corresponding magnetic field component H_x may simply be obtained as $(-E_y/\eta_o)$, where η_o is the characteristic impedance of a vacuum given by 120π.

To complete the problem, modes on the MTL must be defined. In general, the modes are associated with the eigenfunctions of $(-\omega^2 \underline{L}\,\underline{K})$. However, in a homogeneous medium $\underline{L}^{-1} = c^2\underline{K}$ and we need the eigenvectors of $(-\frac{\omega^2}{c^2}\underline{I})$ where $\underline{I}$ is the identity matrix. In this case, we are free to choose the eigenvectors. It is standard to choose one of the voltage eigenvectors for an n-wire line as

$$| b_1 > = \frac{1}{\sqrt{n}} \begin{Bmatrix} 1 \\ \vdots \\ 1 \end{Bmatrix} , \tag{122}$$

which corresponds to the bulk mode, and the other nodes $| b_i >$ as orthonormal differential nodes. The corresponding charge distributions $| Q_i >$ are given by

$$| Q_i > = \underline{K} | b_i > \tag{123}$$

which results in aperture field E_{yi} for each $| Q_i >$. The components of $| e_y >$ and $| h_x >$ are normalized for unit power flow. Thus

$$e_{yi} = \frac{\sqrt{2}\ E_{yi}}{\sqrt{c < b_i | \underline{K} | b_i >}} \tag{124}$$

to give

$$| e_y > = \begin{Bmatrix} e_{y1} \\ \vdots \\ e_{yn} \end{Bmatrix} \tag{125}$$

and

$$| h_x > = - \frac{1}{\eta_o} | e_y > . \tag{126}$$

With these vectors and equation (66), we are prepared to determine an upper bound on the frequency domain voltage and current.

Alternately, the $| b_i >$ may be chosen as the unit normalized eigenvectors of $\underline{L}^{-1}$, then (123) becomes

$$| Q_i > = \frac{\lambda_i}{c^2} | b_i > . \tag{127}$$

The denominator of (124) similarly becomes $\sqrt{\lambda i/v}$. Since E_{yi} is proportional to $\frac{\lambda_i}{c^2}$, (124) can be simplified to

$$e_{y_i} = \frac{\sqrt{2}\, E'_{y_i}}{c} \sqrt{\frac{\lambda_i}{c}} \tag{128}$$

where the prime denotes the electric field due to a charge vector $| b_i >$.

The first problem to consider in this chapter consists of two parallel thin wires in a vacuum as shown in Figure 23. A particular frequency is not chosen, but rather the answer is given as proportional to ω. Using the suggested 1dB/100ft estimate for the loss along with lengths ℓ_4 and ℓ_3 of 5 and 7 meters respectively, $(1 - e^{-\sigma T})^{-1}$ becomes (11.539). These are the same lengths as the example of Chapter VI. Also assuming the same circular aperture, α_m and α_e are given by (1.333×10^{-6}) and (6.666×10^{-7}) respectively.

To determine the eigenvalues and field vectors, we consider the approximate line charge equivalent configuration of Figure 24. To compute the $\underline{P}$ of Equation (121), we may sequentially allow only charge Q_1 and charge Q_2 to be nonzero. From each of these line charges, the electric fields may be determined. We obtain the corresponding voltages by integrating the electric field from the ground plane to the wire edges (dotted line about line charge) along both paths L_1 and L_2. From the latter, the matrix elements of $\underline{P}$ are given for thin wires as

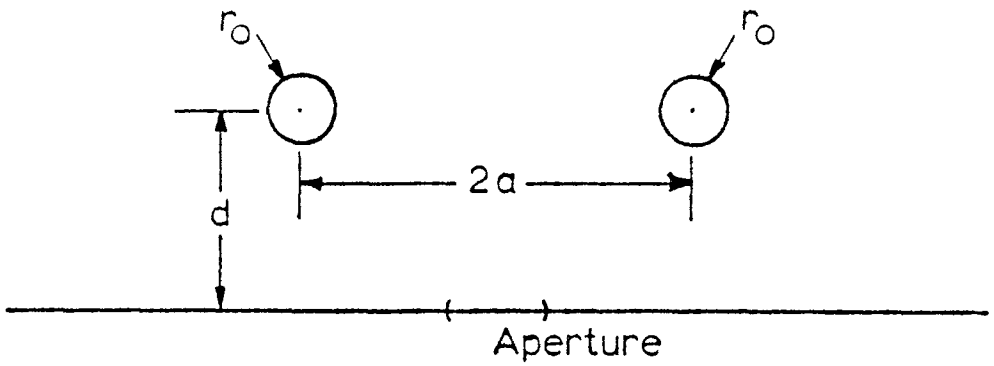

Figure 23. Cross-section of two wires behind an aperture.

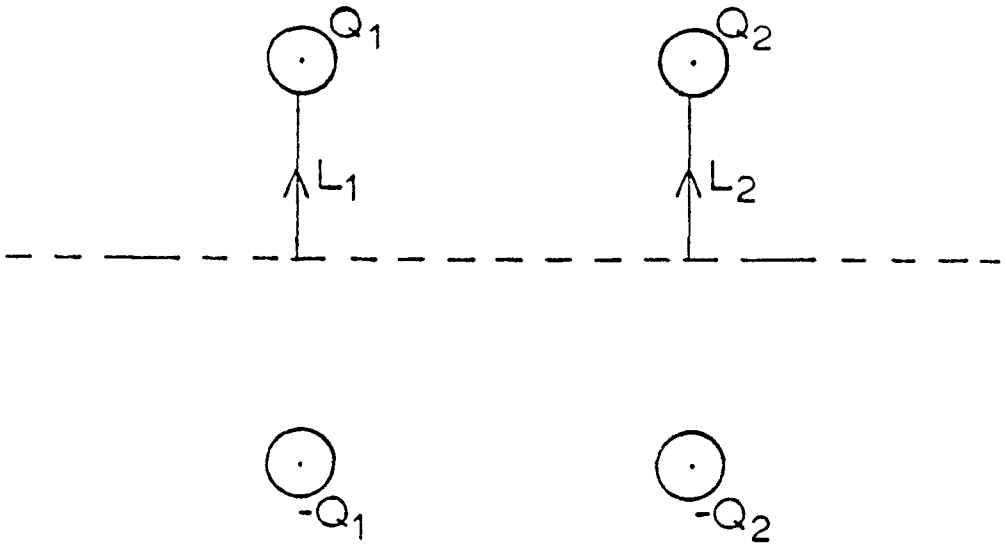

Figure 24. Image charge equivalent of two wires above a ground plane.

$$P_{11} = P_{22} = -\int_{o}^{d-r_o} \left[\frac{1}{2\pi\varepsilon_o(x-d)} - \frac{1}{2\pi\varepsilon_o(x+d)} \right] dx$$

$$= \frac{1}{2\pi\varepsilon_o} \ln\left(\frac{2d - r_o}{r_o}\right) \tag{129}$$

and

$$P_{12} = P_{21} = -\int_{o}^{d-r_o} \left[\frac{x-d}{2\pi\varepsilon_o[(x-d)^2+4a^2]} - \frac{x+d}{2\pi\varepsilon_o[(x+d)^2+4a^2]} \right] dx$$

$$= \frac{1}{4\pi\varepsilon_o} \ln\left[\frac{(2d-r_o)^2 + 4a^2}{r_o^2 + 4a^2} \right]. \tag{130}$$

Thus

$$\underline{L}^{-1} = \frac{c^2}{(P_{11}^2 - P_{12}^2)} \begin{bmatrix} P_{11} & -P_{12} \\ -P_{12} & P_{11} \end{bmatrix} \tag{131}$$

where c is the speed of light (3×10^8 m/s).

It is easily shown that the eigenvalues of $\underline{L}^{-1}$ are given by

$$\lambda_i = c^2/(P_{11} \mp P_{12}) \tag{132}$$

with the associated eigenvectors given by

$$|b_i\rangle = \frac{1}{\sqrt{2}} \begin{bmatrix} 1 \\ \mp 1 \end{bmatrix}. \tag{133}$$

If the charges on the two wires are designated as Q_1 and Q_2, then it is easily shown that the electric field at an aperture symmetrically located between the wires is given by

$$\vec{E} = \frac{-d\hat{y}}{\pi\varepsilon_o(d^2+a^2)} (Q_1 + Q_2) \ . \tag{134}$$

Choosing $|\, b_1 >$ to have the plus sign we have

$$E_{y_2} = \frac{-d\sqrt{2}}{\pi\varepsilon_o(d^2+a^2)}$$

and

$$E_{y_1} = 0$$

to give

$$|\, e_y > = \begin{bmatrix} \dfrac{-2\ d\ \eta_o}{\pi(d^2+a^2)} & \sqrt{\dfrac{\lambda_1}{c}} \\ 0 \end{bmatrix} \tag{135a}$$

$$|\, h_x > = \begin{bmatrix} \dfrac{2\ d}{\pi(d^2+a^2)} & \sqrt{\dfrac{\lambda_1}{c}} \\ 0 \end{bmatrix} \ . \tag{135b}$$

We note that λ_1 is the minimum eigenvalue required in Equation (66).

Substituting this information into (66) we obtain

$$|\, \Delta V|_{max} \leqslant (3.077 \times 10^{-5})\omega\varepsilon_o \frac{2\ d\ \eta_o}{\pi(d^2+a^2)} [2|\eta_o H_x^{sc-}| + |E_y^{sc-}|] \ . \tag{136}$$

If $a = d = 1$cm, this becomes

$$|\Delta V|_{max} \leqslant 9.794 \times 10^{-4}\ k_o[2|\eta_o H_x^{sc-}| + |E_y^{sc-}|]$$

where k_o is the wave number $\omega\sqrt{\mu_o\varepsilon_o}$. Using the H_x^{sc-} and E_y^{sc-} of (118) with the associated data, this bound is

$$|\Delta V|_{max} \leq 334\ k_o \qquad V$$

or equivalently

$$|\Delta V|_{max} \leq \omega(1.11 \times 10^{-6}) \qquad V \ . \tag{137}$$

This is approximately five times the level of the parallel plate problem of Chapter VI with a 2 cm spacing.

To obtain the time-domain upper bound for the vacuum filled line we note that the factor $\omega/(1 - e^{-\sigma T})$ of equation (66) must simply be replaced by

$$\sum_{j=1}^{m} \frac{|s_j||f_j|}{1 - e^{-2\eta_j \tau}}$$

to obtain equation (108). In (108), the loss has been neglected in comparison to the decay of the short circuit fields as specified by η_j for each mode. Using the data of Kajfez in equation (120), the time domain bound becomes

$$|\Delta V|_{max} \leq 10.98V. \tag{138}$$

The second problem of interest is shown in Figure 25 with wire 2 close to wire 1 and much smaller with both radii much less than d. This problem models a wire at the surface of a wire bundle with an aperture centered below. If one assumes that the only change from the previous problem is in the cross-sectional geometry, only the new λ_i, $|e_y>$, and $|h_x>$ are needed for equation (66) to be used. Fundamental to these quantities is the determination of $\underline{P}$ in (121).

To determine $\underline{P}$, a charge set of $Q_1 = 0$ and $Q_2 = 1$ is first considered. Due to the proximity of the wires, the model of Figure 26 is

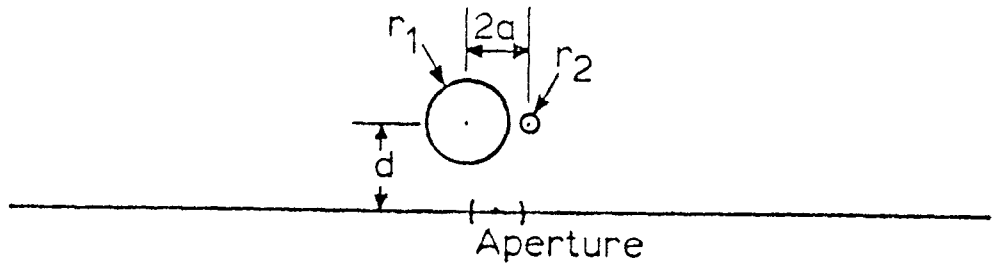

Figure 25. Cross-section of thick and thin wires behind an aperture.

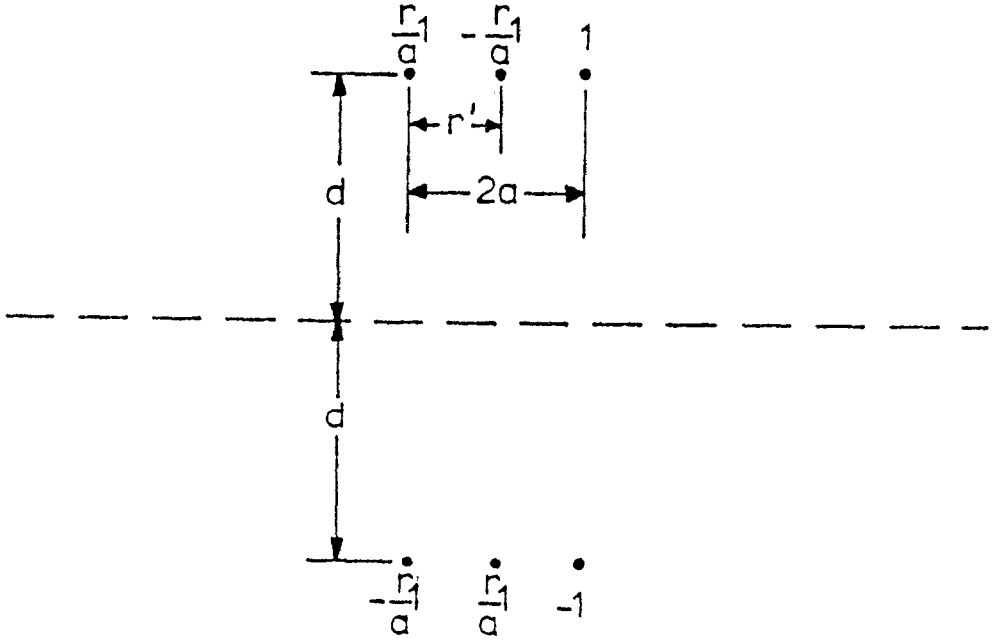

Figure 26. Image charge equivalent for only small wire charged.

required with the center charges representing the cylindrical images of Q_2 in wire 1 and the left charges balancing the center charges to give $Q_1 = 0$. Computing the resulting voltages V_1 and V_2 between the wires and the ground plane, the corresponding forms of P_{12} and P_{22} are obtained as

$$P_{12} = \frac{r_1}{4\pi\varepsilon_o a}\left[\ln\left|\frac{2d - r_1}{r_1}\right| + \frac{1}{2}\ln\left(\frac{r_1^2 + r'^2}{(2d - r_1)^2 + r'^2}\right)\right]$$

$$+ \frac{1}{4\pi\varepsilon_o}\ln\left(\frac{(2d - r_1)^2 + 4a^2}{r_1^2 + 4a^2}\right)$$

and

$$P_{22} = \frac{r_1}{8\pi\varepsilon_o a}\left[\ln\left(\frac{(2d - r_2)^2 + 4a^2}{r_2^2 + 4a^2}\right) + \ln\left(\frac{r_2^2 + (2a - r')^2}{(2d - r_2)^2 + (2a - r')^2}\right)\right]$$

$$+ \frac{1}{2\pi\varepsilon_o}\ln\left|\frac{2d - r_2}{r_2}\right|$$

where r_1 and r_2 are the radii of wires 1 and 2 and $r' = r_1^2/2a$ is the location of the image charge.

For P_{21} and P_{22}, no image is needed in wire 1 and the line charges are simply $Q_1 = 1$ and $Q_2 = 0$ to give

$$P_{11} = \frac{1}{2\pi\varepsilon_o}\ln\left|\frac{2d - r_1}{r_1}\right|$$

and

$$P_{21} = \frac{1}{4\pi\varepsilon_o}\ln\left[\frac{(2d - r_2)^2 + 4a^2}{r_2^2 + 4a^2}\right].$$

Dimensions are chosen similar to the previous problem as d = 1cm, r_1 = 0.5cm, r_2 = 0.1cm, and a = 0.35cm. The image position r' is given by 0.3571cm. The resulting matrices $\underline{P}$ and $\underline{L}^{-1}$ are given by

$$\underline{P} = \frac{1}{2\pi\varepsilon_o}\begin{bmatrix} 1.0986 & 0.7821 \\ 1.0521 & 3.3940 \end{bmatrix}$$

and

$$\underline{L}^{-1} = \frac{2\pi}{\mu_o}\begin{bmatrix} 1.1680 & -0.2692 \\ -0.3621 & 0.3781 \end{bmatrix}.$$

The required eigenvalues and eigenvectors of $\underline{L}^{-1}$ are given by

$$\lambda_1 = \frac{1.6939}{\mu_o}, \quad \lambda_2 = \frac{8.0205}{\mu_o}$$

and

$$|b_1\rangle = \begin{bmatrix} 0.2870 \\ 0.9579 \end{bmatrix}, \quad |b_2\rangle \begin{bmatrix} -0.9275 \\ 0.3738 \end{bmatrix}$$

where $|b_1\rangle$ represents the bulk mode.

The aperture is located half way between the centers of the wires as shown in Figure 25. The aperture electric field for each mode is needed for $|e_y\rangle$ and $|h_x\rangle$. For mode 1, the charge vector is

$$|Q\rangle = \underline{P}^{-1}\,|b_1\rangle = 2\pi\varepsilon_o \begin{bmatrix} 0.0773 \\ 0.2583 \end{bmatrix}.$$

To compute E_y at the aperture, Q_2 must be modeled by three charges above the ground plane as was done in the evaluation of P_{12} and P_{22}. With this in mind the general formula for E_y is

$$E_y = \frac{-1}{\pi\varepsilon_o}\left[(Q_1 + Q_2 + \frac{r_1 Q_2}{2a})\frac{d}{a^2 + d^2} - Q_2 \frac{r_1}{2a}\frac{d}{[d^2 + (a - r_1^2/2a)^2]}\right]$$

to give

$$E_{y1} = -55.78 \text{ V.}$$

Similarly for mode 2,

$$|Q> = 2\pi\varepsilon_o \begin{bmatrix} -1.1839 \\ 0.4772 \end{bmatrix}$$

and

$$E_{y2} = 133.35 \text{ V.}$$

From equation (128), $|e_y>$ becomes with the (λ_i/c^2) scale

$$|e_y> = \begin{bmatrix} -1176.8 \\ 1292.9 \end{bmatrix}.$$

Substituting into (66), the upper bound becomes

$$|\Delta V|_{max} \leq 0.8025\ \omega\varepsilon_o[2|\eta_o H_x^{sc-}| + |E_y^{sc-}|].$$

For the incident form of Kajfez, this bound is

$$|\Delta V|_{max} \leq \omega(2.41 \times 10^{-6}) \text{ V.}$$

In the time domain this bound becomes

$$|\Delta V|_{max} \leq 23.84 \text{ V.}$$

The substantial increase in these bounds compared to the parallel plate

problem is seen as a primary result of the five-fold increase in the L_2 norm of $|e_y>$. This is a consequence of the closeness of the wires and aperture and the stronger interaction.

The last problem is depicted in Figure 27. The wire has been placed at the center of the structure and has a radius equal to b/100. The wire is labeled as conductor 1 with the upper plane as conductor 2. If $Q_1 = 0$ and $Q_2 = 1$, the wire may be neglected in computing P_{12} and P_{22} to obtain

$$P_{12} = \frac{d - a}{\varepsilon_o L}$$

and

$$P_{22} = \frac{b}{\varepsilon_o L} \quad .$$

The computation of P_{11} and P_{21} is more complicated since the images of the wire in the surfaces must be included. The values P_{11} and P_{21} may be obtained by subtracting $-\frac{d}{b}$ times P_{12} or P_{22} from the potentials for a wire between two grounded planes. This removes the effect of charge on conductor 2. For the grounded planes case with the wire charge equal to 1 C/m, the potential between planes is zero and the wire potential is obtained from an infinite sum including the images. If only the lower image is used, the wire potential is approximated by $(4.595/2\pi\varepsilon_o)$. The additional images have a minor contribution changing this value to $(4.0466/2\pi\varepsilon_o)$. Combining these results for the geometry given with L = 10b, one obtains

$$\underline{P} = \frac{1}{\varepsilon_o} \begin{bmatrix} 0.6854 & 0.05 \\ 0.05 & 0.1 \end{bmatrix}$$

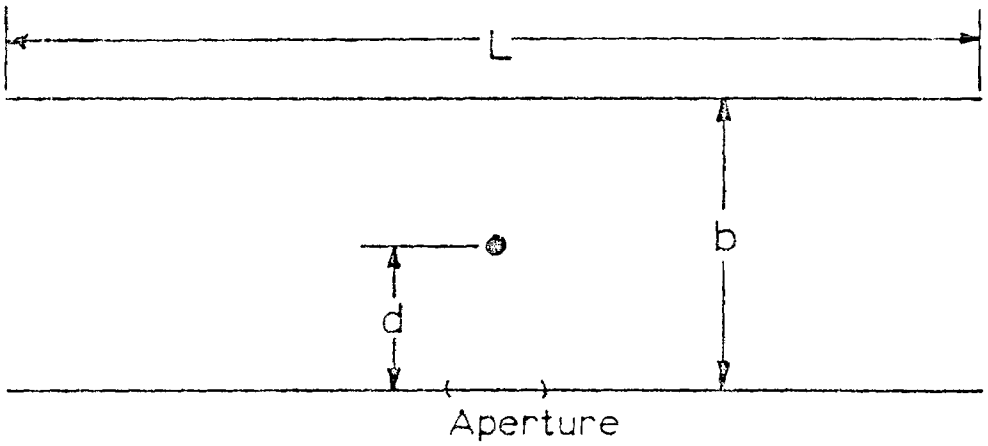

Figure 27. Cross-section of wire between parallel conductors.

and

$$\underline{L}^{-1} = \frac{1}{\mu_o}\begin{bmatrix} 1.5142 & -0.757 \\ -0.757 & 10.378 \end{bmatrix}$$

The corresponding eigenvalues and eigenvectors are

$$\lambda_1 = \frac{1.45}{\mu_o} \quad , \quad \lambda_2 = \frac{10.44}{\mu_o}$$

and

$$|b_1\rangle = \begin{bmatrix} 0.9963 \\ 0.0845 \end{bmatrix} \quad , \quad |b_2\rangle = \begin{bmatrix} -.0845 \\ 0.9964 \end{bmatrix} .$$

The aperture is located directly below the wire for maximum coupling and d is set equal to 1cm. The image summation for E_y can be computed exactly for this problem to give the electric field at the aperture as

$$E_y = Q_1\left[\frac{1}{2L\varepsilon_o} - \frac{1}{4d\varepsilon_o}\right] - \frac{Q_2}{L\varepsilon_o} \quad .$$

Using the $|b_i\rangle$ as charge distributions, the primed fields of (128) are obtained as

$$E_{y_1}' = -22.84/\varepsilon_o$$

and

$$E_{y_2}' = -3.08/\varepsilon_o$$

which give an $|e_y\rangle$ of

$$|e_y\rangle = \begin{bmatrix} -755.2 \\ -273.3 \end{bmatrix} .$$

Since $|e_y>$, $|h_x>$, and λ_i are the only parts of (66) to be modified from the last problem, the upper bound is obtained as

$$|\Delta V|_{max} \leq \omega(1.197 \times 10^{-6}) \quad V$$

with an equivalent time domain bound of

$$|\Delta V|_{max} \leq 11.84 \quad V.$$

The primary observation of interest which seems to link these three problems is that for similar dimensional relationships, the bound takes on the same order of magnitude. This would suggest the applicability of canonical problems as bounds for more complex problems.

CHAPTER VIII
CONCLUSIONS

This report developed a computational technique for upper bounds on signal levels at terminations of multiconductor transmission lines (MTL) located behind an aperture-perforated conducting screen. This was accomplished in several stages. First, the electromagnetic coupling through small aperture was described using the concept of aperture polarizabilities. The idea of coupling was then extended to the MTL excitation behind an aperture where the aperture was represented by the equivalent current dipole moments. A source of traveling waves was introduced to replace the aperture and the aperture coupled energy. These traveling waves transferred the energy from the aperture region to the terminations. The amount of transferred energy in terms of the traveling waves was found by introducing a signal flow graph of the whole system. It was assumed that the aperture had no other significant interactions with the MTL as might be described by additional reflections in the aperture region.

Having computed the amount of energy at the terminations, a transformation was used to represent the traveling waves in terms of the voltages and currents. The mathematical properties of vector norms and their associated matrix norms were discussed. The idea of two-norm was used to formulate upper bounds on the voltages and currents at the terminations. At this stage, it was assumed that the terminals were passive and the losses associated with each mode traveling on the MTL were of exponential form. Although the radiation and termination losses

were not explicitly taken into account, it was mentioned that these losses, if non-negligible, could be considered by modifying the term due to propagation loss. Further, after some mathematical manipulations, it was found that the bounds depend primarily on the source and termination local geometries. Finally, considering the fact that the maximum voltage between any two lines might be the sum of the individual voltages to ground, an additional factor of two was incorporated in the upper bound. The upper bound on the termination voltages was formulated in the frequency domain. An upperbound on the currents in frequency domain was simply obtained from this voltage bound.

This idea was extended to the time domain where it was assumed that the waveforms launched from the sources were non-dispersive (quasi-TEM), thus reaching the terminations without any distortion. Several assumptions were made regarding the medium, the termination, and the modal propagation. It was assumed that the elements of the termination are all real and constant and the propagation constant of all the modes are equal to that in a vacuum. The multiple reflection phenomenon was taken into account and its formulation was simplified by using the pole expansion of the incident field characterized in the Singularity Expansion Method (SEM). Using vector and matrix norms, an upper bound for the voltage and the current was formulated. It was observed that the upperbounds basically depend on the geometry of the system, the properties of the external time-varying fields, and the shape of the aperture.

Having formulated the upperbounds on the signal levels in both time

and frequency domain, a comprehensive example was presented in order to elaborate the use of the technique. The parameters and the geometry were chosen exactly the same as a problem introduced by Kajfez [12] in order to facilitate the comparison of results. It was found that the maximum voltage in Kajfez's example for a moderate mismatched termination was found by a multiplicative factor of approximately ten. It was noted that for upperbound calculations under the worst possible conditions a factor of ten was in reasonable agreement with his results. The reason being that at several stages of computation various types of inequalities were used that doubled the exact value. Also, the velocity of all the modes were assumed to be the velocity of light in a vacuum which were greater than the actual velocity of the modes in their respective media, contributing to the increase of the voltage at the termination. In addition, a factor of two was used to account for the potential difference between any two wires and not just to ground. In the whole, it was observed that final results obtained by using the developed techniques were in good and reasonable agreement with Kajfez's results.

Several other problems were also approached directly by the techniques developed. Two bundles of wires over a ground plane were bound above by modeling them as two wires over a ground plane. A wire at the surface of a bundle of wires was modeled by separate thick and thin wires over a ground plane. A last example considered a wire between parallel plates. The problems all had comparable dimensions but interestingly had similar voltage bounds.

There are several suggestions for future research. It would be desirable to find signal levels on wires behind composite panels which couple the external field by a diffusion mechanism. Also of some importance is the problem of wires passing through an aperture corresponding to antennas or aircraft control cables. Another area of research would be large aperture problems such as conformed antennas or large windows.

Appendix (A)

POLARIZABILITY OF SMALL APERTURES

The diffracted field in the vicinity of an aperture depends on the excitation field and upon the shape and size of the aperture. The moments of the equivalent dipoles are related to the components of the known exciting field through special constants of proportionality called the aperture electric and magnetic polarizabilities.

Due to the importance of the use of dipole moments, a great deal of attention has been devoted to determination of the polarizabilities. Cohn in [A1] and [A2] has experimentally determined the constants for several shapes, while Van Bladel [A3], has computed by numerical methods the polarizabilities for a rectangle, diamond, cross, and a rounded-off rectangle. Table (A1) gives the electric and magnetic polarizabilities for a circle of radius (R), an ellipse of eccentricity (ε), and a narrow ellipse. The following remarks should be made concerning the table:

1) $\overline{\overline{\alpha_m}} = \alpha_{m,xx}\,\hat{x}\hat{x} + \alpha_{m,yy}\,\hat{y}\hat{y}$

2) $\varepsilon = \sqrt{1 - (W/e)^2}$

3) K and E are the complete elliptic integrals of the first and second kind, as in [A5].

By the study of the data given by De Meulenaere [A3], when an inaccuracy in the polarizabilities of 10% can be tolerated, one can use a normalization factor of [(aperture area)$^{3/2}$], and use elliptic polarizabilities in order to calculate the polarizabilities of the

rectangle and rounded-off rectangle.

The polarizabilities of other shapes may be obtained by either measurement or numerical solution of the quasi-static aperture problem.

Table (A1): Aperture Polarizabilities [13]

Shape	α_e	$\alpha_{m,\,xx}$	$\alpha_{m,\,yy}$
circle (Radius = R)	$\frac{2}{3} R^3$	$\frac{4}{3} R^3$	$\frac{4}{3} R^3$
Ellipse	$\frac{1}{3} \frac{(\pi)\ W^2\ \ell}{E(\epsilon)}$	$\frac{1}{3} \frac{(\pi)\ \ell^3\ \epsilon^2}{K(\epsilon) - E(\epsilon)}$	$\frac{1}{3} \frac{(\pi)\ \ell^3\ \epsilon^2}{\left[\frac{\ell}{W}\right]^2 E(\epsilon) - K(\epsilon)}$
Narrow Ellipse ($W<<\ell$)	$\frac{1}{3}\ (\pi)\ W^2\ \ell$	$\frac{1}{3} \frac{(\pi)\ \ell^3}{\ell n \left[\frac{4\ell}{W}\right] - 1}$	$\frac{1}{3}\ (\pi)\ W^2\ \ell$
2ℓ = major diameter of ellipse $2W$ = minor diameter of ellipse			

Appendix (B)

APERTURE REPRESENTATION BY A PAIR OF CURRENT DIPOLES

Consider Figure (B1) where an aperture-perforated screen is shown [B1]. In order to evaluate the scattered field in the interior region, one only needs to know about the tangential electric field $\vec{E}_t$ over the aperture. It is convenient to close the aperture with a metalic lid and place a magnetic surface current density $\vec{J}_S^{\,m}$ over it given by

$$\vec{J}_S^{\,m} = \vec{E}_t \times \vec{n} \tag{B1}$$

where $\vec{n}$ is the normal vector as shown in Figure (B2). The vector $\vec{E}_t$ is the total aperture field typically obtained by solution of a quasi-static integral equation [B2].

Now, one can invoke the reciprocity theorem to compute the scattered field at any point in the interior region due to surface magnetic current. For the purpose of this discussion, the reciprocity theorem as introduced in [B3] will be used. As shown in Figure (B3), the scattered field $\vec{E}(r')$ at a point $(\vec{r}')$ is to be computed with respect to the origin which is taken at the center of the closed aperture region. By introducing a unit magnitude electric dipole $\vec{P}$ at the point $(\vec{r}')$ [B1], as shown in Figure (B3), one can write the reciprocity theorem as

$$\vec{E}(r') \cdot \vec{a}_p = \int_V (\vec{J}_e \cdot \vec{E}_b - \vec{J}_m \cdot \vec{H}_b)\, dV \tag{B2}$$

where $\vec{P}$ is an electric current dipole given by

$$\vec{P} = \vec{a}_p\, \delta(\vec{r} - \vec{r}') \tag{B3}$$

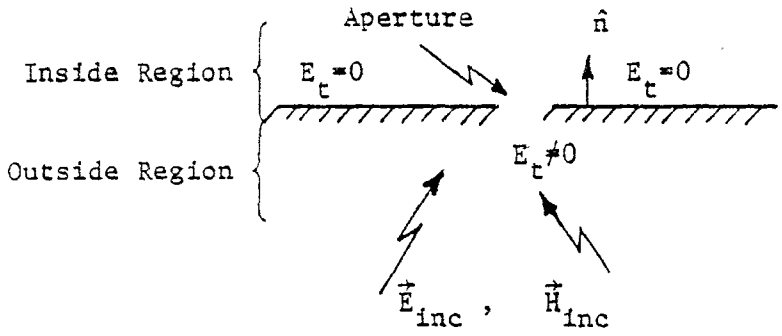

Figure (B1). Aperture-perforated screen [8].

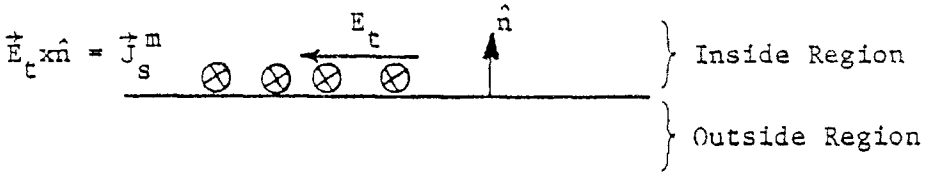

Figure (B2). Aperture replaced by $\vec{J}_s^m$ [8].

Figure (B3). Evaluation of scattered field [8].

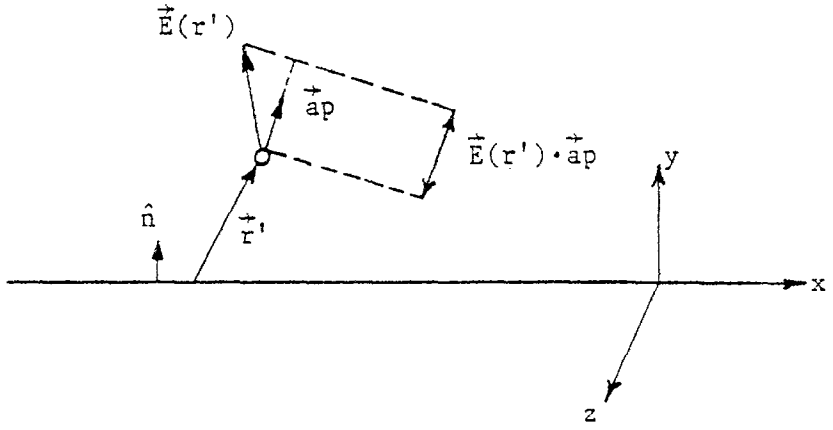

and $\vec{a}_p$ is a unit vector characterizing the orientation of the testing dipole $\vec{P}$. The vectors $\vec{E}_b$ and $\vec{H}_b$ are the fields produced by the source $\vec{P}$, evaluated at the surface of the closed aperture, and $\vec{J}_e$ and $\vec{J}_m$ are volume electric and magnetic current densities which are the sources of the field scattered by the aperture. In the case of this discussion, $\vec{J}_e$ is equal to zero and equation (B2) for the surface current $\vec{J}_S^{\,m}$ becomes

$$\vec{E}(r') \cdot \vec{a}_p = \int_S - (\vec{J}_S^{\,m} \cdot \vec{H}_b)\, dS. \qquad \text{(B4)}$$

From Maxwell's equations, one can write

$$\nabla \times \vec{H}_b = j\omega\varepsilon\, \vec{E}_b. \qquad \text{(B5)}$$

The vector H_b can be expanded in Taylor's series as

$$\vec{H}_b(\vec{r}) = \vec{H}_b(\vec{o}) + \vec{r} \cdot (\nabla\vec{H})\Big|_{\vec{o}} + \ldots \qquad \text{(B6)}$$

where the higher order terms are assumed to be negligible. One can write $\vec{r} \cdot (\nabla\vec{H})\big|_{\vec{o}}$ as

$$\vec{r} \cdot (\nabla\vec{H})\Big|_{\vec{o}} = (\nabla\vec{H})\Big|_{\vec{o}} \cdot \vec{r} - \vec{r} \times (\nabla \times \vec{H})\Big|_{\vec{o}}. \qquad \text{(B7)}$$

The term $(\nabla H)\big|_{\vec{o}} \cdot \vec{r}$ gives rise to a quadrupole which is neglected [B2]. Substituting equation (B5) in equation (B7), one may rewrite equation (B6) as

$$\vec{H}_b(\vec{r}) = \vec{H}_b(\vec{o}) - \vec{r} \times [j\omega\varepsilon\, \vec{E}_b(\vec{o})]. \qquad \text{(B8)}$$

If equation (B8) is substituted in equation (B4), one obtains

$$\vec{E}(r') \cdot \vec{a}_p = \int_S -[\vec{H}_b(\vec{o}) - j\omega\varepsilon\vec{r} \times \vec{E}_b(\vec{o})] \cdot \vec{J}_S^{\,m}\, dS \qquad \text{(B9)}$$

One may define $\vec{C}_e$ and $\vec{C}_m$ as electric and magnetic dipole current moments respectively by

$$\vec{C}_e = j\omega\varepsilon \int_S \vec{r} \times \vec{J}_S^{\,m}\, dS \tag{B10}$$

$$\vec{C}_m = \int_S \vec{J}_S^{\,m}\, dS \,. \tag{B11}$$

With these definitions, equation (B9) can be written as

$$\vec{E}(r') \cdot \vec{a}_p = - \vec{E}_b(\bar{o}) \cdot \vec{C}_e - \vec{H}_b(\bar{o}) \cdot \vec{C}_m \tag{B12}$$

By comparison of equations (B2) and (B12), one may write equivalent currents as

$$\vec{J}_m = \delta(y)\, \vec{J}_m^{\,S} = \vec{C}_m \delta(\bar{r}) \tag{B13}$$

$$\vec{J}_e = \delta(y)\, \vec{J}_e^{\,S} = \vec{C}_e \delta(\bar{r}) \tag{B14}$$

where $\delta(\bar{r})$ is the three dimensional Dirac delta distribution. The equivalent dipole current moment representation of an aperture is shown in Figure (B4).

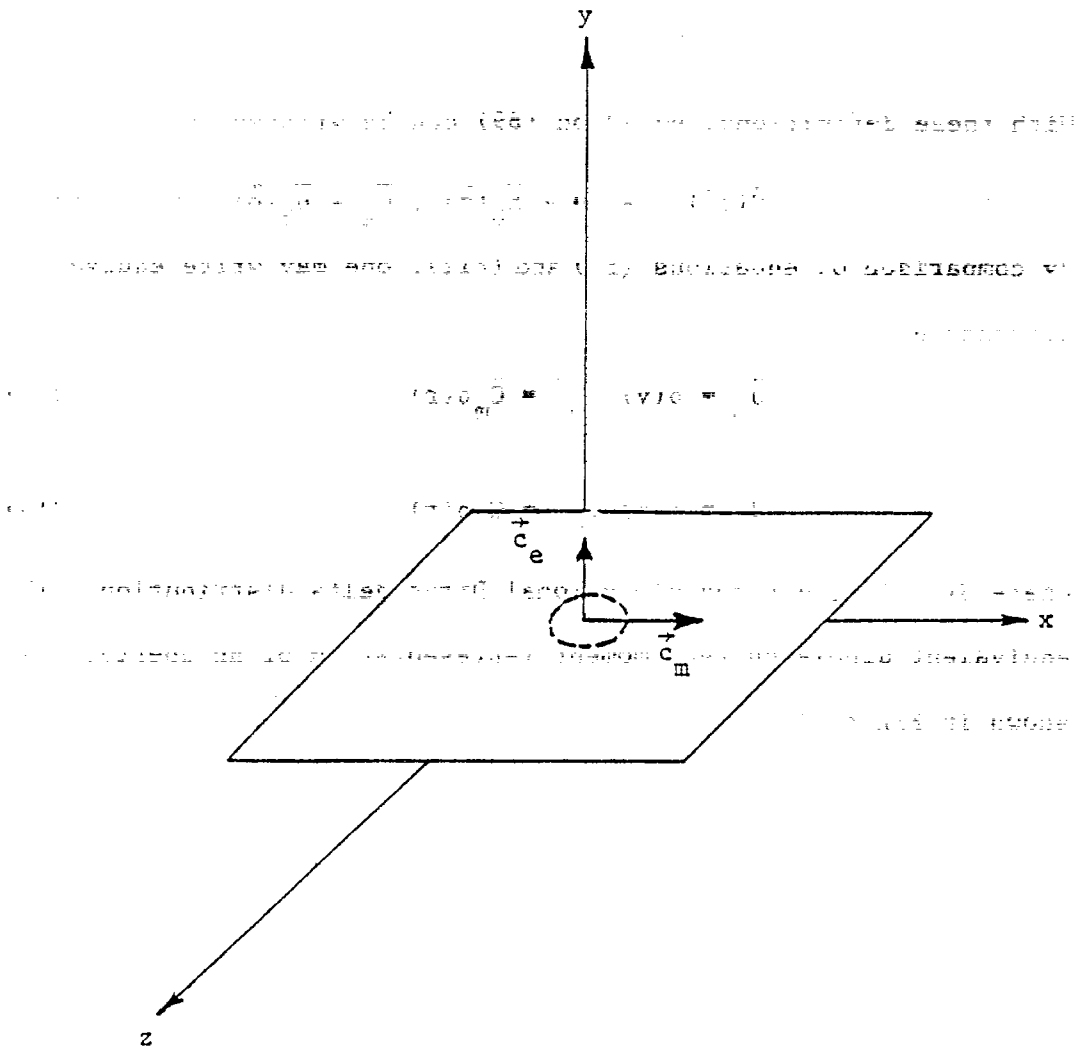

Figure (B4). $\vec{J}_s^m$ replaced by a pair of current dipoles.

Appendix (C)

DIRAC'S NOTATION OF MATRICES

The following material is an introduction to matrix algebra using Dirac's Notation which was introduced in Quantum theory by P.A.M. Dirac. The presented material is a summary of B. Friedman [C1], S. Gasiorowicz [C2], and A. Messiah [C3].

In Dirac's Notation, an N-dimensional column vector is denoted by

$$|x\rangle = \begin{bmatrix} x_1 \\ x_2 \\ x_3 \\ \vdots \\ x_N \end{bmatrix}$$

When matrix $\underline{A}$, an $N \times N$ matrix operates on vector $|x\rangle$, the resulting operation is another column vector $|V\rangle$. By elementary properties of matrix multiplication, the kth element of the vector $|V\rangle$ is computed as

$$V_k = \sum_{j=1}^{N} A_{kj} x_j \tag{C1}$$

The complex conjugate transpose of a column vector $|x\rangle$ is a row vector denoted by $\langle x|$ whose elements are the complex conjugate elements of $|x\rangle$ ordered as

$$\langle x| = (x_1^* \quad x_2^* \ldots x_N^*) \tag{C2}$$

where (*) means complex conjugate.

The (†) notation is used for complex conjugate transpose of $\underline{A}$ given by

$$\underline{A}^{\dagger} = \begin{bmatrix} a_{11}^{*} & \cdots & a_{N1}^{*} \\ a_{12}^{*} & \cdots & a_{N2}^{*} \\ \vdots & & \vdots \\ a_{1N}^{*} & \cdots & a_{NN}^{*} \end{bmatrix}$$

Using matrix properties for conjugation and multiplication the following product is obtained:

$$< M | = (\underline{A}\,\underline{B}\,|x>)^{\dagger} = < x | \underline{B}^{\dagger}\underline{A}^{\dagger} \qquad (C3)$$

where $<M|$ is a N×1 row vector and $\underline{B}^{\dagger}$ and $\underline{A}^{\dagger}$ are both N×N matrices.

One of the most important types of matrices is the Hermitian matrix which is equal to its own complex conjugate transpose, i.e.,

$$\underline{A}^{\dagger} = \underline{A}$$

A Hermitian matrix has the following properties:

1) Instead of (N^2) distinct elements, it only has $\frac{1}{2}N(N+1)$ distinct elements.
2) The elements on the main diagonal are real.
3) The elements which are located symmetrically across the main diagonal are complex conjugate of each other.

Multiplication of a row vector with a compatible column vector results in a complex number as

$$< x \mid y> = (x_1^* \quad x_2^* \ldots x_N^*) \begin{bmatrix} y_1 \\ y_2 \\ \vdots \\ y_N \end{bmatrix} = \sum_{j=1}^{N} x_j^* y_j \qquad \text{(C4)}$$

It may be observed that $< x|y > = < y|x >^*$. If $< V| = < x|\underline{A}^\dagger$, then $< V|y > = < x|\underline{A}^\dagger|y>$, and the result of such an operation is scalar.

Sometimes it may happen that the order of multiplication in (C4) is interchanged, then the result is a N×N square matrix

$$|y>< x| = \begin{bmatrix} y_1 \\ y_2 \\ \vdots \\ y_N \end{bmatrix} (x_1^* \quad x_2^* \quad x_3^* \ldots x_N^*). \qquad \text{(C5)}$$

One of the benefits of representing matrices in Dirac's Notation is that by observing the position of symbols, one can readily determine the format of the resulting operation. For example, assuming that β is a scalar, $|x >$ and $|y >$ are vectors, and $\underline{A}$ is a square matrix, then $< x|\underline{A}|y >$ and $\beta < y|x >$ are scalars, $\underline{A}|x >$ is a vector, and $|x >< y|$ is a square matrix.

Appendix (D)

MULTICONDUCTOR-LINE FORMULATION

The computation of voltages and currents on a multiconductor transmission line (MTL) in terms of eigenvectors have been analyzed by Amemiya [D1] and Marx [D2]. This approach has been used for both transient and steady-state waveforms. D. Kajfez [D3] has extended the eigenvector treatment by using a simultaneous diagonalization of two matrices. This section presents the main ideas of method of diagonalization by using only one composite matrix instead of two separate matrices.

Consider the N-conductor transmission line with a conducting ground plane as shown in Figure (D1). The reference direction has been chosen such that real, positive values of V_i and I_i represent power flow in the positive z direction.

References [D1], [D2], and [D4] derive the following two formulas for a lossless MTL in sinusoidal steady-state analysis with isotropic, nonmagnetic dielectrics:

$$\frac{d}{dz}\,|V> = -j\omega\underline{L}|\,I> \qquad \text{(D1)}$$

$$\frac{d}{dz}\,|I> = -j\omega\underline{K}|\,V> \qquad \text{(D2)}$$

The matrix $\underline{L}$ is called the induction matrix and the matrix $\underline{K}$ is the induction coefficient matrix.

There are two types of propagation on these lines. If the

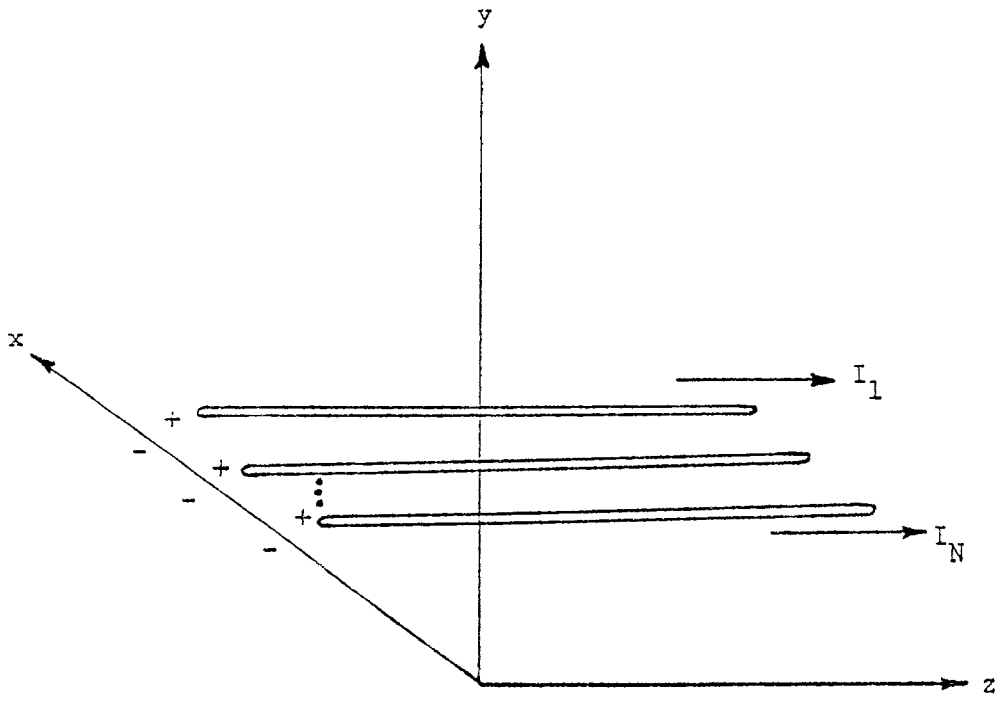

Figure (D1). Voltage and currents on a MTL with a ground plane in the (x-z) plane.

dielectric is homogeneous, transverse electromagnetic (TEM) modes propagate. If the dielectric is inhomogeneous, hybrid electromagnetic (HEM) modes propagate [D5]. In HEM mode both the electric and magnetic vectors have a longitudinal component. At low frequencies, the longitudinal component is small and may be neglected, giving rise to quasi-TEM modes.

Using the analysis presented by Friedman [D6], the first step is to decouple equations (D1) and (D2) by taking derivatives of both sides and substituting in the same equations to obtain

$$\frac{d^2}{dz^2} |V> = -\omega^2 \underline{L}\,\underline{K} |V> \tag{D3}$$

$$\frac{d^2}{dz^2} |I> = -\omega^2 \underline{K}\,\underline{L} |I>. \tag{D4}$$

As $\underline{L}$ and $\underline{K}$ represent stored energy of a passive network, they are both positive definite and thus qualify for the method of Friedman [D6]. This method of solution for $|V>$ and $|I>$ consists first of obtaining a set of orthonormal eigenvectors $|\zeta_i>$ and corresponding eigenvalues $(-\beta_i^2)$ for the matrix $\underline{B} = -\omega^2 \underline{L}\,\underline{K}$. Since $\underline{L}$ and $\underline{K}$ are positive definite, $\underline{L}\,\underline{K}$ is also positive definite and the β_i^2's are all positive. The eigenvalue problem is given by

$$-\omega^2 \underline{L}\,\underline{K} |\zeta_i> = -\beta_i^2 |\zeta_i>. \tag{D5}$$

The eigenvalues may be obtained from

$$\det[-\omega^2 \underline{L}\,\underline{K} + \beta_i^2 \underline{I}] = 0 \tag{D6}$$

where

$$\langle \zeta_i | \zeta_j \rangle = \delta_{ij} \tag{D7}$$

and δ_{ij} is the Kroneker delta.

One may now form a square matrix $\underline{G}$ whose columns are the $|\zeta_i\rangle$

$$\underline{G} = [\, |\zeta_1\rangle, |\zeta_2\rangle, \ldots, |\zeta_N\rangle] \tag{D8}$$

This matrix may be used to diagonalize $\underline{B}$ as

$$\underline{\Lambda} \equiv \underline{G}^{\dagger}\, \underline{B}\, \underline{G} = \mathrm{Diag}[-\beta_1^2, \ldots, -\beta_N^2] \tag{D9}$$

where

$$\underline{G}\,\underline{G}^{\dagger} = \underline{I}. \tag{D10}$$

The matrix $\underline{G}$ is an orthogonal real matrix, $(\dagger)$ denotes the transpose of the matrix, and $\underline{I}$ is the identity matrix.

The corresponding eigenvalue problem of the decomposed matrix $\underline{\Lambda}$ becomes

$$\frac{d^2}{dz^2} |Y\rangle = \underline{\Lambda}\, |Y\rangle \tag{D11}$$

where

$$|Y\rangle = \underline{G}^{\dagger} |V\rangle \tag{D12}$$

Because of the fact that $\underline{\Lambda}$ is real and diagonal, equation (D11) can be decomposed into a second order differential equation for each mode as

$$\frac{d^2}{dz^2} y_i = -\beta_i^2\, y_i \tag{D13}$$

The solution is of the exponential form

$$y_i = y_i^+ \, e^{-j\beta_i z} + y_i^- \, e^{+j\beta_i z} \tag{D14}$$

where $\beta_i = \frac{\omega}{v_i}$, and v_i is the velocity of the ith mode. This velocity relation can be shown by the usual method of multiplying (D14) with $e^{+j\omega t}$ and then taking the real part in order to obtain the rate of change of the phase. In equation (D14), y_i^+ and y_i^- refer to the amplitudes of positive and negative travelling waves in the z direction.

$|Y>$ can now be written as (D15)

$$|Y> = \sum_{i=1}^{N} y_i |u_i> \tag{D15}$$

where $|u_i>$ denotes a column vector having all zero elements except for the ith element which is unity.

Equation (D12) can now be used to find $|V>$ as

$$|V> = \sum_{i=1}^{N} y_i |\zeta_i> \tag{D16}$$

Similarly, $|I>$ can be obtained from equations (D1) and (D16) as

$$|I> = \sum_{i=1}^{N} \left(\frac{-1}{j\omega} \right) \left(\frac{dy_i}{dz} \right) \underline{L}^{-1} |\zeta_i> \tag{D17}$$

The above equation can also be written as

$$|I> = \sum_{i=1}^{N} \left(\frac{\beta_i}{\omega} \right) [y_i^+ \, e^{-j\beta_i z} - y_i^- \, e^{+j\beta_i z}] \underline{L}^{-1} |\zeta_i> \tag{D18}$$

From these expressions for voltage and current, the total power carried on a MTL is the average real power defined by

$$P = \tfrac{1}{2}\,\mathrm{Re} < V|I > \tag{D19}$$

Substituting equations (D18) and (D16) into (D19), P becomes

$$P = \tfrac{1}{2}\,\mathrm{Re}\left\{ \sum_{i,j=1}^{N} \left(\frac{\beta_i}{\omega}\right) y_i^{*} y_j < \zeta_i|\underline{L}^{-1}|\zeta_j > \right\}, \tag{D20}$$

where (*) denotes the complex conjugate. If y_i^- is equal to zero then the power travelling in positive z direction is

$$P^{+} = \tfrac{1}{2}\,\mathrm{Re}\left\{ \sum_{i,j=1}^{N} \left(\frac{\beta_j}{\omega}\right) y_i^{*+} y_j^{+} < \zeta_i|\underline{L}^{-1}|\zeta_j > \right\} \tag{D21}$$

It is useful to relate the positive traveling power (P^+) to a power wave (a_i) such that

$$P^{+} = \tfrac{1}{2} \sum_{j=1}^{N} |a_i|^2 \tag{D22}$$

assuming that the travelling modes are orthogonal. In this case, a_i is given by

$$a_i = \frac{y_i^{+}}{\sqrt{v_i}} \sqrt{<\zeta_i|\lambda_i|\zeta_i>} \tag{D23}$$

where the λ_i's are the eigenvalues of the matrix $\underline{L}^{-1}$. Generalizing, the total power can be written as

$$P = \tfrac{1}{2} \sum_{i=1}^{N} [\, |a_i|^2 + |b_i|^2 \,] \tag{D24}$$

where the b_i's are defined by

$$b_i = \frac{y_i^-}{v_i} \sqrt{\langle \zeta_i | \lambda_i | \zeta_i \rangle} \tag{D25}$$

The voltage vector $|V\rangle$ may be written in terms of the voltage eigenvectors $|\phi_i\rangle$, normalized to unity power as

$$|V\rangle = \sum_{i=1}^{N} (a_i e^{-j\beta_i z} + b_i e^{j\beta_i z}) |\phi_i\rangle \tag{D26}$$

where

$$|\phi_i\rangle = \frac{\sqrt{v_i}}{\sqrt{\langle \zeta_i | \lambda_i | \zeta_i \rangle}} |\zeta_i\rangle \tag{D27}$$

Similarly, $|\psi_i\rangle$ is the corresponding normalized current eigenvector giving rise to

$$|I\rangle = \sum_{i=1}^{N} (a_i e^{-j\beta_i z} - b_i e^{+j\beta_i z}) |\psi_i\rangle \tag{D28}$$

where

$$|\psi_i\rangle = \frac{1}{v_i} \underline{L}^{-1} |\phi_i\rangle . \tag{D29}$$

It can be easily shown that

$$\langle \phi_i | \psi_j \rangle = \delta_{ij} \tag{D30}$$

In order to transform from the power wave formulation back to the desired voltages and currents, one defines two matrices whose columns are the voltage and current eigenvectors given by

$$\underline{M}_V = (|\phi_1\rangle, \ldots, |\phi_N\rangle) \tag{D31}$$

$$\underline{M}_I = (|\psi_1\rangle, \ldots, |\psi_N\rangle) \tag{D32}$$

From equation (D30), it is easily shown that

$$\underline{M}_I \, \underline{M}_V^{\dagger} = \underline{I} \tag{D33}$$

and

$$\underline{M}_V \, \underline{M}_I^{\dagger} = \underline{I} \, . \tag{D34}$$

In the bounding process of Chapter IV, an inhomogeneous medium would be replaced by a homogeneous medium with a dielectric constant less than or equal to the minimum dielectric constant of the inhomogeneous medium. This typically leads to the use of a vacuum model with the $(\beta_i^2 = \frac{\omega^2}{v_i^2})$ replaced by $(\beta^2 = \frac{\omega^2}{c^2})$, where c is the speed of light in vacuum. In this instance, equation (D13) becomes

$$\frac{d^2}{dz^2} y_i = -\beta^2 y_i \tag{D35}$$

The corresponding $|\zeta_i\rangle$ and $|\phi_i\rangle$ would also change to account for the homogeneity.

APPENDIX (E)

TRAVELING WAVE FORMULATION

The voltages and currents on a MTL as described in Appendix (D) are

$$|V(z)\rangle = \sum_{i=1}^{N} \left(a_i \, e^{-j\beta_i z} + b_i \, e^{+j\beta_i z} \right) |\phi_i\rangle \tag{E1}$$

$$|I(z)\rangle = \sum_{i=1}^{N} \left(a_i \, e^{-j\beta_i z} - b_i \, e^{+j\beta_i z} \right) |\psi_i\rangle \tag{E2}$$

where $|\phi_i\rangle$ and $|\psi_i\rangle$ are normalized voltage and current eigenvectors, a_i and b_i represent the amplitudes of the ith mode waves traveling in the positive and negative (z) directions respectively, and (β_i) is the propogation constant of the ith mode.

Using $\underline{M}_V$ and $\underline{M}_I$ matrices as introduced in Appendix (D), equations (E1) and (E2) can be written in more compact form as

$$|V(z)\rangle = \underline{M}_V \left[\underline{F}^*(z) |a\rangle + \underline{F}(z) |b\rangle \right] \tag{E3}$$

$$|I(z)\rangle = \underline{M}_I \left[\underline{F}^*(z) |a\rangle - \underline{F}(z) |b\rangle \right] \tag{E4}$$

where

$$\underline{F}(z) = \text{diag} \left(e^{j\beta_1 z}, \ldots, e^{j\beta_N z} \right) \tag{E5}$$

Equations (E3) and (E4) can be written as

$$\underline{F}^*(z) |a\rangle = \frac{1}{2} \left[\underline{M}_I^{\dagger} |V(z)\rangle + \underline{M}_V^{\dagger} |I(z)\rangle \right] \tag{E6}$$

$$\underline{F}(z) |b\rangle = \frac{1}{2} \left[\underline{M}_I^{\dagger} |V(z)\rangle - \underline{M}_V^{\dagger} |I(z)\rangle \right] \tag{E7}$$

In the above formulas, (a_i) is the complex amplitude of ith mode such that the power contained in the positive (z) direction is

$$P_i^+ = \frac{1}{2} |a_i|^2 \tag{E8}$$

Hence, the entire power transmitted along the positive (z) direction is

$$P_{Total}^+ = \frac{1}{2} \langle a|a\rangle \tag{E9}$$

Similarly, the total power contained in the negative (z) direction is

$$P_{Total}^- = \frac{1}{2} \langle b|b\rangle \tag{E10}$$

where it is assumed that there is no transfer of power among different modes.

It is convenient to introduce a composite MTL, as shown in Figure (E1), with $\underline{Z}_4$ and $\underline{Z}_3$ impedance matrices respectively located at $z = \ell_4$ and $z = -\ell_3$ with respect to the origin where the source is coupled to the MTL [E1]. The amplitudes of the ith mode introduced by the source are a_{si} and b_{si}. The total amplitude a_i of the ith mode consists of a_{si} due to the source and the reflected b_{si} coming from the left hand termination at $z = -\ell_3$. From equations (E6) and (E7) the following relations can be obtained:

$$|a(\ell_4)\rangle = \frac{1}{2} \left[\underline{M}_I^+ |V(\ell_4)\rangle + \underline{M}_V^+ |I(\ell_4)\rangle\right] \tag{E11}$$

$$|b(\ell_4)\rangle = \frac{1}{2} \left[\underline{M}_I^+ |V(\ell_4)\rangle - \underline{M}_V^+ |I(\ell_4)\rangle\right] \tag{E12}$$

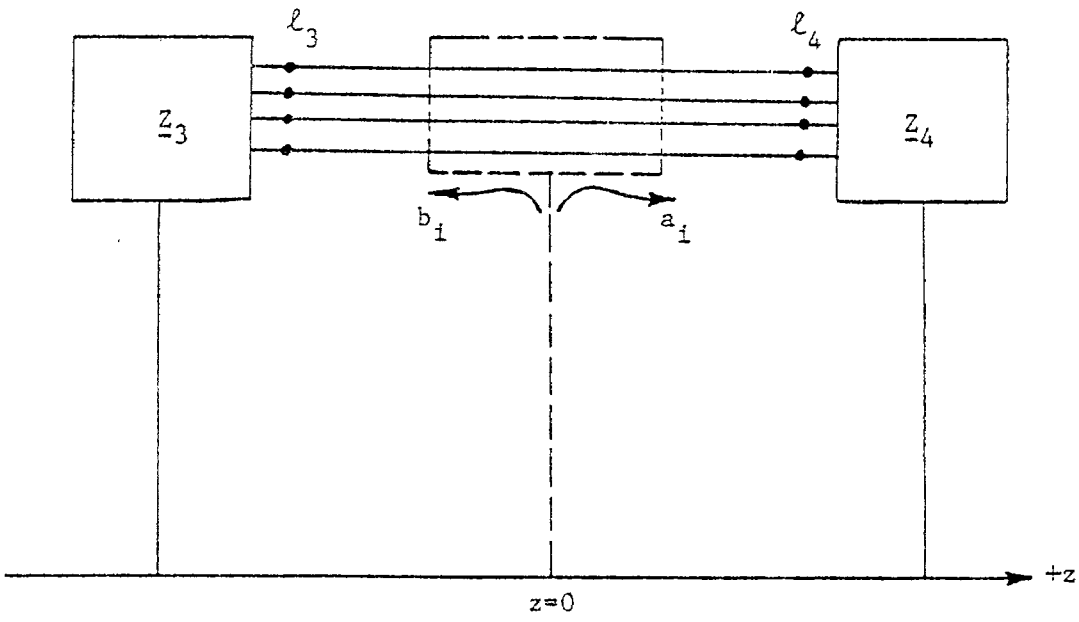

Figure (E1). Terminated MTL with a source located at z=0 [E1].

By Ohm's law, one obtains

$$|V(\ell_4)> = \underline{Z}_4 |I(\ell_4)> \tag{E13}$$

Combining equations (E11), (E12), and (E13), one obtains

$$|b(\ell_4)> = \underline{\Gamma}_4 |a(\ell_4)> \tag{E14}$$

where $\underline{\Gamma}_4$ is called the reflection matrix given by

$$\underline{\Gamma}_4 = \left(\underline{M}_I^{\dagger} \underline{Z}_4 \underline{M}_I - \underline{I}\right)\left(\underline{M}_I^{\dagger} \underline{Z}_4 \underline{M}_I + \underline{I}\right)^{-1} \tag{E15}$$

The matrix $\underline{\Gamma}_4$ may contain non-zero off-diagonal elements creating mode coupling. Similarly, at $z = -\ell_3$, one can obtain

$$|a(-\ell_3)> = \underline{\Gamma}_3 |b(-\ell_3)> \tag{E16}$$

where

$$\underline{\Gamma}_3 = \left(\underline{M}_I^{\dagger} \underline{Z}_3 \underline{M}_I - \underline{I}\right)\left(\underline{M}_I^{\dagger} \underline{Z}_3 \underline{M}_I + \underline{I}\right)^{-1} \tag{E17}$$

One can also look at the problem in time-domain assuming that the quasi-TEM waves are non-dispersive, and each mode is launched and transmitted without a distortion. Assuming that the starting amplitude at (z=0) is denoted by $a_{i0}(t)$, then at $z = \ell_4$ the amplitude becomes

$$a_{i4}(t) = a_{i0}\left(t - \frac{\ell_4}{v_i}\right) \tag{E18}$$

where v_i is the velocity of the ith mode. If the load network consists of passive elements such as capacitor and inductors, the shape of the reflected waves will be distorted as compared to the incident waves.

APPENDIX (F)

COUPLING COEFFICIENTS FOR TRANSVERSE ELECTROMAGNETIC (TEM) MODE EXCITED BY LOCALIZED CURRENT SOURCES

Figure (F1) represents an electric current source $\vec{J}$ located inside a parallel plate waveguide which produces outgoing waves that carry energy to ports Z_1 and Z_2. The total electric and magnetic fields traveling in the positive z direction have been derived by Collin [F1] as

$$\vec{E}^{+} = \sum_{n=1}^{\infty} c_n^{+} \, (\vec{e}_n + \vec{e}_{nz}) \, e^{-j\beta_n z} \tag{F1}$$

$$\vec{H}^{+} = \sum_{n=1}^{\infty} c_n^{+} \, (\vec{h}_n + \vec{h}_{nz}) \, e^{-j\beta_n z} \tag{F2}$$

where n stands for the nth outward propagating mode, c_n^{+} is the wave amplitude, and β_n is the nth mode propagation constant. The vectors $\vec{e}_n$ and $\vec{h}_n$ are normalized transverse electric and magnetic fields of the nth quasi-TEM mode and are real functions normalized to unit power as

$$\int_s (\vec{e}_m \times \vec{h}_n) \cdot d\vec{s} = \delta_{mn} \tag{F3}$$

where δ is the Kroneker delta and s is the cross section of the waveguide. Collin has used the reciprocity theorem for Figure (F1) and has obtained

$$c_n^{+} = \frac{-1}{2} \int_V (\vec{e}_n - \vec{e}_{nz}) \cdot \vec{J} \, e^{j\beta_n z} \, dV \tag{F4}$$

where the volume of integration encloses the current $\vec{J}$.

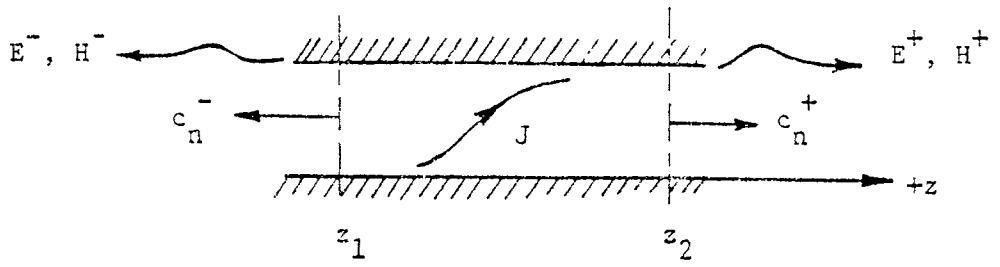

Figure (F1). A current source excitation of a waveguide [F1].

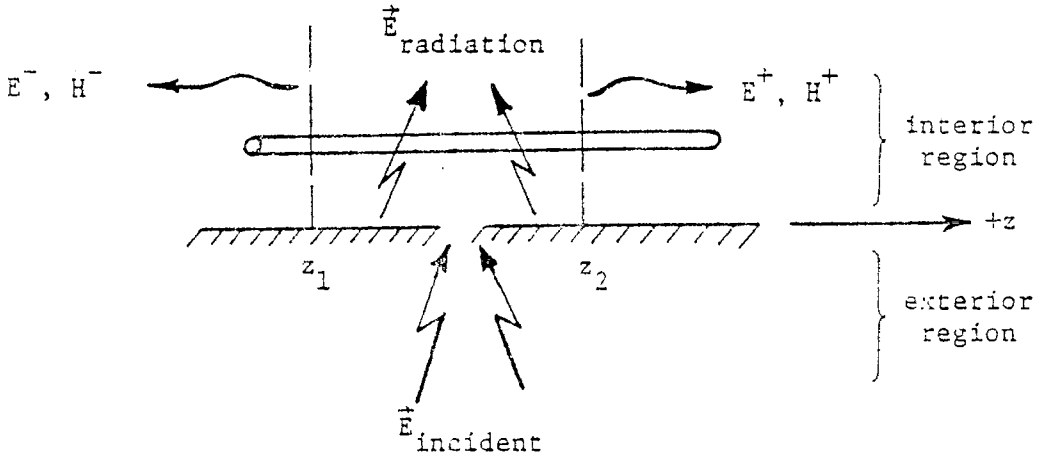

Figure (F2). Incident, radiated, and guided waves for the open region with aperture-perforated screen [F1].

The above method can be used in aperture problems where a wire is located behind a conducting screen as shown in Figures (F2). The incident field from exterior region produces both a radiation field and a guided transverse electromagnetic wave (TEM) in the interior region. The radiation field ($\vec{E}_{rad}$) radiates into a free space and the TEM wave propagates along the wire. In order to use the method of Collin, one must assume that the radiated field is negligible. Kajfez [F2] has attempted to justify this assumption in his coupling formulation [F2]. Davis [F3] has also compared the radiated and the transmitted TEM energy for such problems to justify the assumption that only TEM modes need to be considered.

Shown in Figure (F3) are the electric and magnetic dipoles above a closed aperture which replace the aperture. The discussion of the dipole equivalence in aperture problems is formulated in Appendix (B). The situation in Figure (F3) is entirely the same as Figure (F1) with the two dipoles $\vec{J}_s^m$ and $\vec{J}_s^e$ being the effective sources. Now, one can apply the reciprocity method of Collin to obtain

$$c_n^+ = \frac{1}{2} \int_{\text{Aperture}} \left(\vec{h}_n \cdot \vec{J}_s^m - \vec{e}_n \cdot \vec{J}_s^e \right) e^{j\beta_n z} \, ds \qquad \text{(F5)}$$

where the integration is over the surface of the aperture.

The computation is simplified if the source currents are assumed to take a Dirac delta distribution form of $\delta(x)$ and $\delta(z)$. For such a distribution equations (B11) and (B12) become

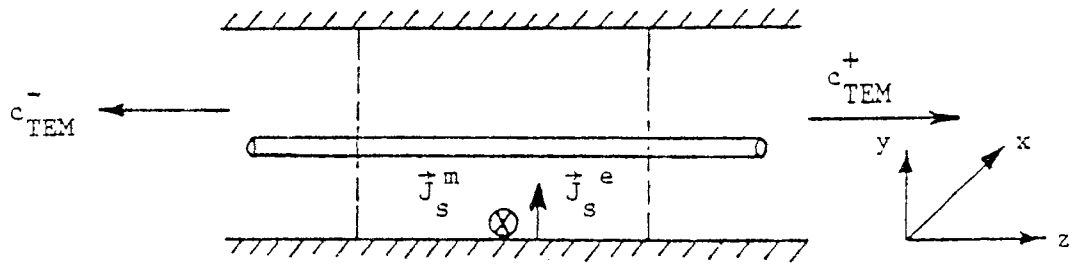

Figure (F3). Aperture representation by electric and magnetic dipoles [F1].

$$\vec{J}_s^{\,m} = \vec{c}_m \, \delta(x - x_0) \, \delta(z - z_o) \tag{F6}$$

$$\vec{J}_s^{\,e} = \vec{c}_e \, \delta(x - x_0) \, \delta(z - z_o) \tag{F7}$$

Substitution of equations (F6) and (F7) in (F5) gives

$$c_n^+ = \frac{1}{2} e^{+j\beta_n z_0} \left[h_{xn}(x_0, 0) \, c_{mx} - e_{yn}(x_0, 0) \, c_{ey} \right] \tag{F8}$$

Similarly, one can show that

$$c_n^- = \frac{1}{2} e^{-j\beta_n z_0} \left[-h_{xn}(x_0, 0) \, c_{mx} - e_{yn}(x_0, 0) \, c_{ey} \right] \tag{F9}$$

where the minus on $h_{xn}(x_0, 0)$ and in the exponent are due to the reference direction for propagation in the (-z) direction. Equations (F8) and (F9) completely define the source coupling to a wire behind an aperture.

REFERENCES

[1] C. M. Butler, Y. Rahmat-Samii, and R. Mittra, "Electromagnetic Penetration through Apertures in Conducting Surfaces," IEEE Trans. Ant. Prop. AP-26, 82-93, January, 1978.

[2] Lord Rayleigh, "On the passage of waves through apertures in plane screen," Philos. Mag., Vol. 43, No. 263, April, 1897.

[3] Lord Rayleigh, "On the incidence of aerial and electric waves on small obstacles in the form of ellipsoids or elliptic cylinders, on the passage of electric waves through a circular aperture in a conducting screen," Philosophical Magazine, Vol. 44, P. 28, 1897.

[4] H. A. Bethe, "Theory of diffraction by small holes," Phys. Rev. Vol. 66, PP. 163-182, 1944.

[5] C. J. Bouwkamp, "Diffraction Theory," Rep. Progr. Phys. Vol 17 - PP. 35-100, 1954.

[6] C. M. Butler, "Formulation of integral equations for an electrically small aperture in a conducting screen," Interaction Note 149, AFWL, Kirtland, NM, December 1973.

[7] C. M. Butler, K. R. Umashankar, "A numerical solution procedure for small aperture integral equations," Interaction Notes 212, AFWL, Kirtland, NM, Sept., 1974.

[8] D. Kajfez, "Excitation of a terminated TEM transmission line through a small aperture," AFWL Interaction Note 215, July 1974.

[9] C. M. Butler and K. R. Umashankar, "Electromagnetic excitation of a wire through an aperture-perforated conducting screen," IEEE Trans. Ant. Prop, AP-24, PP. 456-462, July, 1976.

[10] K. S. H. Lee and F. C. Yang, "A wire passing by a circular aperture in an infinite ground plane," AFWL Interaction Note 317, February 1977.

[11] W. A. Davis, "Bounding singal levels at wire terminations behind apertures," AFWL Interaction Note 384, February 1980.

[12] D. Kajfez, "Small aperture on a multiconductor transmission line filled with inhomogeneous dielectrics," AFWL Interaction Notes 347, November 1977.

[13] C. M. Butler, "A review of electromagnetic diffraction by small apertures in conducting surfaces," Invited Paper, IEEE 1978 International Symp. on EMC, June 20-22, 1978, PP. 86-91, Atlanta, GA. U.S.A.

[14] R. E. Collin, Field Theory of Guided Waves, McGraw-Hill Book Company, New York; 1960.

[15] W. A. Davis, "Bounding Signal Levels at Wire Terminations Behind Apertures," USAF SCEEE Research Program, Final Report, AFWL, Kirtland, NM; 20 August, 1979.

[16] C. H. Papas, Theory of Electromagnetic Wave Propagation, McGraw Hill Company, 1965.

[17] J. H. Wilkinson, Rounding Errors In Algebraic Processes, Englewood Cliffs, N.J. Prentice-Hall, Inc., 1963, P. 80.

[18] L. B. Felsen, Transient Electromagnetic Fields, Topics in Applied Physics, Volume 10, Chapter 3, Springer-Verlag, New York, 1976.

[A1] S. B. Cohn, "Determination of Aperture Parameters by Electrolytic-Tank Measurements," Proceedings of the IRE, Vol. 39, PP. 1416-1421; November, 1951.

[A2] S. B. Cohn, "The Electric Polarizability of Apertures of Arbitrary Shape," Proceedings of IRE, Vol. 40, PP. 1069-1071; September, 1952.

[A3] F. DeMeulenaere, J. Van Bladel, "Polarizability of Some Small Apertures," IEEE Trans. Ant. and Prop., Vol. AP-25, No. 2, PP. 198-205; March, 1977.

[A4] C. M. Butler, "A review of electromagnetic diffraction by small apertures in conducting surfaces," Invited papers, IEEE 1978 International Symp. on EMC, June20, 1978, PP. 86-91.

[A5] H. B. Dwight, Tables of Integrals and Other Mathematical Data, 4th ed. Macmillan, New York; 1961.

[B1] D. Kajfez, "Excitation of a termianted TEM transmission line through a small aperture," Interaction Notes 215, July 1974.

[B2] W. A. Davis, "Bounding signal lavels at wire terminations behind apertures," AFWL Interaction Note 384, February 1980.

[B3] W. L. Weeks, Electromagnetic Theory for Engineering Applciations, New York: Wiley, 1964, PP. 318-323.

[C1] B. Friedman, Principles and Techniques of Applied Mathematics, New York: J. Wiley, 1956, PP. 26-33.

[C2] S. Gasiorowicz, Quantum Physics, New York: J. Wiley, 1974, PP. 495-499.

[C3] A. Messiah, Quantum Mechanics, Volume I, Amsterdam: North Holland, 1965, PP. 162-179.

[D1] H. Amemiya, "Time-domain Analysis of Multiple Parallel Transmission Lines," RCA Review, Vol. 28, PP. 241-276, June 1967.

[D2] K. D. Marx, "Propagation Models, Equivalent Circuits, and Characteristic Terminations For Multiconductor Transmission Lines with Inhomogeneous Dielectrics," IEEE Trans. Microwave Theory & Tech, Vol. MTT-21 PP. 456-457, July 1973.

[D3] D. Kajfez, D. R. Wilton, "Small Aperture on a Multiconductor Transmission Line Filled with Inhomogeneous Dielectrics," AFWL Interaction Note 347, November 1977.

[D4] L. A. Pipes, "Matrix Theory of Multiconductor Transmission Lines," Phil. Mag, Vol. 24, PP. 97-113, July 1937.

[D5] IRE Standards on Antennas and Waveguides: Definition of Terms, Proc. I.R.E., PP. 1721-1728, December 1953.

[D6] B. Friedman, Principles and Techniques of Applied Mathematics, New York: J. Wiley, 1956, PP. 107-110.

[E1] D. Kajfez, D. R. Wilton, "Small Aperture on a Multiconductor Transmission Line Filled With Inhomogeneous Dielectrics," AFWL Interaction Note 347, November 1977.

[F1] R. E. Collin, Foundations for Microwave Engineering, New York: McGraw Hill, 1966, PP. 183-187.

[F2] D. Kajfez, "Excitation of a terminated TEM transmission line through a small aperture," Interaction Notes 215, July 1974.

[F3] W. A. Davis, "Bounding signal levels at wire terminations behind aperture;" AFWL Interaction Note 384, February 1980.

☆U.S. GOVERNMENT PRINTING OFFICE: 1982-576-115/525